MODELING THE CONSEQUENCES OF EPIDERMAL GROWTH FACTOR RECEPTOR INHIBITION ON CARDIAC DEVELOPMENT, FUNCTION, AND HOMEOSTASIS

Cordelia Johnson Barrick

A dissertation submitted to the faculty of the University of North Carolina at Chapel Hill in partial fulfillment of the requirements for the degree of Doctor of Philosophy in the Curriculum of Toxicology

Chapel Hill

2007

Approved by:

David Threadgill

Curtis Harper

William Coleman

Joan Taylor

Mark Majesky

ABSTRACT

Cordelia Johnson Barrick: MODELING THE CONSEQUENCES OF EPIDERMAL GROWTH FACTOR RECEPTOR INHIBITION ON CARDIAC DEVELOPMENT, FUNCTION, AND HOMEOSTASIS

(Under the direction of David Threadgill)

The epidermal growth factor receptor (EGFR/ERBB1) is the prototypical and first discovered member of the ERBB family of receptor tyrosine kinases. As transmembrane receptors, their primary function is to translate extracellular signals into cellular response. Signaling is initiated through binding by members of the EGF ligand family, which induces receptor homodimerization or heterodimerization with other ERBB receptors (ERBB2, ERBB3 or ERBB4). Activation of downstream cytoplasmic signaling pathways occurs, leading to alterations in biological responses such as cellular proliferation, survival, motility, and adhesion. As EGFR is expressed in most developing and adult tissues, misregulation or dysfunction of EGFR activity severely impacts embryonic viability, tissue maintenance and multiple disease processes. Since EGFR was first proposed as a cancer drug target over twenty years ago, substantial research has defined a central role for aberrant ERBB signaling in cancer and led to the design of targeted therapies that effectively inhibit receptor activity. However, significant cardiotoxicity was observed in clinical trials targeting the closely related ERBB2 receptor, necessitating further studies on the role of ERBB signaling in cardiac development and function. Genetic ablation of any of the ERBB receptors, select ligands, or ligand-processing enzymes results in severe congenital cardiac defects, often causing embryonic lethality. Direct stimulation of ERBB2/ERBB4 heterodimers by the

ligand neuregulin-1 (NRG1) supports cardiomyocyte survival, while GPCR mediated transactivation of EGFR likely plays a significant role in cardiac hypertrophy and hypertension. These discoveries have fostered interest in novel therapies targeting the EGFR signaling pathway for the treatment of several common cardiovascular diseases. However, the effects of chronic EGFR inhibition on cardiovascular homeostasis have not been evaluated. Through the use of mouse models, we demonstrated that genetic or pharmaceutical repression of EGFR signaling significantly altered cardiac function and homeostasis. Since the cardiac phenotype of mice harboring a hypomorphic mutation in *Egfr* was strongly dependent on genetic background, we broadly localized quantitative trait loci (QTL) which modulate the cardiac phenotype. These studies should be useful in predicting degenerative cardiac changes associated with EGFR inhibition which may be overlooked in short term clinical trials, and may advance understanding of the role of EGFR in cardiac development and function.

In loving memory of James Harris Johnson, III

ACKNOWLEDGEMENTS

Graduate school requires a special combination of good luck, tenacity and personal motivation.

I was fortunate to join a laboratory headed by David Threadgill, who gives his students an extraordinary amount of freedom. As a result, there is always an interesting and eclectic mix of ongoing research and graduate students in the Threadgill laboratory. Choosing one's research project is a bit like picking a piece of chocolate out of a Whitman's sampler box, except that there is less certainty about what is really in the center of the chocolate. Is that brown piece that appears so appetizing really a truffle? Or, when you pick it up, does it smell bad? When making this choice, I was also lucky, as I inherited a well-tended project from Reade Roberts, an exceptional scientist and friend. I was also privileged to meet and work closely with Susan Smyth while she was at UNC-Chapel Hill. Susan has been a source of encouragement, a fantastic mentor, and has contributed greatly to my overall development as a scientist. As far as tenacity is concerned, my innate stubbornness has proved to be an asset in completion of this research project. The unexpected loss of my father to cardiovascular disease has motivated me in my research efforts, far beyond completion of the doctoral degree.

I am especially grateful to my husband, Brian Barrick, my family, and friends for their love and support which sustained my resolve to complete this endeavor.

TABLE OF CONTENTS

LIST OF TABLES

Table

LIST OF FIGURES

Figure

LIST OF ABBREVIATIONS

AKT	protein kinase B
ANOVA	analysis of variance
AREG	amphiregullin
AS	aortic stenosis
BTC	betacellulin
dpc	days post coitus
DTR/HB-EGF	diphtheria toxin receptor
ECC	endocardial cushions
ECM	extracellular matrix
EGF	epidermal growth factor
EGFR	epidermal growth factor receptor
EH	essential hypertension
EMT	endocardial mesenchymal transdifferentiation
EPGN	epigen
EREG	epiregulin
FS	fractional shortening
GPCR	G protein coupled receptor
H&E	hemotoxylin and eosin
HR	heart rate
HW	heart weight
IF	intermale fighting

LV	left ventricle
LVED,d	left ventricular end diastolic diameter
LVED,s	left ventricular end systolic diameter
LVH	left ventricular hypertrophy
LVMI	left ventricle mass index
LVPWTh,d	left ventricular posterior wall thickness, diastole
LVPWTh,s	left ventricular posterior wall thickness, systole
MAP	mean arterial pressure
MAPK	mitogen-activated protein kinase
NRG	neuregulin
RCE	restraint and cold exposure
TAC	transverse aortic constriction
TGFA	transforming growth factor alpha
TKI	tyrosine kinase inhibitor
TTE	transthoracic echocardiography
wa2	waved-2

CHAPTER 1

THE ROLES OF EGFR/ERBB1 SIGNALING IN CARDIAC DEVELOPMENT AND DISEASE

Abstract

The epidermal growth factor receptor (EGFR/ERBB1) is the prototypical and first discovered member of the ERBB family of receptor tyrosine kinases. As transmembrane receptors, their primary function is to translate extracellular signals into cellular response. Signaling is initiated through by members of the EGF ligand family, which induces receptor homodimerization or heterodimerization with other ERBB receptors (ERBB2, ERBB3 or ERBB4). Activation of downstream cytoplasmic signaling pathways occurs, leading to alterations in biological responses such as cellular proliferation, survival, motility, and adhesion. As EGFR is expressed in most developing and adult tissues, misregulation or dysfunction of EGFR activity severely impacts embryonic viability, tissue maintenance and multiple disease processes. Since EGFR was first proposed as a cancer drug target over twenty years ago, substantial research has defined a central role for aberrant ERBB signaling in cancer and led to the design of targeted therapies that effectively inhibit receptor activity. However, a major side effect on cardiac function was observed, necessitating further studies on the role of ERBB signaling in cardiac development and function. Genetic ablation of any of the ERBB receptors, select ligands, or ligand-processing enzymes results in severe congenital cardiac defects, often causing embryonic lethality. Direct stimulation of ERBB2/ERBB4 heterodimers by the ligand neuregulin-1 (NRG1) supports cardiomyocyte

survival, while GPCR mediated transactivation of EGFR likely plays a significant role in cardiac hypertrophy and hypertension. These discoveries have fostered interest in novel therapies targeting the EGFR signaling pathway for the treatment of common cardiovascular diseases. However, the effects of chronic EGFR inhibition on cardiovascular homeostasis have not been evaluated. Here, we review current research in ERBB signaling in cardiac development and disease, with particular emphasis on EGFR signaling. Through the use of mouse models, we demonstrate that genetic or pharmaceutical reduction of EGFR activity results in significant alterations in cardiac development and homeostasis; moreover the severity of these alterations is modified by genetic background. Genetic mapping studies also identify loci conferring susceptibility to EGFR-related degenerative cardiac pathology. Together, these studies should be useful in predicting degenerative cardiac changes associated with EGFR inhibition which may be overlooked in short term clinical trials.

Introduction

The EGFR (HER1) is the prototypical and first discovered member of the ERBB/HER family of membrane receptors, which also includes ERBB2/HER2, ERBB3/HER3 and ERBB4/HER4 [2]. These receptor tyrosine kinases have a conserved molecular structure with an extracellular, cysteine-rich ligand-binding domain, a single alpha-helix transmembrane domain and an intracellular domain with tyrosine kinase (TK) activity in the carboxy-terminal tail (except for ERBB3/ HER3) [3]. Ligand binding by members of the epidermal growth factor (EGF) family induces homodimerization or heterodimerization with other ERBB receptors, resulting in tyrosine kinase activity [4]. Subsequently, autophosphorylation or transphosphorylation of tyrosine residues in the carboxy-terminal tail directs binding for adaptor proteins and signaling molecules [5]. The

net result of intracellular signaling cascades is altered biological processes, including proliferation, differentiation, motility and survival [3].

The ERBB signaling pathway is complex and strongly associated with other central intracellular and extracellular signaling pathways [6, 7]. In addition to EGF [8], there are ten additional known ligands which bind to ERBB homo and heterodimers with differing degrees of preference, including transforming growth factor-α (TGF-α) [9], amphiregulin (AREG) [10, 11], diphtheria toxin receptor/ heparin-binding, EGF-like growth factor (HB-EGF/DTR) [12], betacellulin (BTC) [13, 14], epiregulin (EREG) [15], epigen (EPG) [16], and neuregulins (NRG1-4) [17-19]. As illustrated in Figure 1-1, EGF, TGF-α, and AR show specificity to EGFR, and HB-EGF/DTR, EPR and BTC bind to both EGFR and ERBB4. NRG1 and NRG2 bind to both ERBB3 and ERBB4, while NRG3 and NRG4 are specific to the ERBB4 receptor. Adding to the complexity, ERBB2 has no known ligand but enhances and stabilizes dimerization with other ERBBs, while ERBB3 is catalytically inactive [20-23]. Receptor homodimer or heterodimer combinations induce phosphorylation of unique tyrosine sites which in turn serve as docking sites for specific SH-2 adaptor proteins that initiate intracellular signaling cascades. The Ras- and Shc-activated mitogen-activated protein kinase (MAPK) pathway is a target of all ERBB receptors, while the PI(3)K-activated AKT and p70S6K/p85S6K pathways are downstream of only some ERBB dimers [7]. Activation of signaling networks translates in the nucleus into distinct transcriptional programs involving the proto-oncogenes FOS, JUN and MYC, and several transcription factors, including SP1 and EGR1. An additional control of biological outcomes is signal duration. The kinetics of signal termination is dependent upon ligand-mediated receptor endocytosis and receptor composition [7].

Cross activation by other receptor families also contributes to ERBB signaling intricacy. For example, members of the G protein coupled receptor superfamily (GPCR) transactivate EGFR via metalloproteinase activation and subsequent cleavage and extracellular release of EGF-like ligands [24]. This is thought to be how GPCR agonists, such as angiotensin II (ANG-II), endothelin-1 (ET-1) and thrombin elicit growth effects via activation of the MAPK pathway, circumventing the lack of intrinsic tyrosine kinase activity of their cognate receptors [25, 26]. Recently, it was proposed that in the heart, ERBB2 forms a heterocomplex with GPCRs in a ligand-dependent fashion, leading to a direct activation of MAPK signaling [27].

ERBB signaling in cardiac development, function and homeostasis. Gene targeting studies in mice demonstrate that all four ERBB receptors, select ligands and ligand-processing enzymes are required for normal cardiac development (summarized in Table 1-1). Mice lacking *Erbb2*, *Erbb4*, and *Nrg1* all die around 10.5 days post-coitus (dpc) primarily due to defects in cardiomyocyte development [28-30]. While *Erbb3* $^{-/-}$ mice have normal cardiomyocyte development, defective cardiac valve formation and function results in embryonic lethality by 13.5 dpc [31]. Mice nullzygous for *Egfr* show strain-dependent lethality varying from early pre-implantation to three weeks after birth [32-34]. On the CD-1 background, which supports survival to term, *Egfr* null mice have cardiac valve enlargement in addition to severe neurological and gastrointestinal defects [35, 36]. Of the ten known ligands, only genetic ablation of *Nrg1* or *Dtr/Hb-egf* affects cardiovascular development. The precursor, membrane-bound form of DTR is cleaved by members of the "α disintegrin and metalloprotease" [37] family of convertases, resulting in the shedding of soluble HB-EGF/DTR which can bind and activate EGFR and ERBB4 homodimers as well as ERBB2/3

heterodimers. *Dtr/Hb-egf* $^{-/-}$ mice exhibit severe defects in heart chamber and valve formation [35, 38], while mice lacking members of the ADAM family (*t*umor necrosis factor-*a*lpha *c*onverting *e*nzyme (TACE*)* or ADAM19) show similar valve phenotypes [1, 35]. Homozygous deletion of other ligands individually, or even combined *Egf/Areg/Tgf-*α deletion, does not result in embryonic lethality or cardiovascular defects, suggesting significant signaling pathway redundancy in development [39, 40]. Cumulatively, these knock-out models suggest distinct, chronological roles of ERBB receptors and ligands during cardiovascular development, with NRG-1-ERBB2/4 signaling being of central importance in cardiomyocyte development and maturation, while DTR/HB-EGF and/or NRG-1 activation of EGFR, ERBB3 (and possibly ERBB2) being central to normal cardiac valve development. In order to define these roles in context, a brief outline of cardiac development follows.

Outline of heart development:

A. **Cardiac crest formation**. At approximately 7 days post-coitus (dpc) in the mouse, cardiac progenitor cells derived from the mesoderm and neural crest migrate towards the anterior and anterio-lateral portion of the embryo to form the "cardiac crescent" or primary heart field. Specification of the myocardial and endocardial cell lineages occurs during this stage (Figure 2A) [41].
B. **Formation of the primitive heart tube.** By 8.0 dpc in the mouse, the cardiac crescent has fused at the ventral midline to form a heart tube, consisting of an incomplete outer layer of myocardium and an inner lining of endocardial cells separated by an extensive extracellular matrix (ECM) referred to as the cardiac jelly (Figure 1-2B). At this stage, the forming heart is centrally located within the embryo and is bilaterally symmetrical. Marking studies have shown that the base of the tube is destined to give rise to the atria,

the middle region will give rise to a common ventricle, and the conus truncus, with contributions from a secondary heart field, will give rise to the outflow tract of the heart [41].

C. **Cardiac looping**. A crucial remodeling process of the heart tube known as cardiac looping occurs during 8.5-10.5 dpc in the mouse (Figure 1-2C). This positions the atrial region of the tube posterior to the common ventricle, setting the stage for the formation and maturation of the four chambers as well as establishment of separate pulmonary and systemic circulation (Figure 1-2C).

D. **Cardiac maturation.** Maturation of the heart occurs in multiple stages: (1) formation of trabeculated myocardium, (2) formation of endocardial cushions (ECC), which contribute to septation of the heart and cardiac valves and (3) compaction of the spongy myocardium coinciding with establishment of the coronary circulation. Ventricular trabeculation, whereby myocardial cells are activated by endocardium-derived signals to proliferate and invade the interior of the cardiac chambers, begins soon after right forward looping of the heart tube (Figure 1-2D). This process serves primarily as a means to increase myocardial oxygenation in the absence of coronary circulation and is necessary for circulation in the early stages of cardiac morphogenesis. Coinciding with ventricular septation, trabeculae start to compact at their base adjacent to the outer compact myocardium, adding to its thickness (beginning at Figure 1-2E). In the mouse, this process is fairly rapid, occurring between 13 and 14 dpc with the establishment of coronary circulation.[42]Non-compaction of the myocardium, even in small localized regions of the ventricular wall, results in serious functional consequences and is associated with heart failure and sudden cardiac death [43].

E. Cardiac valve development. Formation of the endocardial cushion (ECC) tissues is extremely important for cardiac morphogenesis, as they provide the "glue" for virtually all of the septal structures in the heart [42]. Dysmorphogenesis of the ECC or failure of proper fusion are generally thought to play a major role in the etiology of congenital heart defects [43]. ECC formation is characterized by endothelial-mesenchymal transdifferentiation (EMT), where a subset of endocardial cells in the cushion-forming regions delaminates and invades the cardiac jelly shortly after cardiac looping (Figure 1-3A). These cells proliferate and complete their differentiation into mesenchymal cells, forming cushions that subsequently give rise to the septa of the four-chambered heart as well as the cardiac valves. ECC formation is complete by 12.5 dpc in the mouse, and is followed by a valvular remodeling stage in which cell proliferation ceases and apoptosis increases, together remodeling the cushions into slender valve leaflets by 15.5 dpc. In normal mouse and human cardiac valve development, cell proliferation is significant during cushion development, decreases significantly during late embryonic development and early postnatal life (coinciding with valve remodeling), and is undetectable in adult valves [44].

Proportional valve growth after birth is largely attributable to increased ECM production. Stratification of the ECM into three overlapping layers also begins in valve remodeling stages but is not complete until postnatal life. In aortic valves, the arterial aspect of the cusp (fibrosa) is composed predominantly of collagen fibers; the central aspect (spongiosa) consists largely of loosely arranged proteoglycans; while the ventricular aspect (ventricularis) contains elastin fibers [44]. Defective stratification and

degeneration of these layers is a pathological characteristic of congenital and acquired aortic stenosis (AS) which has profound consequences on valve function.

ERBB signaling and cardiac development. ERBB signaling is particularly important in mid-to late gestational cardiac processes, particularly in cardiomyocyte trabeculation and cardiac valve development, both of which depend upon reciprocal signaling between endocardial cells, ECM and cardiomyocytes to regulate cellular proliferation, differentiation and invasion. As mentioned previously, mice lacking ERBB2, ERBB4, and NRG1 die around 10.5 dpc, primarily due to reduced blood flow resulting from a lack of ventricular trabeculae [28-30]. In wild-type 9.5/10.5 dpc embryos, ERBB2 and ERBB4 expression is specific to developing cardiomyocytes, whereas NRG is localized to the endocardium. Although ERBB2 is the preferred dimerization partner for ERBB3 and ERBB4 upon NRG stimulation, ventricular trabeculation is relatively normal in *Erbb3*$^{-/-}$ mice [31]. Since neither ERBB2 nor ERBB4 can compensate for the loss of the other receptor in the heart, cardiac NRG-1 signaling likely requires ERBB2/4 heterodimers. Moreover, genetic rescue of *Erbb2*$^{-/-}$ and *Erbb4*$^{-/-}$ embryos by myocardial expression of *Erbb2* or *Erbb4* cDNA under the control of cardiac specific promoters circumvents cardiac defects and embryonic lethality [45, 46]. These data are consistent with a paracrine model whereby NRG1 is released by endocardial cells, diffuses through the cardiac jelly and activates ERBB2/4 receptors localized on cardiomyocytes, thus triggering proliferation and invasion to form ventricular trabeculae.

During cardiac development, ERBB3 expression appears to be restricted to endocardial cushion mesenchyme [30]. Embryos lacking ERBB3 have thinned ECC completely lacking mesenchymal cells. These defects lead to significant blood reflux and

lethality at 13.5 dpc due to inability to sustain cardiac function [31]. While ERBB3 on its own lacks biological activity, NRG-1 activation of ERBB2/3 heterodimers generates a potent signal [47]. Although not as severe as the *Erbb3* $^{-/-}$ phenotype, *Nrg1*$^{-/-}$ or *Erbb2* $^{-/-}$embryos also have underdeveloped ECC at 10.5 dpc, suggesting that NRG1-ERBB2/3 signaling plays a role in early stages of cellular proliferation and differentiation in ECC formation. Recent work has uncovered additional modulators of ERBB3 activity in this developmental context. The extracellular matrix component hyaluronic acid appears to regulate ERBB2/3 signaling during cushion formation, while the transcription factors GATA binding protein 4 (GATA-4) and SRY (sex determining region Y)-box 9 (SOX9) are upstream mediators of ERBB3 expression in differentiated mesenchymal cells [48-50].

EGFR signaling and cardiac development. Mice lacking EGFR, its ligand DTR/HB-EGF or the convertases TACE or ADAM19, have enlarged, hyperplastic cardiac valves [1, 35, 36, 38]. While these mutant embryos exhibit enlargement of all four cardiac valves, embryos homozygous for the hypomorphic *waved-2* mutation have hyperplastic semilunar (SL, i.e. aortic and pulmonic) valves, suggesting there is greater requirement for EGFR signaling in SL valve development [35, 36]. Exposure to EGFR inhibitors or knockdown of *Egfr* expression in developing zebrafish results in a narrowed outflow tract, ventricular and atrial enlargement, and decreased circulation, suggesting that the cardiac phenotype resulting from disrupted EGFR signaling is conserved across species [51].

Cardiac cushions form normally in *Dtr/Hb-egf* $^{-/-}$embryos, but are only modestly condensed during remodeling stages (12.5-14.5 dpc) and thus remain significantly enlarged compared to wild-type controls by 15.5 dpc [35]. Aberrant mesenchymal cell proliferation, rather than decreased apoptosis, appears responsible for this phenotype. *Egfr*$^{-/-}$ and *Tace* $^{-/-}$

embryos have similarly enlarged, hyperplastic valves at 15.5 dpc, suggesting that impaired remodeling also underlies valve enlargement in these mutants [35]. During the valve remodeling stage in wild-type embryos, and TACE expression is detected throughout the heart but enriched in cardiac cushions while DTR/HB-EGF is expressed exclusively by the endocardial cells lining the developing valves, but not in differentiated mesenchymal cells [35, 38]. Additionally, mice with *Dtr* knocked-out in endothelial and smooth muscle cell lineages, or homozygous for an uncleavable form of DTR/HB-EGF, have a similar valve phenotype [52, 53]. Together, this strongly suggests a paracrine model where DTR is processed and released from the endocardial cells by TACE or ADAM19, diffuses through the extracellular matrix, and activates EGFR on invading, differentiating cells to negatively regulate proliferation.

Several findings suggest that signaling through EGFR may counterbalance bone morphogenic protein (BMP) signaling to suppress mesenchymal cell proliferation. Genetic studies using knockout mouse models established that endocardial outflow track cushion growth is largely controlled by the amount of BMP signaling, with diminished and excessive signaling correlating to hypo and hyperplastic cushions, respectively [54, 55]. Since the enlarged valves of *Dtr/Hb-egf* $^{-/-}$ embryos have dramatic increases in activated BMP signaling effectors SMAD1/5/8 and since EGFR downregulates BMP signaling by inactivating SMAD1 *in vitro*, EGFR activation by TACE-derived soluble DTR may normally limit BMP signaling during the transition from cushion formation/growth to valve remodeling [46]. Potential binding partners for EGFR in this process include ERBB3 or ERBB4 since both are expressed in remodeling valves. Since *Erbb4* $^{-/-}$ embryos rescued by cardiomyocyte specific ERBB4 expression do not have enlarged valves, while *Erbb3* $^{-/-}$

embryos have defective cushion formation, ERBB3 seems a likely heterodimer candidate in DTR/EGFR signaling during valve remodeling.

More recently, phospholipase C epsilon (PLCε), a phosphoinositide-specific phospholipase C, was proposed as a downstream effector of EGFR signaling in valve remodeling [56]. Mice homozygous for a targeted, inactivating mutation in *Plcε* (*Plcε*$^{\Delta X/\Delta X}$) have hyperplastic semilunar valves, ventricular dilation, aortic stenosis and aortic regurgitation. Increased SMAD1/5/8 activity is detected in the remodeling valves of *Plcε*$^{\Delta X/\Delta X}$ 15.5 dpc embryos. The authors conclude that PLCε may play an important role in EGFR-mediated negative regulation of the SMAD1/5/8 activation at a late stage of valve remodeling [56].

ERBB signaling in cardiac disease. A role for ERBB signaling in adult cardiac homeostasis and heart disease is also emerging. Three of the four receptors (EGFR, ERBB2 and ERBB4) remain expressed in the adult human and rodent heart; among these ERBB4 appears to be the most abundant [57-60]. The expression and activity of ERBB2 and ERBB4 receptors is depressed in clinical and experimentally induced heart failure [61-63] and signaling via NRG-1/ERBB2/4 activation is critical for neonatal and adult cardiomyocyte survival and growth [57, 64-67]. The importance of this signaling pathway in cardiac homeostasis was not fully appreciated until the unexpected cardiotoxicity reported in breast cancer clinical trials using trastuzmab (Herceptin, Genetech San Francisco, CA), a humanized monoclonal antibody designed to repress ERBB2 activity by blocking the ligand binding site [66, 68-70]. While approximately 8% of patients had cardiac changes with trastuzmab monotherapy, 30% of patients receiving combinatorial therapy with

anthracycline, a commonly used chemotherapeutic drug, developed dilated cardiomyopathy. Mouse models with ventricular specific deletion of *Erbb2* or *Erbb4* have normal cardiac development, but progressive postnatal degeneration that mimics the cardiotoxicity observed in clinical trials [71-73]. *Erbb2* conditional knock out (CKO) mice have up to 70% reduction of cardiomyocyte ERBB2 expression, with no alterations in ERBB4 expression. These mice develop ventricular dilation, reactivation of embryonic gene expression, increased normalized heart weight, and depressed cardiac contractility. *Erbb4* CKO mice have almost 80% reduction in ventricular ERBB4 protein levels, no alterations in ERBB2 protein levels, and cardiac phenotypes that match *Erbb2* CKO mice as well as significant mortality by one year of age [73]. Although the authors do not report cardiomyocyte apoptosis in *Errb2* or *Erbb4* CKO hearts, isolated cardiomyocytes from *Erbb2* CKO mice display increased sensitivity to the anthracycline doxorubicin, consistent with the enhanced cardiotoxicity observed with concurrent trastuzmab therapy [72]. In addition, overexpression of the anti-apoptotic gene *Bcl2/1* partially rescues ventricular dilation and contractility in *Erbb2* CKO mice, suggesting decreased cell survival contributes to cardiac dysfunction.

Consistent with these results, mice lacking one copy of *Nrg1* (*Nrg1*$^{+/-}$) have decreased survival due to heart failure when exposed to doxorubicin [74]. Cardiomyocyte anti-apoptotic ERBB signaling involves activation of the serine/threonin kinase AKT, which attenuates apoptosis by phosphorylating, and thus inactivating, a variety of pro-apoptotic proteins. Doxorubicin-treated *Nrg1* $^{+/-}$ mice have significantly decreased levels of phosphorylated ERBB2, AKT, and ERK-1/2 compared to similarly exposed wild type controls [74]. Conversely, short term intravenous administration of a recombinant NRG1 peptide fragment substantially improves cardiac function and survival in multiple cardiac

injury models (infarct-, viral-, anthracyline, and pacing models) in rodents and dogs [64]. Consequently, there is interest in exploiting this pathway as a novel therapy for heart failure or as means to prevent chemotherapy-associated cardiotoxicity [75].

EGFR signaling in cardiac disease. Signaling through the EGFR has been shown to modulate pathological processes underlying common cardiovascular diseases, including cardiomyocyte apoptosis and hypertrophy, fibrosis and hypertension [26, 37, 76-79]. *In vitro* studies of isolated cardiomyocytes demonstrate that exposure to EGF increases cardiomyocyte contractile frequency [80], while EGF or DTR/HB-EGF induce hypertrophy and cardiac fibroblast proliferation [81] [82-84]. On a molecular level, these changes are accompanied by increased protein synthesis, MAPK activation and increased transcription of early response genes, suggesting that ligand-dependant EGFR activation can directly influence cardiac remodeling.

Several GPCR agonists, such as angiotensin II (ANGII), endothelin-1 (ET-1) and thrombin, provoke cardiomyocyte hypertrophy, vascular smooth muscle proliferation, vasoconstriction and fibrosis [26, 78, 85-91]. Since GPCRs lack intrinsic tyrosine kinase activity, recent work proposes that these receptors "hijack" EGFR activity via activating metalloproteases which cleave membrane-bound ligands, and in this manner access downstream EGFR-dependent mitogenic pathways [24, 26, 92]. Cardiomyocyte hypertrophy induced by over stimulation of the renin-angiotensin (RAS) depends upon GPCR/EGFR transactivation [25]. Physiological actions of ANGII are mediated via the angiotensin type 1 (AT1R) and angiotensin type 2 (AT2R) GPCRs, which are expressed in cardiomyocytes. In isolated neonatal cardiomyocytes, overexpression of AT1R stimulates robust hypertrophy accompanied by activation of MAPK, induction of the immediate-early response genes and

re-expression of atrial natriuretic peptide (ANP) [93]. These responses are blocked *in vitro* by AG-1478, an EGFR inhibitor, or KB-R7785, which inhibits the metalloprotease ADAM12 [93, 94]. Since treatment with KB-R7785 blocks processing of DTR/HB-EGF and attenuates pressure-overload induced hypertrophy *in vivo*, disruption of GPCR/EGFR transactivation at this junction has been proposed as a novel therapy for left ventricular hypertrophy [94].

EGFR activation is also cardioprotective against the effects of sustained β-adrenergic stimulation and acute stress [79, 95]. Intermale fighting (IF) and restraint-and-cold (4°C) exposure (RCE) are two mouse models of intense acute stress. Following IF, but not RCE, plasma EGF concentrations increase up to 1,000-fold. Cardiac necrotic lesions and elevated plasma activity of creatine kinase (CK, a biomarker for cardiac injury) are seen with RCE, but not IF [79]. Administration of AG-1478 (25mg/kg ip) prior to IF leads to increased plasma activities of CK and other biomarkers, while administration of endogenous EGF significantly reduces biomarker activity in RCE mice compared to vehicle treated controls. Co-administration of AG-1478 and EGF eliminates the cardioprotective effect in RCE mice, providing additional evidence that EGFR activation may protect the heart against stress-induced injury. Activation of EGFR generates a potent survival signal in cardiomyocytes and other cell types [37]; conversely, EGFR inhibition enhances apoptosis in normal and cancerous epithelial cells [96] and in regenerating tissue [97, 98]. Since prolonged β-adrenergic stimulation is known to trigger cardiomyocyte apoptosis, these studies suggest that chronic EGFR inhibition may exacerbate some types of heart disease.

Conclusions

The EGFR/ERBB1 signaling pathway is complex, intricately intertwined with many extracellular and intracellular signaling pathways, and required for normal development and homeostasis of most tissues. Genetically engineered mouse models have advanced our understanding of ERBB receptor function in cardiac development and predicted cardiotoxicity arising from ERBB2/HER2 targeted therapy. The current use of EGFR inhibitors for cancer treatment and proposal of novel therapies repressing EGFR activity are proposed for cardiovascular diseases necessitates a better understanding of roles of this signaling pathway in cardiac development, function and disease.

Mouse models with genetically reduced EGFR activity resulting from the *waved-2* hypomorphic allele (*Egfr* ^{wa2}) have assisted in defining the role of EGFR in carcinogenesis; moreover, phenotypes of *Egfr* $^{wa2/wa2}$ mice mimic common side effects observed with EGFR-targeted therapy [99, 100]. Despite extensive use of this mouse model, congenital valve defects and AS were discovered rather recently. Previous studies revealed the severity and penetrance of phenotypes associated with EGFR activity are highly dependent upon genetic background. To determine if genetic modifiers play a similar role in EGFR-related cardiac phenotypes, we backcrossed the mutation onto the commonly used C57BL/6J (B6) and 129S1/SvImJ (129S1) inbred strains, creating *Egfr* ^{wa2} congenic lines and an F_1 *Egfr* ^{wa2} population. Because we found impressive genetic-background-dependent differences in cardiac phenotypes associated with congenitally enlarged aortic valves, we designed experiments investigating cardiac response to similar afterload in B6, 129S1 and F_1 wild-type mice. In order to partition EGFR-related congenital defects from effects on cardiac homeostasis, we conducted toxicity studies where adult wild-type mice were chronically

exposed to EGFR small molecule inhibitors. Finally, to broadly localize genetic modifiers which confer susceptibility to EGFR-related cardiac hypertrophy and failure, we conducted preliminary genetic mapping experiments. Together, these studies should be useful in predicting degenerative cardiac changes associated with EGFR inhibition which may be overlooked in short term clinical trials.

Figure 1-1. ERBB ligand binding specificity is depicted for the four ERBB receptors. Epidermal growth factor (EGF), transforming growth factor alpha (TGF-a), amphiregulin (AREG), epiregulin (EREG), betacellulin (BTC), epigen (EPG), and neuregulins 1-4 (NRG1-4).

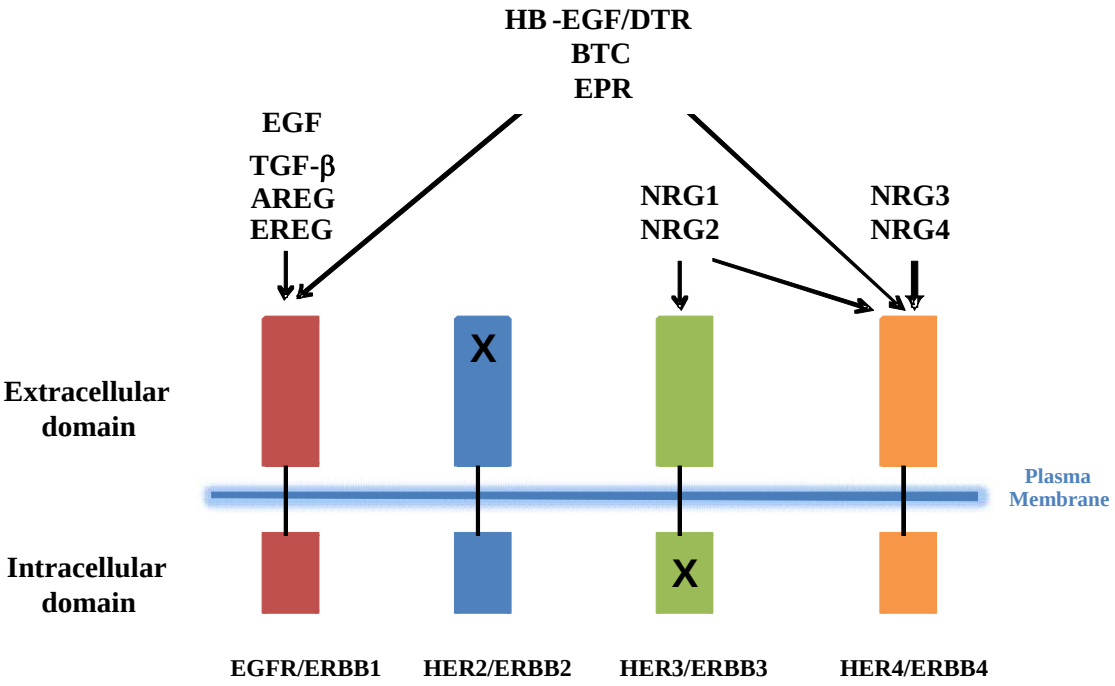

Table 1-1. Phenotypes resulting from genetic ablation of ERBB receptors, ERBB ligands or ligand processing enzymes.

ERBB receptor	Survival	Embryonic timepoint	Cardiovascular defect	Other defects	References
ERBB1/EGFR	Genetic background dependent	Embryonic, perinatal or postnatal lethality	Semilunar valve enlargement	Placental defects Eye, pulmonary, skin, kidney, brain, liver, GI tract	[32-34]
HER2/ERBB2	Embryonic lethal	E 10.5	Trabeculation defects	Nervous system	[28]
HER3/ERBB3	Embryonic lethal	E13.5	Hypoplastic cardiac cushions	Nervous system Stomach pancreas	[31, 101]
HER4/ERBB4	Embryonic lethal	E 10.5	Trabeculation defects	Nervous system	[29]
EGF ligand	**Survival**	**Embryonic timepoint**	**Cardiovascular defect**	**Other defects**	**References**
EGF	Normal	N/A	None reported	None	[39]
Amphiregulin (AR)	Normal	N/A	None reported	Mammary gland	[39]
TGF-a	Normal	N/A	None reported	Skin, eye	[102]
EGF/AR/TGF-a	Normal	N/A	None reported	Mammary gland, growth, small intestine	[39, 40]
HB-EGF/DTR	Peri/postnatal	N/A	Cardiac dilatation Valve enlargement	Skin, pulmonary, eye	[35, 38, 103]

EGF ligand	Survival	Embryonic timepoint	Cardiovascular defect	Other defects	References
Betacellulin (BTC)	Normal	N/A	None reported	None reported	[35]
Epiregulin (ER)	Normal	N/A	None reported	Intestinal damage	[104]
Neuregulin (NRG)-1	Embryonic lethal	E 10	Trabeculation defects Cardiac conduction	Nervous system	[30]
NRG-2	Normal	N/A	None reported	Growth, reproduction	[105]
Ligand processing	**Survival**	**Embryonic timepoint**	**Cardiovascular defect**	**Other defects**	**References**
ADAM17(TACE) Processing of : NRG1 and 2, HB-EGF, TGFα and AR	Perinatal/postnatal [39]	N/A	SL and AV valve enlargement VSD	Pulmonary	[35, 106]
ADAM19 Processing of: HB-EGF, NRG1, AR	Perinatal/postnatal	N/A	SL and AV valve enlargement VSD Overriding aorta Vasculature defects	None reported	[1]
ADAM17/19	Embryonic lethality	> E14.5	Trabeculation SL and AV valve	None reported	[106]

Figure 1-2. Developmental stages of heart development. A. Specification of precardiac mesoderm and formation of cardiac crescent. B. Fusing of the cardiac mesoderm to form linear heart tube. C. Right forward lopping of the heart tube and determination of segments giving rise to cardiac chambers and cardiac valves. D. Cardiac looping leads to formation of cardiac chambers and outflow tract. An example of an E12.5 embryonic heart is shown below (E). F. Later stages of cardiac maturation include remodeling of cardiac cushions to form mature valves as well as thickening of the ventricular chamber walls. An example of an E14.5 embryonic heart is shown below (G). A, Atria; V, ventricle; CT, conus truncus; SV, sinus venous; RA, right atrium; LA, left atrium. Figures adapted from [107, 108].

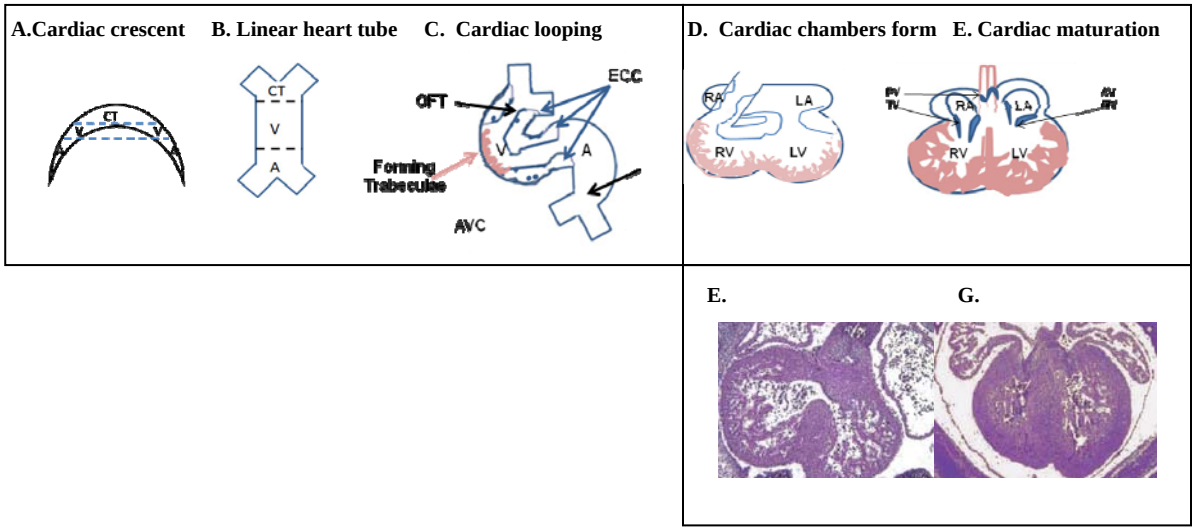

Figure 1-3. Developmental stages of cardiac valve development. A. Formation of the endocardial cushions begins when a subpopulation of endocardial cells is activated by signals released by the myocardium to delaminate and invade the underlying cardiac jelly. B. These cells differentiate, migrate towards the myocardium and proliferate. C. During remodeling of the endocardial cushions, decreased proliferation and increased apoptosis results in mature slender valve leaflets. Stratification of the extracellular matrix also occurs. Molecules within the ECM and released from endocardial cells are thought to mediate this process. Figures adapted from [107, 108].

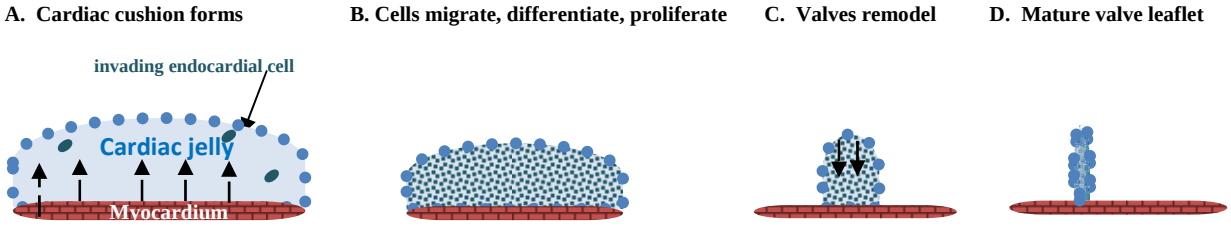

References

1. Zhou, H.M., et al., *Essential role for ADAM19 in cardiovascular morphogenesis.* Mol Cell Biol, 2004. **24**(1): p. 96-104.

2. Gullick, W.J., *Type I growth factor receptors: current status and future work.* Biochem Soc Symp, 1998. **63**: p. 193-8.

3. Wells, A., *EGF receptor.* Int J Biochem Cell Biol, 1999. **31**(6): p. 637-43.

4. Weiss, F.U., H. Daub, and A. Ullrich, *Novel mechanisms of RTK signal generation.* Curr Opin Genet Dev, 1997. **7**(1): p. 80-6.

5. Schlessinger, J., *Cell signaling by receptor tyrosine kinases.* Cell, 2000. **103**(2): p. 211-25.

6. Oda, K., et al., *A comprehensive pathway map of epidermal growth factor receptor signaling.* Mol Syst Biol, 2005. **1**: p. 2005 0010.

7. Yarden, Y., *The EGFR family and its ligands in human cancer. signalling mechanisms and therapeutic opportunities.* Eur J Cancer, 2001. **37 Suppl 4**: p. S3-8.

8. Cohen, S., *Isolation of a mouse submaxillary gland protein accelerating incisor eruption and eyelid opening in the new-born animal.* J Biol Chem, 1962. **237**: p. 1555-62.

9. Marquardt, H., et al., *Rat transforming growth factor type 1: structure and relation to epidermal growth factor.* Science, 1984. **223**(4640): p. 1079-82.

10. Ciardiello, F., et al., *Expression of cripto, a novel gene of the epidermal growth factor gene family, leads to in vitro transformation of a normal mouse mammary epithelial cell line.* Cancer Res, 1991. **51**(3): p. 1051-4.

11. Ciardiello, F., et al., *Differential expression of epidermal growth factor-related proteins in human colorectal tumors.* Proc Natl Acad Sci U S A, 1991. **88**(17): p. 7792-6.

12. Higashiyama, S., et al., *A heparin-binding growth factor secreted by macrophage-like cells that is related to EGF.* Science, 1991. **251**(4996): p. 936-9.

13. Barnard, J., *Betacellulin: newest addition to the epidermal growth factor family.* J Pediatr Gastroenterol Nutr, 1993. **17**(3): p. 343-4.

14. Shing, Y., et al., *Betacellulin: a mitogen from pancreatic beta cell tumors.* Science, 1993. **259**(5101): p. 1604-7.

15. Toyoda, H., et al., *Epiregulin. A novel epidermal growth factor with mitogenic activity for rat primary hepatocytes.* J Biol Chem, 1995. **270**(13): p. 7495-500.

16. Kochupurakkal, B.S., et al., *Epigen, the last ligand of ErbB receptors, reveals intricate relationships between affinity and mitogenicity.* J Biol Chem, 2005. **280**(9): p. 8503-12.

17. Carraway, K.L., 3rd, et al., *Neuregulin-2, a new ligand of ErbB3/ErbB4-receptor tyrosine kinases.* Nature, 1997. **387**(6632): p. 512-6.

18. Harari, D., et al., *Neuregulin-4: a novel growth factor that acts through the ErbB-4 receptor tyrosine kinase.* Oncogene, 1999. **18**(17): p. 2681-9.

19. Peles, E., et al., *Isolation of the neu/HER-2 stimulatory ligand: a 44 kd glycoprotein that induces differentiation of mammary tumor cells.* Cell, 1992. **69**(1): p. 205-16.

20. Horan, T., et al., *Binding of Neu differentiation factor with the extracellular domain of Her2 and Her3.* J Biol Chem, 1995. **270**(41): p. 24604-8.

21. Kim, H.H., et al., *Signal transduction by epidermal growth factor and heregulin via the kinase-deficient ErbB3 protein.* Biochem J, 1998. **334 (Pt 1)**: p. 189-95.

22. Sternberg, M.J. and W.J. Gullick, *Neu receptor dimerization.* Nature, 1989. **339**(6226): p. 587.

23. Klapper, L.N., et al., *The ErbB-2/HER2 oncoprotein of human carcinomas may function solely as a shared coreceptor for multiple stroma-derived growth factors.* Proc Natl Acad Sci U S A, 1999. **96**(9): p. 4995-5000.

24. Daub, H., et al., *Role of transactivation of the EGF receptor in signalling by G-protein-coupled receptors.* Nature, 1996. **379**(6565): p. 557-60.

25. Saito, Y. and B.C. Berk, *Transactivation: a novel signaling pathway from angiotensin II to tyrosine kinase receptors.* J Mol Cell Cardiol, 2001. **33**(1): p. 3-7.

26. Shah, B.H. and K.J. Catt, *Matrix metalloproteinase-dependent EGF receptor activation in hypertension and left ventricular hypertrophy.* Trends Endocrinol Metab, 2004. **15**(6): p. 241-3.

27. Negro, A., et al., *erbB2 is required for G protein-coupled receptor signaling in the heart.* Proc Natl Acad Sci U S A, 2006. **103**(43): p. 15889-93.

28. Lee, K.F., et al., *Requirement for neuregulin receptor erbB2 in neural and cardiac development.* Nature, 1995. **378**(6555): p. 394-8.

29. Gassmann, M., et al., *Aberrant neural and cardiac development in mice lacking the ErbB4 neuregulin receptor.* Nature, 1995. **378**(6555): p. 390-4.

30. Meyer, D. and C. Birchmeier, *Multiple essential functions of neuregulin in development.* Nature, 1995. **378**(6555): p. 386-90.

31. Erickson, S.L., et al., *ErbB3 is required for normal cerebellar and cardiac development: a comparison with ErbB2-and heregulin-deficient mice.* Development, 1997. **124**(24): p. 4999-5011.

32. Miettinen, P.J., et al., *Epithelial immaturity and multiorgan failure in mice lacking epidermal growth factor receptor.* Nature, 1995. **376**(6538): p. 337-41.

33. Threadgill, D.W., et al., *Targeted disruption of mouse EGF receptor: effect of genetic background on mutant phenotype.* Science, 1995. **269**(5221): p. 230-4.

34. Sibilia, M. and E.F. Wagner, *Strain-dependent epithelial defects in mice lacking the EGF receptor.* Science, 1995. **269**(5221): p. 234-8.

35. Jackson, L.F., et al., *Defective valvulogenesis in HB-EGF and TACE-null mice is associated with aberrant BMP signaling.* Embo J, 2003. **22**(11): p. 2704-16.

36. Chen, B., et al., *Mice mutant for Egfr and Shp2 have defective cardiac semilunar valvulogenesis.* Nat Genet, 2000. **24**(3): p. 296-9.

37. Howes, A.L., et al., *Galphaq expression activates EGFR and induces Akt mediated cardiomyocyte survival: dissociation from Galphaq mediated hypertrophy.* J Mol Cell Cardiol, 2006. **40**(5): p. 597-604.

38. Iwamoto, R., et al., *Heparin-binding EGF-like growth factor and ErbB signaling is essential for heart function.* Proc Natl Acad Sci U S A, 2003. **100**(6): p. 3221-6.

39. Luetteke, N.C., et al., *Targeted inactivation of the EGF and amphiregulin genes reveals distinct roles for EGF receptor ligands in mouse mammary gland development.* Development, 1999. **126**(12): p. 2739-50.

40. Troyer, K.L., et al., *Growth retardation, duodenal lesions, and aberrant ileum architecture in triple null mice lacking EGF, amphiregulin, and TGF-alpha.* Gastroenterology, 2001. **121**(1): p. 68-78.

41. Moorman, A., et al., *Development of the heart: (1) formation of the cardiac chambers and arterial trunks.* Heart, 2003. **89**(7): p. 806-14.

42. Wessels, A. and D. Sedmera, *Developmental anatomy of the heart: a tale of mice and man.* Physiol Genomics, 2003. **15**(3): p. 165-76.

43. Waller, B.F., et al., *Congenital hypoplasia of portions of both right and left ventricular myocardial walls. Clinical and necropsy observations in two patients with parchment heart syndrome.* Am J Cardiol, 1980. **46**(5): p. 885-91.

44. Hinton, R.B., Jr., et al., *Extracellular matrix remodeling and organization in developing and diseased aortic valves.* Circ Res, 2006. **98**(11): p. 1431-8.

45. Woldeyesus, M.T., et al., *Peripheral nervous system defects in erbB2 mutants following genetic rescue of heart development.* Genes Dev, 1999. **13**(19): p. 2538-48.

46. Tidcombe, H., et al., *Neural and mammary gland defects in ErbB4 knockout mice genetically rescued from embryonic lethality.* Proc Natl Acad Sci U S A, 2003. **100**(14): p. 8281-6.

47. Sliwkowski, M.X., et al., *Coexpression of erbB2 and erbB3 proteins reconstitutes a high affinity receptor for heregulin.* J Biol Chem, 1994. **269**(20): p. 14661-5.

48. Camenisch, T.D., et al., *Heart-valve mesenchyme formation is dependent on hyaluronan-augmented activation of ErbB2-ErbB3 receptors.* Nat Med, 2002. **8**(8): p. 850-5.

49. Rivera-Feliciano, J., et al., *Development of heart valves requires Gata4 expression in endothelial-derived cells.* Development, 2006. **133**(18): p. 3607-18.

50. Akiyama, H., et al., *Essential role of Sox9 in the pathway that controls formation of cardiac valves and septa.* Proc Natl Acad Sci U S A, 2004. **101**(17): p. 6502-7.

51. Goishi, K., et al., *Inhibition of zebrafish epidermal growth factor receptor activity results in cardiovascular defects.* Mech Dev, 2003. **120**(7): p. 811-22.

52. Nanba, D., et al., *Loss of HB-EGF in smooth muscle or endothelial cell lineages causes heart malformation.* Biochem Biophys Res Commun, 2006. **350**(2): p. 315-21.

53. Yamazaki, S., et al., *Mice with defects in HB-EGF ectodomain shedding show severe developmental abnormalities.* J Cell Biol, 2003. **163**(3): p. 469-75.

54. Grazette, L.P., et al., *Inhibition of ErbB2 causes mitochondrial dysfunction in cardiomyocytes: implications for herceptin-induced cardiomyopathy.* J Am Coll Cardiol, 2004. **44**(11): p. 2231-8.

55. Delot, E.C., *Control of endocardial cushion and cardiac valve maturation by BMP signaling pathways.* Mol Genet Metab, 2003. **80**(1-2): p. 27-35.

56. Tadano, M., et al., *Congenital semilunar valvulogenesis defect in mice deficient in phospholipase C epsilon.* Mol Cell Biol, 2005. **25**(6): p. 2191-9.

57. Zhao, Y.Y., et al., *Neuregulins promote survival and growth of cardiac myocytes. Persistence of ErbB2 and ErbB4 expression in neonatal and adult ventricular myocytes.* J Biol Chem, 1998. **273**(17): p. 10261-9.

58. Zhao, Y.Y., et al., *Neuregulin signaling in the heart. Dynamic targeting of erbB4 to caveolar microdomains in cardiac myocytes.* Circ Res, 1999. **84**(12): p. 1380-7.

59. Srinivasan, R., et al., *Expression of the c-erbB-4/HER4 protein and mRNA in normal human fetal and adult tissues and in a survey of nine solid tumour types.* J Pathol, 1998. **185**(3): p. 236-45.

60. Fuchs, I.B., et al., *Analysis of HER2 and HER4 in human myocardium to clarify the cardiotoxicity of trastuzumab (Herceptin).* Breast Cancer Res Treat, 2003. **82**(1): p. 23-8.

61. Uray, I.P., et al., *Left ventricular unloading alters receptor tyrosine kinase expression in the failing human heart.* J Heart Lung Transplant, 2002. **21**(7): p. 771-82.

62. Rohrbach, S., et al., *Neuregulin receptors erbB2 and erbB4 in failing human myocardium -- depressed expression and attenuated activation.* Basic Res Cardiol, 2005. **100**(3): p. 240-9.

63. Rohrbach, S., et al., *Neuregulin in cardiac hypertrophy in rats with aortic stenosis. Differential expression of erbB2 and erbB4 receptors.* Circulation, 1999. **100**(4): p. 407-12.

64. Liu, X., et al., *Neuregulin-1/erbB-activation improves cardiac function and survival in models of ischemic, dilated, and viral cardiomyopathy.* J Am Coll Cardiol, 2006. **48**(7): p. 1438-47.

65. Fukazawa, R., et al., *Neuregulin-1 protects ventricular myocytes from anthracycline-induced apoptosis via erbB4-dependent activation of PI3-kinase/Akt.* J Mol Cell Cardiol, 2003. **35**(12): p. 1473-9.

66. Schneider, J.W., A.Y. Chang, and T.P. Rocco, *Cardiotoxicity in signal transduction therapeutics: erbB2 antibodies and the heart.* Semin Oncol, 2001. **28**(5 Suppl 16): p. 18-26.

67. Pugatsch, T., et al., *Anti-erbB2 treatment induces cardiotoxicity by interfering with cell survival pathways.* Breast Cancer Res, 2006. **8**(4): p. R35.

68. Schneider, J.W., A.Y. Chang, and A. Garratt, *Trastuzumab cardiotoxicity: Speculations regarding pathophysiology and targets for further study.* Semin Oncol, 2002. **29**(3 Suppl 11): p. 22-8.

69. Ewer, M.S., et al., *Cardiotoxicity in patients receiving transtuzumab (Herceptin): primary toxicity, synergistic or sequential stress, or surveillance artifact?* Semin Oncol, 1999. **26**(4 Suppl 12): p. 96-101.

70. Schaller, G., et al., *Therapy of metastatic breast cancer with humanized antibodies against the HER2 receptor protein.* J Cancer Res Clin Oncol, 1999. **125**(8-9): p. 520-4.

71. Ozcelik, C., et al., *Conditional mutation of the ErbB2 (HER2) receptor in cardiomyocytes leads to dilated cardiomyopathy.* Proc Natl Acad Sci U S A, 2002. **99**(13): p. 8880-5.

72. Crone, S.A., et al., *ErbB2 is essential in the prevention of dilated cardiomyopathy.* Nat Med, 2002. **8**(5): p. 459-65.

73. Garcia-Rivello, H., et al., *Dilated cardiomyopathy in Erb-b4-deficient ventricular muscle.* Am J Physiol Heart Circ Physiol, 2005. **289**(3): p. H1153-60.

74. Liu, F.F., et al., *Heterozygous knockout of neuregulin-1 gene in mice exacerbates doxorubicin-induced heart failure.* Am J Physiol Heart Circ Physiol, 2005. **289**(2): p. H660-6.

75. Freedman, N.J. and G.S. Ginsburg, *Novel--and "neu"--therapeutic possibilities for heart failure.* J Am Coll Cardiol, 2006. **48**(7): p. 1448-50.

76. Zhai, P., et al., *An angiotensin II type 1 receptor mutant lacking epidermal growth factor receptor transactivation does not induce angiotensin II-mediated cardiac hypertrophy.* Circ Res, 2006. **99**(5): p. 528-36.

77. Chan, H.W., et al., *Effect of dominant-negative epidermal growth factor receptors on cardiomyocyte hypertrophy.* J Recept Signal Transduct Res, 2006. **26**(5-6): p. 659-77.

78. Chan, H.W., et al., *Tackling the EGFR in pathological tissue remodelling.* Pulm Pharmacol Ther, 2006. **19**(1): p. 74-8.

79. Pareja, M., et al., *Activated epidermal growth factor receptor (ErbB1) protects the heart against stress-induced injury in mice.* Am J Physiol Regul Integr Comp Physiol, 2003. **285**(2): p. R455-62.

80. Rabkin, S.W., *The effect of alteration of extracellular Na+ or Ca2+ and inhibition of Ca2+ entry, Na(+)-H+ exchange, and Na(+)-Ca2+ exchange by diltiazem, amiloride, and dichlorobenzamil on the response of cardiac cell aggregates to epidermal growth factor.* Exp Cell Res, 1990. **188**(2): p. 262-6.

81. Perrella, M.A., et al., *Regulation of heparin-binding epidermal growth factor-like growth factor mRNA levels by hypertrophic stimuli in neonatal and adult rat cardiac myocytes.* J Biol Chem, 1994. **269**(43): p. 27045-50.

82. Ushikoshi, H., et al., *Local overexpression of HB-EGF exacerbates remodeling following myocardial infarction by activating noncardiomyocytes.* Lab Invest, 2005. **85**(7): p. 862-73.

83. Clerk, A., et al., *Peptide growth factors signal differentially through protein kinase C to extracellular signal-regulated kinases in neonatal cardiomyocytes.* Cell Signal, 2006. **18**(2): p. 225-35.

84. Rabkin, S.W., *Indapamide accentuates cardiac chronotropic responses to epidermal growth factor in chick cardiomyocytes.* Tissue Cell, 1996. **28**(4): p. 469-72.

85. Sadoshima, J. and S. Izumo, *Molecular characterization of angiotensin II--induced hypertrophy of cardiac myocytes and hyperplasia of cardiac fibroblasts. Critical role of the AT1 receptor subtype.* Circ Res, 1993. **73**(3): p. 413-23.

86. Suzuki, T., et al., *Endothelin-1 stimulates hypertrophy and contractility of neonatal rat cardiac myocytes in a serum-free medium. II.* J Cardiovasc Pharmacol, 1991. **17 Suppl 7**: p. S182-6.

87. Neyses, L., et al., *Induction of immediate-early genes by angiotensin II and endothelin-1 in adult rat cardiomyocytes.* J Hypertens, 1993. **11**(9): p. 927-34.

88. Harada, M., et al., *Significance of ventricular myocytes and nonmyocytes interaction during cardiocyte hypertrophy: evidence for endothelin-1 as a paracrine hypertrophic factor from cardiac nonmyocytes.* Circulation, 1997. **96**(10): p. 3737-44.

89. Piacentini, L., et al., *Endothelin-1 stimulates cardiac fibroblast proliferation through activation of protein kinase C.* J Mol Cell Cardiol, 2000. **32**(4): p. 565-76.

90. Glembotski, C.C., et al., *Myocardial alpha-thrombin receptor activation induces hypertrophy and increases atrial natriuretic factor gene expression.* J Biol Chem, 1993. **268**(27): p. 20646-52.

91. Obreztchikova, M., et al., *Distinct signaling functions for Shc isoforms in the heart.* J Biol Chem, 2006. **281**(29): p. 20197-204.

92. Prenzel, N., et al., *EGF receptor transactivation by G-protein-coupled receptors requires metalloproteinase cleavage of proHB-EGF.* Nature, 1999. **402**(6764): p. 884-8.

93. Thomas, W.G., et al., *Adenoviral-directed expression of the type 1A angiotensin receptor promotes cardiomyocyte hypertrophy via transactivation of the epidermal growth factor receptor.* Circ Res, 2002. **90**(2): p. 135-42.

94. Asakura, M., et al., *Cardiac hypertrophy is inhibited by antagonism of ADAM12 processing of HB-EGF: metalloproteinase inhibitors as a new therapy.* Nat Med, 2002. **8**(1): p. 35-40.

95. Lorita, J., et al., *Effects of epidermal growth factor on epinephrine-stimulated heart function in rodents.* Am J Physiol Heart Circ Physiol, 2002. **283**(5): p. H1887-95.

96. Gilmore, A.P., et al., *Activation of BAD by therapeutic inhibition of epidermal growth factor receptor and transactivation by insulin-like growth factor receptor.* J Biol Chem, 2002. **277**(31): p. 27643-50.

97. Bernal, N.P., et al., *Epidermal growth factor receptor signaling regulates Bax and Bcl-w expression and apoptotic responses during intestinal adaptation in mice.* Gastroenterology, 2006. **130**(2): p. 412-23.

98. O'Brien, D.P., et al., *Selective inhibition of the epidermal growth factor receptor impairs intestinal adaptation after small bowel resection.* J Surg Res, 2002. **105**(1): p. 25-30.

99. Roberts, R.B., C.L. Arteaga, and D.W. Threadgill, *Modeling the cancer patient with genetically engineered mice: prediction of toxicity from molecule-targeted therapies.* Cancer Cell, 2004. **5**(2): p. 115-20.

100. Roberts, R.B., et al., *Importance of epidermal growth factor receptor signaling in establishment of adenomas and maintenance of carcinomas during intestinal tumorigenesis.* Proc Natl Acad Sci U S A, 2002. **99**(3): p. 1521-6.

101. Riethmacher, D., et al., *Severe neuropathies in mice with targeted mutations in the ErbB3 receptor.* Nature, 1997. **389**(6652): p. 725-30.

102. Luetteke, N.C., et al., *TGF alpha deficiency results in hair follicle and eye abnormalities in targeted and waved-1 mice.* Cell, 1993. **73**(2): p. 263-78.

103. Mine, N., R. Iwamoto, and E. Mekada, *HB-EGF promotes epithelial cell migration in eyelid development.* Development, 2005. **132**(19): p. 4317-26.

104. Lee, D., et al., *Epiregulin is not essential for development of intestinal tumors but is required for protection from intestinal damage.* Mol Cell Biol, 2004. **24**(20): p. 8907-16.

105. Britto, J.M., et al., *Generation and characterization of neuregulin-2-deficient mice.* Mol Cell Biol, 2004. **24**(18): p. 8221-6.

106. Horiuchi, K., et al., *Evaluation of the contributions of ADAMs 9, 12, 15, 17, and 19 to heart development and ectodomain shedding of neuregulins beta1 and beta2.* Dev Biol, 2005. **283**(2): p. 459-71.

107. Iwamoto, R. and E. Mekada, *ErbB and HB-EGF signaling in heart development and function.* Cell Struct Funct, 2006. **31**(1): p. 1-14.

108. Armstrong, E.J. and J. Bischoff, *Heart valve development: endothelial cell signaling and differentiation.* Circ Res, 2004. **95**(5): p. 459-70.

CHAPTER 2

CARDIAC RESPONSE TO PRESSURE OVERLOAD IN 129S1/SVIMJ AND C57BL/6J MICE: TEMPORAL AND BACKGROUND DEPENDENT DEVELOPMENT OF CONCENTRIC LEFT VENTRICULAR HYPERTROPHY

Abstract

Left ventricular hypertrophy (LVH), a risk factor for cardiovascular morbidity and mortality, is commonly caused by essential hypertension (EH). Three geometric patterns of LVH can be induced by hypertension: concentric remodeling, concentric hypertrophy, and eccentric hypertrophy. Clinical studies suggest that different underlying etiologies, genetic modifiers, and risk of mortality are associated with LVH geometric patterns. Since pressure-overload induced LVH can be modeled experimentally using transverse aortic constriction and since C57BL/6J (B6) and 129S1/SvImJ (129S1) strains, which have different baseline cardiovascular phenotypes, are commonly used, we conducted serial echocardiographic studies to assess cardiac function up to eight weeks post-TAC in male B6, 129S1, and B6129S1F_1 (F_1) mice. B6 mice had earlier onset and more pronounced impairment in contractile function, with corresponding LV and RV dilatation, fibrosis, change in expression of hypertrophy marker, and increased liver weights at five weeks post-TAC. These observations suggest that B6 mice had eccentric hypertrophy with systolic dysfunction and right-sided heart failure. By contrast, we found that 129S1 and F_1 mice delayed transition to decompensated heart failure, with 129S1 mice exhibiting preserved systolic function until eight weeks post-TAC, and relatively mild alterations in histology and markers of hypertrophy at five weeks post-surgery. Consistent with concentric hypertrophy, our results show that these strains manifest different cardiac responses to pressure overload in a time-

dependent manner and that genetic susceptibility to initial concentric hypertrophy is dominant to eccentric hypertrophy. These results also imply that genetic background differences can complicate interpretation of TAC studies when using mixed genetic backgrounds.

Introduction

Left ventricular hypertrophy (LVH), or increased LV mass, is associated with many cardiovascular disorders and is recognized as an independent risk factor for cardiac-related morbidity and mortality [1-6]. Although it can be associated with mechanical stress, growth factors, catecholamines, cytokines and primary genetic abnormalities, a principle determinant of LVH is systemic hypertension. Of the nearly one in three adult Americans who have essential hypertension (EH), 20-60% will have evidence of LVH [7]. Moreover, the beneficial effects of reversing LVH with anti-hypertensive therapy have been well documented in clinical trials [8-10].

Three patterns of LVH are observed in patients with EH and can be classified according to LV mass index (LVMI) and relative wall thickness (RWT, or ratio of diastolic LV posterior wall thickness to LV chamber cavity radius): concentric hypertrophy, characterized by an increase in both LVMI and RWT, eccentric hypertrophy, characterized by an increase in LVMI with normal RWT, and concentric remodeling, characterized by normal LVMI in the setting of an increased RWT. Additionally, some individuals maintain normal LV geometry in the face of EH [11]. The geometric pattern of LVH appears to be closely related to LV function and patient prognosis, and may be a better predictor of outcome than traditional cardiovascular risk factors [12, 13]. LV geometry and LV mass are highly variable among patients with comparable systolic blood pressure, environmental and other known predisposing factors, suggesting a significant heritable susceptibility to specific geometric patterns of LVH. Recent estimates

attribute as much as 60% of the blood pressure (BP)-independent variation in cardiac mass to genetic factors; moreover, a significant correlation exists between adjusted relative risk for concentric LVH and elevated LVMI with race and ethnic background, suggesting the presence of genetic modifiers conferring differential susceptibility to pressure-overload induced LV remodeling and LVH [14-18]. Recent studies identifying polymorphisms in genes encoding ghrelin, angiotensin converting enzyme, bradykinin B2 receptor, and in genes involved with carnitine transport as candidate modifiers of LV remodeling and LVM, further support a strong genetic link [19-26].

Surgical transverse aortic constriction [27] in mice causes chronic LV pressure overload, progressive LVH remodeling and subsequent cardiac failure, providing an experimental model for human cardiac response to systemic hypertension [28-31]. Since its development, the TAC model has been used extensively on genetically engineered mice to investigate the role of specific genes during the development of LVH and cardiac failure *in vivo*. However, there is considerable variation in the degree of hypertrophy, LV geometry, and time to heart failure in this experimental model [32]. Since many studies use engineered mouse models maintained on outbred or mixed genetic backgrounds, genetic variability may contribute to observed phenotypic variability [27, 33-35], including cardiac response to TAC.

C57BL/6J (B6) and 129S1/SvImJ (129S1) inbred mouse strains are some of the most widely used strains to generate genetically engineered mice [36-38], with many subsequent analyses being done on a mixed B6 and 129 genetic background. Since B6 and 129S1 mice have different baseline cardiovascular phenotypes [39, 40] and dissimilar response to various cardiovascular stressors [41, 42], it is likely that varied combinations of B6 and 129S1 alleles will cause divergent cardiac responses to chronic pressure overload.

Although several studies have investigated the B6 response to TAC, no comparative studies exist using 129S1 and B6129S1F_1 (F_1) mice. Because of the strain-based variation in baseline cardiac phenotypes, we hypothesized that the cardiac response to TAC would also vary by genetic background, and that strain-specific genetic modifiers may be a source of variability in previous studies on LVH, LV geometry, and cardiac failure. Furthermore, inter-strain variability in response to TAC may provide experimental models for different geometric patterns of LVH response to hypertension observed in humans. Therefore to identify potential strain-specific differences in response to TAC, we quantified the effects of pressure overload induced by TAC on cardiac morphology, histology, hypertrophy-associated gene expression, and LV function in B6, 129S1 and F_1 male mice. We found these strains manifest very different cardiac responses to pressure overload, suggesting that genetic background modifiers are important determinants of the response to pressure overload, possibly complicating interpretation of TAC studies using genetically-engineered mice on mixed genetic backgrounds. Our results also identify the 129S1 strain as a model for concentric LVH and indicate that concentric LVH is dominant to the eccentric LVH observed in B6 mice. These models will be useful in determining how similar cardiac insults can result in very different responses among individuals and for the identification of therapeutic strategies for specific geometric patterns of LVH. The results also emphasize the importance of using proper genetic controls for studies investigating gene function using engineered mouse model

Materials and Methods

Animals. Mice were obtained from The Jackson Laboratory (Bar Harbor, ME). Ten-week old 129S1/SvImJ (129S1), C57BL/6J (B6), and B6129S1F_1 (F_1) males were acclimated to the local environment for one week, which included housing in ventilated cages with HEPA-filtered air and Purina 5058 rodent chow provided *ad libitum*.

Aortic banding. Pressure overload of the left ventricle was induced by transverse aortic constriction [27] of nine mice each from B6, 129S1, and F_1 genetic backgrounds, as described [29]. The aorta was ligated between the innominate and left common carotid arteries by tying a 7-0 silk suture around a tapered 27-gauge needle placed on top of the aorta. 33The tapered needle was removed, leaving the suture to produce a defined stenosis of the vessel. The skin was closed with separate sutures (6-0 silk) and buprenorphine was administered for analgesia. To estimate the load produced by TAC, Doppler velocities were measured in the right and left carotid arteries before and after ligation using a hand-held 20 mHz Doppler probe (Indus Instruments, Houston, Texas). Work by others has demonstrated that the RCA/LCA peak velocity ratio significantly correlates with heart weight after TAC and with peak jet across the banding site and can thus be used to estimate the pressure drop across the banding site (24). Peak systolic gradients post-TAC were similar among the genetic backgrounds (44±10 mmHg, B6 versus 40±12 mmHg, F_1 versus 48 ±12 mmHg, 129S1). Six mice of each genetic background received a sham operation in which the aortic arch was isolated and a band was twined around the aorta, but not ligated, and subsequently removed. Surgery was also performed on a smaller cohort of mice from each genetic background (n = 2-3 sham, 3-5 TAC) to assess cardiac function past eight weeks.

Echocardiography. Transthoracic echocardiography (TTE) was performed at baseline and at

five weeks post-TAC using a 30 mHz probe and the Vevo 660 Ultrasonograph (VisualSonics, Toronto, Canada). Mice were lightly anaesthetized with 1-1.5% isofluorane, maintaining heart rate at 400-450 beats per minute, and a topical depilatory agent applied, before placing in the left lateral decubitus position under a heat lamp to maintain body temperature at 37°C. The heart was imaged in the 2D mode in the parasternal long-axis view. From this view, an M-mode cursor was positioned perpendicular to the interventricular septum and posterior wall of the LV at the level of the papillary muscles. Diastolic and systolic LV wall thickness, LV end-diastolic dimensions (LVDD), and LV end-systolic chamber dimensions (LVSD) were measured. All measurements were done from leading edge to leading edge according to the American Society of Echocardiography guidelines [43]. Two dimensional short and long axis views of the left ventricle were obtained. M-mode tracings were recorded and used to determine LV end-diastolic diameter (LVED,d), LV end systolic diameter (LVED,s), LV posterior wall thickness diastole (LVPWTh,d), and LV posterior wall thickness systole (LVPWTh,s), over three cardiac cycles. LV fractional shortening was calculated using the formula % FS= (LVED,d-LVED,s)/(LVED,d). LV mass was calculated according to uncorrected cube assumptions with some modifications using the equation:

LV mass [44] = $1.055[(\text{LVED,d} + \text{LVPWTh,d} + \text{LVIVSTh, d})^3 - (\text{LVED,d})^3]$ [45], where 1.055 is the gravity of myocardium, LVPWTh,d is diastolic posterior wall thickness, and LVIVSTh,d is diastolic ventricular septal thickness. Stroke volume [46] was estimated by the formula $SV=(LV_{\text{volume d}} - LV_{\text{volume,s}})$, and was multiplied by mean HR to estimate cardiac output (CO). Percent ejection fraction (%EF) was calculated using the formula $\%EF= (LV_{\text{volume, d}} - LV_{\text{volume s}})/(LV_{\text{volume d}})$. Relative wall thickness (RWT) was approximated using the

formula RWT=(LVPWTh,d+LVIVSTh,d)/(LVED,d), where LVIVSTh,d indicates diastolic intraventricular septal wall thickness. Serial TTE under anesthesia was performed on a smaller cohort of mice at additional time points (0, 2, 4, 5, 6, and 8 weeks post-surgery; n = 2-3 sham, 3-5 TAC). Conscious TTE was also performed on a smaller cohort of mice (n = 3 sham, 5 TAC) at 5 weeks post-TAC. All measurements were made by an independent observer with no knowledge of treatment or genetic background.

Histology. Mice were weighed, and hearts, lungs, liver, and kidneys were dissected five weeks after TAC (n = 6) or sham surgery (n = 4) from mice of each genetic background, rinsed in PBS and weighed. Hearts were cut in cross-section just below the level of the papillary muscle. The top half of the heart was formalin-fixed and embedded in paraffin. Sections (5 μm) were prepared at 200 μm intervals. The sections were stained with hematoxylin and eosin (H&E) for examination of gross appearance, while Masson's Trichrome [47] or Periodic Acid-Schiff (PAS-H) counterstained with hematoxylin (PAS-H) was employed in order to facilitate quantification of fibrosis and cardiomyocyte size, respectively. Cardiomyocyte hypertrophy was assessed by measuring cross-sectional area of 100 cardiomyocytes per PAS-H stained section in ten randomly selected fields having nearly circular capillary profiles and centered nuclei in the left ventricular free wall. Cardiac fibrosis was determined by calculating the percent of MT stained area of interstitial fibrosis per total area of cardiac tissue. Inflammatory cells were detected using the pan rat anti-mouse monoclonal IgG macrophage/monocyte marker MCA519G (clone number MOMA-2) (Accurate Chemical, Westbury, New York) followed by biotinylated goat anti-rat IgG (Jackson ImmunoResearch, West Grove, Pennsylvania) with visualization using the ABC Elite kit (Vector, Burlingame, California). Positively stained cells per cross-section were

manually counted in three sections per heart. Histological images were analyzed using Nova Prime 6.75.10 software (BioQuant Image Analysis, San Diego, California). Blinded measurements were made by two independent observers.

Gene expression. Total RNA was extracted from the lower half of the LV using TRIzol (Invitrogen, Carlsbad, California). After DNAse treatment, 500 ng of total RNA was reverse transcribed using the High Capacity cDNA Archive Kit (Applied Biosystems, Foster City , California). The expression of α-myosin heavy chain (*Myh6*), β-myosin heavy chain (*Myh7*), atrial nautriuretic peptide (*Nppa*), brain nautriuretic peptide (*Nppb*), and medium chain acyl dehydrogenase (*Acadm*) was determined by real-time quantitaive PCR (qPCR) using Taqman Univeral Master Mix and Assays-on Demand primers and probes (Applied Biosystems, Foster City, California). β-actin (*Actb*) was used as an internal control for the results presented here; similar results were obtained using beta glucuronidase, (*Gusb*) as an internal control. There were no significant differences by genetic background or treatment in *Actb* expression levels. Reactions were run on a Stratagene MX3000P machine with analysis software. Threshold cycles [48] were determined by an in-program algorithm assigning a fluorescence baseline based on readings prior to exponential amplification. Fold change in expression was calculated using the $2^{-\Delta\Delta CT}$ method [49] using *Actb* as the endogenous control. Results are represented as mean fold changes relative to B6 sham LV expression.

Statistical analysis. All results were expressed as mean ± standard error of the mean [50]. Statistical analysis was performed using Statview version 5 (SAS Institute, Cary, North Carolina). The Kolmogorov-Smirnov test was used to test for normal distribution. Statistical significance within genetic backgrounds was determined using the two-tailed unpaired Student's t-test or nonparametric Mann-Whitney test, while a two-way ANOVA or the

Kruskal-Wallis test was used to determine statistical significance within treatment groups. A *p*-value of less than 0.05 was considered significant.

Results

Previous studies suggest that many cardiovascular phenotypes vary by genetic background. Consequently, strain-specific genetic modifiers may have been a source of variability in previous studies using engineered models of LVH, LV geometry, and cardiac failure. To evaluate and characterize genetic background-specific responses, the effects of pressure overload induced by TAC were used to identify experimental models for different geometric patterns of LVH response to hypertension that is observed in humans.

Baseline strain-specific differences in cardiovascular phenotypes. Sham treated B6 and 129S1 control mice had natural baseline variation in cardiac morphology (Figure 2-1, A-D). Sections taken through the hearts showed that B6 hearts were rounded at the apex, with a larger LV diameter, while 129S1 hearts were longer and narrower with a thicker septal wall and with a smaller LV diameter. Histologic analysis indicated that the 129S1 hearts had more tightly packed cardiomyocytes in the septal and free LV wall (Figure 2-1, B compared to D). The hearts of F_1 sham mice were similar to those of 129S1 mice in morphology and cardiomyocyte density (data not shown).

These baseline differences among the strains were also observed by transthoracic echocardiography (TTE). 129S1 mice had the smallest left ventricular end diastolic diameter (LVED,d) and left ventricular end systolic diameter (LVED,s), but longer LV length than B6 mice (Figure 2-1G and Table 2-1). Baseline calculated values of percent fractional shortening [51] and percent ejection fraction (%EF) were significantly lower in F_1 mice

compared to 129S1 and B6 mice, while LVvol, d and LVvol, s were smaller in 129S1 mice compared to B6 and F_1 mice suggesting intrinsic strain-dependent variation in cardiac contractility and left ventricular geometry (Table 2-1 and Table 2-2).

Differences in body and organ weights across the strains were also observed (Table 2-3). 129S1 sham mice were lighter, and had smaller wet organ weights compared to B6 and F_1 mice. However when normalized to body weight, there was no significant difference in organ weights by genetic background. There was also no significant difference in mean aortic diameter measured at the level of the aortic root at systole or diastole by genetic background at baseline. As previously reported, 129S1 mice had higher systolic blood pressures as compared to B6 mice (122 ± 5 mmHg versus 116 ± 3 mmHg; Table 2-4).

Pressure overload induces strain-specific differences in cardiac function. Because it is possible that baseline differences could impact cardiovascular pathophysiological responses, we subjected B6, 129S1 and F_1 hybrid mice to TAC to identify strain-dependent cardiac responses to elevated pressure overload (Figure 2-1E and F). No significant differences in heart rate were detected at baseline or after treatment or by genetic background. Following TAC, peak systolic gradients across the left and right carotid arteries were similar in B6, F_1, and 129S1 mice (43.5 ± 10, 40± 12, and 48 ±12 mmHg, respectively), indicating a similar initial pressure gradient. Approximately 20% of B6 mice died between one-to-three weeks post-TAC, similar to published mortality rates for this strain, with only 40% of B6 TAC mice surviving to eight weeks post-surgery [31]. No mortality occurred in 129S1, F_1, or sham mice followed up to eight weeks post-TAC.

To determine whether the increased mortality in B6 mice could reflect more severe LV dysfunction, changes in LV geometry and function were non-invasively measured by

TTE. Five weeks post-TAC, B6 mice had LV chamber dilatation, reduced %FS, and reduced %EF, with no significant change in RWT as compared to sham B6 mice (Table 2-1), consistent with eccentric hypertrophy and depressed systolic function. Both 129S1 and F_1 mice developed concentric hypertrophy five weeks post-TAC, as marked by significantly reduced chamber size, increased wall thickness, increased RWT, and increased %FS and %EF compared to controls (Table 2-1 and 2-2). Although LV wall posterior wall thickness (LVPWTh) increased in all three genetic backgrounds with chronic pressure overload, 129S1 TAC mice manifested the greatest percent increase in LVPWTh compared to sham-operated controls (Table 2-1). In contrast, calculated LV mass also increased in all TAC mice compared to sham-operated mice, but a significantly greater increase was observed in B6 TAC mice compared to other genetic backgrounds (% increase LV mass over baseline 89.9±14.9, B6 versus 66.3±16.3, F_1 versus 56.1±7.1, 129S1; $p < 0.05$). Sections taken through the hearts confirmed that B6 TAC mice developed a dilated cardiomyopathy with RV enlargement, whereas 129S1 TAC mice had concentric hypertrophy (Figure 2-1, E and F). Interestingly, measurements of mean aortic diameter proximal to the constriction site taken five weeks post-surgery were significantly greater in B6 TAC mice compared to shams as well as compared to F_1 and 129S1 TAC mice, suggesting possible strain differences in the aortic response to load (Table 2-2).

Initial assessment of LV geometry and function by TTE was performed on mice anethestized with inhaled isoflurane, which in published studies has been found to have mild effects on cardiac function and has been proposed to be the best anesthetic for repeated measurement in the same animal [52-57]. To exclude the possibility that differences we were observing in the cardiac geometry and function in B6, F_1, and 129S1 mice by TTE could be

ascribed to differential strain susceptibility to anesthesia, we performed conscious echocardiographic and compared the results to those obtained under isoflurane. TTE on conscious mice yielded similar patterns to those observed with isoflurane anesthetized animals with 129S1 and F_1 TAC mice having reduced LVED,d, LVED,s and increased %FS and %EF consistent with concentric hypertrophy, while B6 TAC mice had increased LVED,d, LVED,s and reduced %FS and %EF consistent with LV dilatation (Table 2-5).

Five weeks post-TAC, significant strain differences were observed in body weight (BW), organ weights and organ:BW ratios (Table 2-3). Pressure overload significantly increased heart weight (HW), and HW:BW on all three genetic backgrounds relative to controls. However, wet lung weight and Lu:BW were significantly increased in F_1 and 129S1 TAC mice ($p < 0.02$ versus shams), while wet liver weight (LiW) was significantly higher in TAC B6 mice ($p < 0.03$ versus shams), but when corrected for BW did not reach significance ($p < 0.06$ versus shams). There were no differences in wet kidney weight (KiW) or Ki:BW between banded and sham mice (data not shown). When wet organ weights were expressed as percent increase over sham mice, B6 TAC mice had the largest relative increase in HW and LiW whereas 129S1 mice had the largest relative increase in LuW. Since B6 mice also have evidence of RV dilatation (Figure 2-1, E) it is likely they manifest passive liver congestion and right-sided heart failure in response to chronic pressure overload, whereas 129S1 mice have significant pulmonary congestion.

B6 mice have heightened cellular responses to pressure overload. Cardiomyocyte hypertrophy was assessed by histomorphometry in mice from all three genetic backgrounds. Changes in cardiomyocyte size varied with background, approximately doubling in B6 TAC hearts, while only increasing 1.6 fold in F_1 TAC hearts and 1.3-fold in 129S1 TAC hearts

relative to sham controls (Figure 2-2, A). Within the TAC group, B6 cardiomyocytes had the largest cross-sectional area (Figure 2-2, B and C).

The hypertrophic response to pathological stimuli often involves fibrosis [58]. Quantitative analysis of Masson's Trichrome stained sections, in which collagen stains a bright blue color, indicated increased interstitial fibrosis (IS) in B6 and 129S1 TAC mice compared to shams (Figure 2-3, A). B6 TAC mice had significantly greater IS fibrosis than respective TAC mice on other genetic backgrounds (Figure 2-3, C and E). Additionally, only B6 TAC mice tended to have extensive perivascular fibrosis (Figure 2-3, B and D). B6 TAC mice also had inflammatory infiltrate found in regions of fibrosis (Figure 2-4, A). Comparably fewer inflammatory cells were detected in the hearts of sham mice on all genetic backgrounds as well as F_1 and 129S1 TAC mice (Figure 2-4, C), and were not associated with fibrosis (Figure 2-4, B).

Strain-specific hypertrophic response is supported by expression of molecular markers. Pressure overload and other cardiac stressors typically initiate induction of the fetal hypertrophic gene program, which is associated with pathological ventricular remodeling [59]. The expression of atrial natriuretic peptide (*Nppa*/ANP), brain natriuretic peptide (*Nppa*/BNP), medium chain acyl dehydrogenase (*Acadm*/MCAD), α-myosin heavy chain (*Myh6*/α–MHC) and β-myosin heavy chain (*Myh7*/β-MHC), signature markers for cardiac hypertrophy, was measured by qPCR using LV total RNA (Figure 2-5). The re-expression of ventricular *Nppb* and *Nppa*, both cardioprotective hormones, is recognized as a marker for the induction of the embryonic gene program in ventricular hypertrophy [60]. Although *Nppa* and *Nppb* expression was elevated in the LV of mice on all backgrounds after TAC relative to sham-treated mice of the same background, only LV from B6 and F_1 mice showed

significant changes (Figure 2-5, A and B). Interestingly, B6 mice (both sham and TAC) had nearly 3-fold greater *Nppb* LV expression in the LV as compared to F_1 and 129S1 mice in respective treatment groups.

In failing mouse and human hearts, a shift in myosin heavy chain isoform expression from the adult form (*Myh6*) to the fetal form (*Myh7*) can occur, and a change in the ratio of these isoforms is associated with pathological hypertrophy. Pressure overload of C57BL/6J X SJL/J mice was previously reported to suppress expression of *Myh6* by more than 50% after ten weeks of banding [61]. We also found decreased *Myh6* expression (by approximately 75%) while *Mhy7* expression was dramatically increased in B6 TAC LVs compared to controls (Figure 2-5, C and D). Milder alterations in the expression of these markers were also observed in F_1 mice. Additionally, within the TAC cohort, B6 mice had significantly lower *Myh6* expression and higher *Myh7* expression than F_1 and 129S1 mice ($p < 0.05$).

During the transition to heart failure, the chief myocardial energy source switches from fatty acid beta-oxidation to glycolysis indicating a reversion to the fetal energy substrate preference pattern. Expression of *Acadm*, coding for a rate limiting fatty acid beta-oxidation enzyme, is reported to be down-regulated during the progression from cardiac hypertrophy to failure [62]. Consistent with this expression, *Acadm* expression was significantly decreased in B6 TAC mice compared to shams as well as compared to other TAC mice (Figure 2-5 E; $p < 0.05$). Together with echocardiographic data, altered gene expression of these markers may reflect a transition in the B6 mice to decompensated heart failure.

129S1 genetic modifiers delay transition to decompensated heart failure. To determine if the 129S1 mice would eventually progress to an eccentric, decompensated phenotype,

cardiac geometry and function was assessed serially by TTE for up to eight weeks post-TAC in all three strains (n = 3-4 TAC, 2-3 sham; Figure 2-6 A-E). By week eight post-surgery, LVED,d, LVED,s and LV posterior wall thickness were significantly increased and %FS was significantly decreased in all TAC mice relative to respective sham controls, demonstrating that pressure overload ultimately leads to dilatation and decreased systolic function irrespective of genetic background. However, there was both a blunting and a temporal delay in transition to decompensated heart failure in 129S1 and F_1 mice. Interestingly, both the 129S1 and the B6 mice went through an initial stage characterized by pronounced concentric hypertrophy. In contrast the B6 TAC mice developed characteristics of decompensated heart failure by five weeks; the F_1 and 129S1 TAC mice did not have significant evidence of LV dilation or systolic dysfunction until week six and eight weeks post-TAC, respectively. Even after eight weeks, surviving B6 TAC mice retained the largest percent increase in LV diameter and greatest reduction in %FS relative to baseline values. Together, this data suggests that the 129S1 strain harbors protective genetic modifers that enables prolonged compensation to chronic pressure overload.

Discussion

B6 and 129 strains are known to differ in baseline cardiovascular phenotypes such as blood pressure, morphological traits (*i.e.* atrial and ventricular size), heart rate variability, and cardiac metabolism, as well as in cardiac response to stressors [39-42]. Extending these findings, we present evidence that B6, and 129S1 mice manifest different cardiac phenotypes in response to TAC; moreover, genetic background influences the ability to maintain cardiac function in the face of prolonged cardiac stress as modeled by TAC-induced pressure overload.

While B6 and 129S1 genetic backgrounds have a hypertrophic response, as indicated by increased heart weight and cardiomyocyte area over controls, they differ significantly in LV function over time, LVH geometric pattern and pathological LV remodeling. By five weeks post-surgery, B6 TAC mice have depressed contractile function, LV dilatation proportional to LV wall thickness, extensive fibrosis associated with inflammatory infiltrate, and significantly altered expression of classic hypertrophy markers. B6 mice also have the largest increase in liver weights and RV dilatation, suggesting passive liver congestion. Collectively, these observations suggest that B6 mice have LV remodeling consistent with eccentric hypertrophy (heart mass increases, but RWT does not change), accompanied by systolic dysfunction and right-sided heart failure. Although 129S1 TAC mice eventually progress to a "decompensated" phenotype, this transition is significantly delayed compared to B6 TAC mice. At five weeks post-surgery, 129S1 mice have a phenotype characteristic of concentric hypertrophy in response to TAC, with increased cardiac mass, RWT, and decreased LVED,d. Systolic function, estimated by FS and EF is also enhanced, evidence of an increased contractile status, while CO is significantly decreased, probably due to reduced LV chamber size and stroke volume. Additionally, 129S1 mice have more pronounced increases in lung volumes after pressure overload suggesting pulmonary congestion, possibly due to elevated LVED pressure. These findings are consistent of clinical features observed in patients with diastolic dysfunction in the setting of concentric LVH. In response to TAC, F_1 mice have a cardiac phenotype intermediate to B6 and 129S1 parental strains in many parameters, but appear to be protected from early systolic dysfunction and cardiac fibrosis, responding similarly to parental 129S1 mice. This result implies that 129S1 genetic modifiers may protect against the more severe pathologic changes seen in the hearts of B6 mice in

response to TAC at earlier timepoints as well as delay transition to decompensated heart failure. This protective effect is significant, as, when all studies were combined, approximately 20% of all B6 TAC mice died by three weeks post-TAC, with approximately 60% dying by eight weeks post-TAC. By contrast, no mortality was observed in 129S1 or F_1 TAC mice.

Our echocardiographic and morphologic data are comparable to prior studies investigating B6 response to pressure overload at similar time points [31, 61, 63]. Less data is available for 129S1 mice, and no studies have reported a direct comparison between these widely used strains. Schmitt et al. [50] performed TAC on wild-type 129SvEv mice (substrain not specified) as controls for co-isogenic mice carrying a mutation in alpha cardiac myosin heavy chain ($Myh^{403/+}$). Interestingly, they report that TAC-treated 129SvEv mice had significantly thickened LV walls, reduced LV diameter, and were able to maintain normal contractile function for over 30 weeks post-banding [50]. Data from our lab and others demonstrate that, compared to B6 mice, 129S1 mice have a higher baseline systolic pressure at baseline and in response to cardiovascular stressors [39, 64-66]. Although there are no publications directly comparing B6 to 129S1 blood pressure response after TAC, comparison of independently published values suggest that 129SvEv mice likely continue to maintain higher systolic pressures than B6 post-TAC (10, 22). Thus, 129S1 TAC mice chronically maintain systolic function despite slightly higher afterload than B6 TAC mice.

Our data, together with reports in the literature, consistently indicates that the B6 and 129S1 strains differ greatly in their ability to adapt to acute pressure overload. As many TAC studies use transgenic mice that have not been backcrossed to congenicity, it is possible that a combination of B6 and 129S1 modifiers would influence the response to pressure overload,

contributing to variability. Thus, the significance of an individual gene effect on pressure-overload induced LVH and remodeling could be masked or diluted by unidentified genetic modifiers in studies that do not adequately control for genetic background. Moreover, many published studies examine the cardiac response to TAC from four-to-six weeks post-surgery, timepoints where our studies would predict there would be more pronounced differences in response.

We also found significant differences in gene expression, fibrosis, organ weights and cardiac morphology among control, sham-treated mice, underscoring the inherent cardiovascular differences of the parental strains. Similarly, the phenotype of transgenic mice overexpressing the sarcoplasmic reticulum Ca^{2+}-binding protein calsequestrin (*Casq1*) are highly strain-specific, showing wide variability when mice carrying the transgene are crossed to different inbred mouse strains [67-70]. In contrast to our results using the TAC model, which showed a dominant 129S1 modifier protecting against dilated cardiomyopathy, reciprocal backcrosses between DBA/2 and B6 mice revealed that the B6 background contributes a dominant susceptibility allele to the cardiomyopathic phenotype in the *Casq1* transgene model, leading to dramatically reduced survival. Thus, the same genetic insult may be significantly modified by genetic background, leading to variable cardiovascular compensation, even in the absence of additional stimuli.

Clinical studies suggest that screening for LVH geometric pattern in patients with EH may have prognostic value in stratifying patients based on CV risk. Yet, relatively little is known about the natural history of LV geometric remodeling in human hypertension; for example, whether the remodeling patterns are temporal stages in the development of the hypertensive heart from normal geometry through compensated hypertrophy to dilation and

heart failure or if every pattern is genetically or hemodynamically predisposed. A recent study followed changes in LVM and LV geometry in 100 hypertensive patients for five years and concluded that LV geometry is a rather conservative entity, as transformation from one pattern to another was rarely observed, even in untreated hypertensive patients. In particular, concentric LVH was fairly stable, without transformation to dilatation over the course of the study; however, the development of eccentric hypertrophy in patients with normal baseline geometry was observed [71]. This suggests that independent determinants of LV geometry exist despite similar arterial hypertension.

In light of the unique patterns of LV remodeling in humans, continued exploration and comparison of inbred strain-specific responses to pressure overload will lead to better pre-clinical models for partitioning LVH by LV geometry. These mouse models will provide tools to investigate changes in LV remodeling and LV geometry over time, to decipher genetic networks that may contribute to different LV geometric patterns, and to compare benefits of pharmaceutical intervention based on LV geometry subtype. It is now clear that similar genes and signaling pathways regulate the development of the heart and vasculature, as well as cardiovascular response to stressors, in mice and humans. Molecular genetics will play an important role in discovering novel methods of diagnosing and treating patients with cardiovascular diseases [2, 28, 37], and mouse models for defined subsets of patients will be essential for pre-clinical therapeutic studies. Ultimately, these studies will contribute to understanding why some patients with chronic pressure overload manifest concentric LVH whereas others progress to LV dilatation and systolic dysfunction.

As exemplified in our studies, the selection of appropriate genetic background controls is essential when performing gene function studies using engineered mouse models

to study response to TAC to ensure interpretable results. Although the vast majority of mutations are produced in 129 embryonic stem cells before generating chimeras, the resulting chimeras are typically bred to B6 mice to produce F_1 hybrids followed by intercrossing of the offspring to generate homozygous mutants on a mixed B6 and 129 genetic backgrounds for analysis. Frequently, viable homozygous mutant mice are maintained as closed colonies for study. Our results show that F_1 hybrids from B6 and 129S1 are not appropriate controls for either these experiments since the F_1 response to TAC will not reflect either the B6 or 129 strains. If mutations are maintained as a closed breeding colony, there are no appropriate controls for genetic background since the composition of the background will be variable and unpredictable, and the genetic background effects described here may incorrectly be associated with the mutation under study. Rather, the only adequate controls are littermates with an equivalently random distribution of the B6 and 129 genomes. However, because of the strong genetic background influence on response to TAC-induced pressure overload, significantly larger groups of mice will be required due to high intra-group variation.

Figure 2-1. B6 and 129S1 male mice have innate differences in cardiac morphology. (A-F) Representative H&E staining of cardiac sections from B6 and 129S1 sham (A-C) and TAC (E and F) heart five weeks post-surgery (A,C, E and F, magnification, 1.6x; B and D, magnification, 10x. Bar = 100μm). (G) Representative M-mode tracings taken from the short-axis five-weeks post surgery from B6 and 129S1 mice. LVED,d, LV end diastolic diameter, LVED,s, LV end systolic diameter, LVPWTh, d, LV posterior wall thickness diastole, LVPWTh,s , LV posterior wall thickness systole.

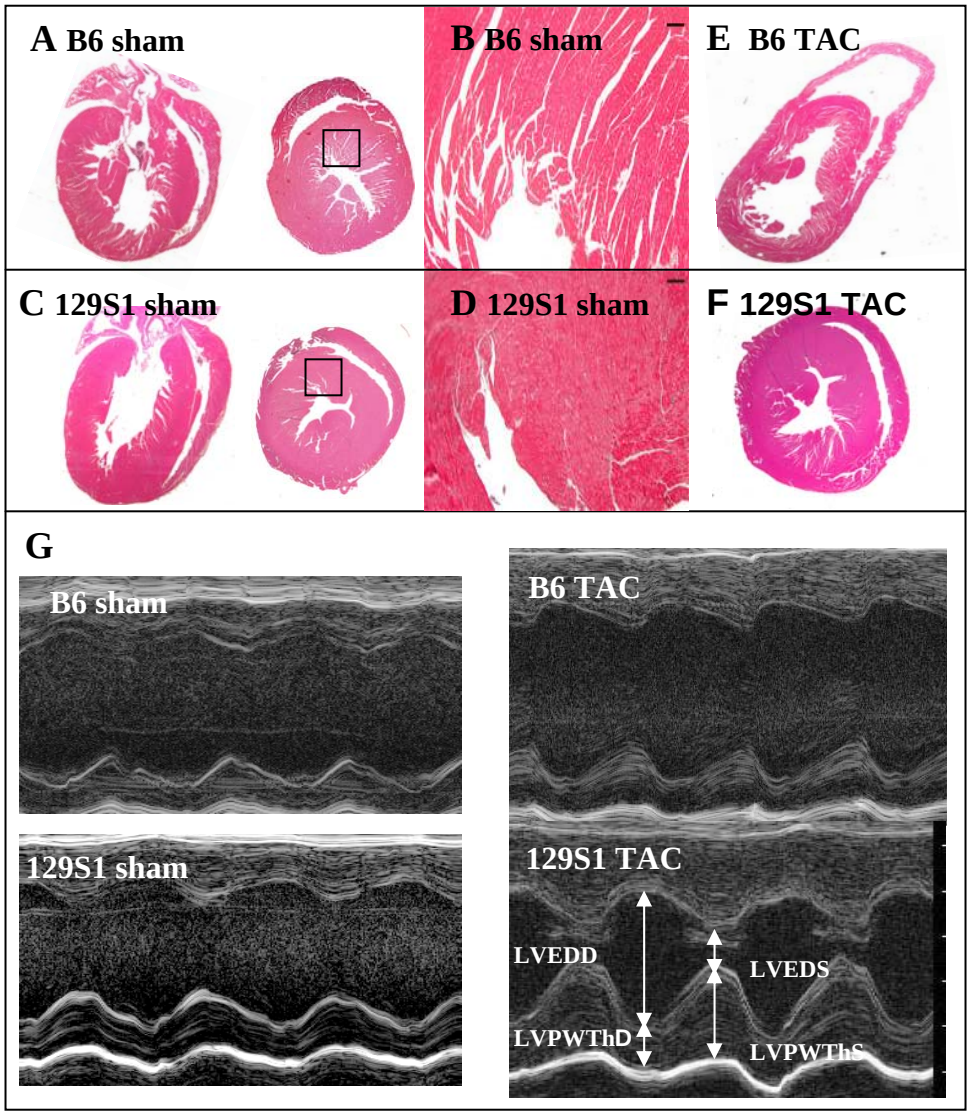

Table 2-1. Echocardiographic analysis in baseline, sham, and banded mice. LVED,d, LV end diastolic diameter; LVED, s, LV end systolic diameter; LVPWTh, d, LV posterior wall thickness diastole; LVPWTh, s, LV posterior wall thickness systole; FS, fractional shortening; RWT, relative wall thickness, LV vol, d; diastolic LV volume, LV vol, s; systolic LV volume, SV; stroke volume, AoD, d; diastolic aortic diameter, AoD, s; systolic aortic diameter, LV length, d; diastolic LV length P-values are shown from comparisons between strains using the non-parametric Kruskal-Wallis test. Echocardiographic measurements are represented as average ± SEM. *$p < 0.05$ vs F1 mice; $^{d}p < 0.01$ vs F_1 mice.

Treatment:		**Baseline**			**SHAM**			**TAC**	
Genetic Background:	B6	F_1	129S1	B6	F_1	129S1	B6	F_1	129
N	15	15	15	6	6	6	9	9	9
HR (BPM)	487.09±10	451±15	482±11	495±16	473±10	448±15	509±18	473±13	460±16
LVED,d(mm)	3.80±0.07	3.80±0.06^{b}	3.56±0.05^{b,d}	3.85±0.10	3.95±0.10	3.53±0.12	4.11±0.13	3.48±0.09^{a}**	2.87±0.23^{b,d}**
LVEDS(mm)	2.27±0.09	2.51±0.07^{a}	1.98±0.05^{a,d}	2.24±0.08	2.42±0.17	2.05±0.19	2.85±0.14**	1.78±0.15^{a}*	1.06±0.15^{b,c}*
LVPWTh, d(mm)	0.62±0.03	0.72±0.06	0.65±0.03	0.62±0.04	0.76±0.10	0.71±0.07	0.85±0.07*	0.97±0.13	1.06±0.09^{c}
LVPWTh, s(mm)	1.11±0.05	0.82±0.06	0.98±0.05	0.91±0.05	0.84±0.14	1.08±0.09	1.36±0.11**	1.39±0.15*	1.70±0.14*
RWT	0.38±0.02	0.36±0.01^{a}	0.46±0.02^{b,d}	0.49±0.06	0.39±0.02	0.43±0.06	0.51±0.02*	0.54±0.04**	0.82±0.05^{b,d}**
%FS	40.41±1.57	33.91±1.16^{b}	44.14±1.34^{d}	41.85±1.99	38.86±3.21	38.48±3.44	29.92±2.17**	48.63±4.18^{b}	59.73±4.88^{b}**
LV vol, d(μl)	62.20±2.67	62.16±2.43^{b}	53.27±1.86^{b,d}	64.18±4.06	68.19±4.27	50.44±5.40	75.61±6.17	50.48±3.05**	34.67±3.14^{b}**
LV vol, s(μl)	18.25±1.82	22.86±1.50	12.61±0.87^{d}	17.09±1.53	21.18±3.93	14.31±3.50	31.74±3.72**	10.22±1.72^{b}**	3.70±1.16^{b,d}**
%EF	71.42±1.93	63.36±1.55^{a}	76.32±1.43^{d}	73.24±2.30	69.42±4.26	72.20±4.44	58.44±3.21*	79.55±3.44^{b}	89.55±6.37^{b}
SV(μl)	43.90±1.40	39.30±1.60^{b}	40.7±1.60^{d}	47.10±3.60	47.00±2.80	36.1±3.40	42.90±3.70	40.30±2.80^{b}	27.5±3.60^{b}
CO(μl/min)	21.41±0.64	21.00±2.30	19.10±0.97	22.3±1.72	22.22±1.47	17.58±1.31	18.00±1.03	19.70±1.31	14.69±0.01^{a,d}*
LV MASS (mg)	82.35±3.01	86.27±4.14	84.82±4.75	89.81±9.86	95.73±9.30	87.04±9.92	150.53±15.72*	137.45±7.99*	120.49±19.11
AoD, d (n=3)(mm)	1.10±0.10	1.33±0.12	1.25±0.07	1.16±0.08	1.35± 0.11	1.28± 0.07	1.62±0.02*	1.47±0.03	1.35±0.09
AoD, s (n=3) (mm)	1.28±0.07	1.39±0.10	1.38±0.10	1.37± 0.05	1.44± 0.11	1.46± 0.06	1.73±0.04*	1.52±0.04	1.53±0.07
LV Length, d (n=3)(mm)	6.67±0.15	6.75±0.15	7.15±0.09	6.6±0.12	6.94±0.10	7.30±0.07	7.0±0.19	7.74±0.24*	7.86±0.09*

Table 2-2. Percent change in echocardiographic parameters compared to baseline five weeks post surgery. HR, heart rate; LVED, d, LV end diastolic diameter; LVED, s, LV end systolic diameter; LVPW, d, LV posterior wall thickness diastole; LVPW, s, LV posterior wall thickness systole; %FS, fractional shortening; % EF, percent ejection fraction. P-values are shown from comparisons between TAC and sham-operated animals using the 2-tailed unpaired Student's t-test. P-values are shown from comparison within strains using two-way ANOVA. Measurements are represented as average percent change over baseline ± SEM. *$p < 0.05$ or **$p < 0.01$ vs sham controls; ns, not significant. [a]$p < 0.01$ vs B6 TAC; [b]$p < 0.05$ vs F1 TAC; [c]$p < 0.01$ vs F_1 TAC.

Treatment:		SHAM		ANOVA		TAC		ANOVA
Genetic Background:	B6	F_1	129S1		B6	F_1	129S1	
N	6	6	6	p <	9	9	9	p <
HR	495±16	473±10	448±11	ns	509±18	473±13	460±16	ns
LVED, d (%)	-0.1±2.2	4.5±1.9	4.7±2.6	ns	9.9±3.9[b]*	-7.9±2.3**	-21.0±2.5[a,b]**	0.01
LVED, s (%)	-2.1±4.9	-1.2±5.9	10.1±12.2	ns	28.3±6.6[c]**	-28.8±4.9**	-48.9±4.3[a]**	0.01
LVPWTh, d (%)	-0.6±9.1	21.6±10.2	0.7±16.8	ns	41.5±10.8*	31.9±10.7	77.1±18.7[b]*	ns
LVPWTh, s (%)	-14.3±5.7	7.1±12.9	3.7±14.4	ns	20.9±8.1[b]**	69.4±16.5*	83.2±10.2[a]**	0.01
%FS (%)	5.1±7.6	11.9±9.1	-1.4±4.1	ns	-32.5±9.1[c]*	46.4±14.2	23.7±12.5a**	0.01
%EF (%)	3.2±5.0	7.7±6.0	-5.7±6.3	ns	-18.2±2.8[c]**	26.6±6.8	6.6±11.6[a,b]**	0.01
CO (%)	7.4±7.6	4.1±2.52	2.4±3.7	ns	-19.3±3.9**	-17.1±7.7*	-18.7±5.5**	ns
LV Mass (%)	-2.1±3.5	9.4±5.7	4.6±5.5	ns	89.9±14.9**	66.3±16.3*	56.1±7.1**	ns

Table 2-3. Comparison of organ weights between SHAM and TAC treated mice. BW, body weight; HW, heart weight; LuW, lung weight; LiW, liver weight; H:BW, heart:body weight; Lu:BW, lung:body weight; Li:BW (liver;body weight) . Percent increase denotes percent increase over sham-operated animals. P-values are shown from comparisons between TAC and sham-operated animals using the Mann-Whitney rank sum test. Comparisons between strains were made using the non-parametric Kruskal-Wallis test. Organ weight measurements are represented as average ± SEM. *$p < 0.05$ or **$p < 0.01$ vs sham of the same genetic background. ns, not significant. Within treatment group: [a]$p < 0.05$ vs B6 mice; [b]$p < 0.01$ vs B6 mice; [c]$p < 0.05$ vs F1 mice; [d]$p < 0.01$ vs F1

Treatment:		SHAM		ANOVA		TAC		ANOVA	% Increase		
Genetic Background:	B6	F_1	129S1		B6	F_1	129S1		B6	F_1	129S1
N	4	4	4	$p <$	6	6	6	$p <$			
BW (g)	31.10±0.42	30.58±1.20	27.63±0.85[a,c]	0.05	30.50 ±0.33	30.50±1.18	26.06± 0.65[a,c]	0.05	-5.64	-2.11	-7.38
HW (mg)	164.00±5.14	153.63±5.58	131.48±3.14[a,c]	0.05	224.83±14.74*	181±13.46*	159.00±7.18[a,c]**	0.05	37.51	17.84	21.37
LuW (mg)	157.00±6.56	159.80±6.72	131.95±3.43[a,c]	0.05	175.53±5.25	172.00±6.22**	154.00±5.46[b,d]**	0.01	12.03	7.33	16.77
LiW (g)	1.41±0.13	1.35±0.43	1.07±0.05[a,c]	0.05	1.66±0.22*	1.28±0 12	1.06±0.04	ns	18.02	-4.97	-1.70
H:BW(mg:g)	5.25±0.30	5.05±0.30	4.76±0.08	ns	7.36±0.42**	6.39±0.37*	6.13±0.29[a,c]**	0.05	40.19	26.53	28.78
Lu:BW(mg:g)	5.44±0.30	5.24±0.24	4.79±0.19	ns	5.76±0.05	6.07±0.19*	5.90±0.09**	ns	5.88	15.84	23.17
Li:BW(mg:g)	45.18±4.54	44.20±0.84	38.87±0.91	ns	54.67±0.11	45.09±2.48	40.56±1.32[b,d]	0.01	21.00	2.01	4.17

Table 2-4. Blood pressure measurements in conscious ten week-old male mice. SYS=systolic pressure, DIAS=diastolic pressure, MAP=mean arterial pressure. Parameters were not significantly different by genetic background.

Genetic Background	SYS (mmHg)	DIAS(mmHg)	MAP	HR (BPM)
B6 (n=7)	116±3	85±2	101±2	702±5
129S1 (n=6)	122±5	87±19	108±7	676±18

Table 2-5. Percent change over baseline in echocardiographic parameters five weeks post-surgery in conscious mice. HR; heart rate, LVED,d, LV end diastolic diameter; LVED,s, LV end systolic diameter; LVPW,d, LV posterior wall thickness diastole; LVPW, s, LV posterior wall thickness systole; %FS, percent fractional shortening; %EF percent ejection fraction; CO; cardiac output, LV Mass; left ventricular mass. P-values are shown from comparisons between TAC and sham-operated animals using the 2-tailed unpaired Student's t-test. P-values are shown from comparisons within treatment group by genetic background using two way ANOVA. No differences were detected between baseline and sham-operated animals of the same strain for any parameters. No differences were detected in heart rate by treatment or strain. Echocardiographic measurements are represented as average percent change over baseline ± SEM. *$p < 0.05$ or **$p < 0.01$ vs sham controls; [a]$p < 0.05$ vs B6 mice (within treatment group).

Genetic Background:	B6	F_1	129S1	ANOVA	B6	F_1	129S1	ANOVA
N	3	3	3	$p <$	3	5	5	$p <$
Treatment:		SHAM				TAC		
HR (BPM)	631±27	621±14.5	611±4	ns	612±10	614±17	635±9	ns
LVED,d (mm)	2.1±0.8	0.7±1.0	7.8±0.1	ns	10.2±5.8*	-12.1±7.6*	-9.4±2.4[a]**	0.01
LVED,s (mm)	-7.4±1.2	0.7±1.0	6.9±1.9	ns	31.1±15.4**	-27.9±3.1[a]*	-25.4±8.0[a]*	0.01
LVPWTh, d (mm)	11.7±5.5	-6.2±0.7	6.2±0.2	ns	34.9±16.2	56.7±25.9*	50.3±11.3*	ns
LVPWTh, s (mm)	-0.2±4.3	6.7±8.3	2.5±7.5	ns	6.7±8.8	28.2±16.1	15.3±7.8	ns
%FS	6.5±1.90	-13.0±16.4	0.5±1.1	ns	-12.9±7.4*	18.0±4.5[a]	9.8±4.8[a]	0.01
%EF	2.6±0.9	6.9±1.9	0.5±0.4	ns	-7.1±4.2*	8.9±1.7[a]*	3.1±1.5[a]	0.01
CO (μl/min)	3.2±1.0	3.6±0.9	2.3±1.7	ns	12.0±6.8	-18.5±10.4	-30.8±4.3[a]**	0.05
LV Mass (mg)	4.4±1.6	7.1±9.1	14.2±4.0	ns	47.3±3.7	52.8±17.7	32.8±9.5	ns

Figure 2-2. Comparison of mean cardiomyocyte area across treatment group and genetic background. A. Cardiomyocyte size was significantly increased in TAC mice relative to mice receiving sham surgery on all genetic backgrounds ($p < 0.05$ versus sham controls). Within the TAC treatment group, the hearts of B6 mice had the greatest increase in cardiomyocyte area ($p < 0.0001$ versus F_1 and 129S1 TAC). Representative histology of PAS-H stained cardiac sections from the LV septal wall of (B) B6 and (C) 129S1 TAC hearts. (Magnification, 20x. Bar = 50 μm). Cardiomyocyte area is represented as average ± SE.

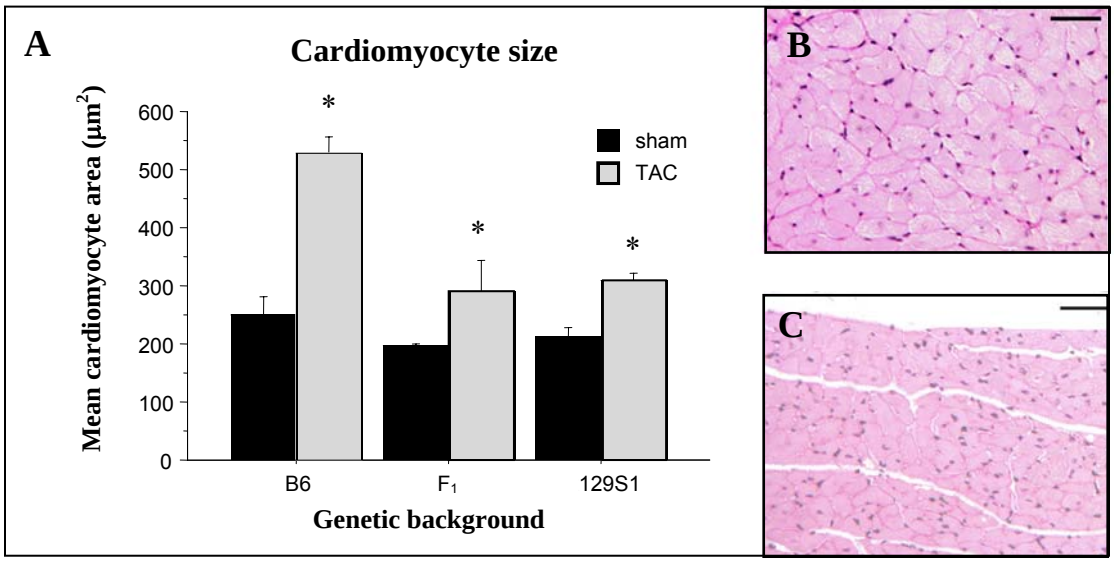

Figure 2-3. Comparison of severity and location of cardiac fibrosis by treatment and genetic background. A. Interstitial fibrosis was significantly increased in B6 and 129S1 TAC mice compared to mice receiving sham surgery ($p < 0.01$ versus sham). B6 sham and TAC mice had more interstitial fibrosis as compared to F_1 and 129S1 mice in their respective groups ($p < 0.05$ versus F_1 and 129S1 shams; $p < 0.01$ versus F_1 and 129S1 TAC). (B-E) Masson's Trichrome stained sections demonstrated that B6 TAC mice have extensive perivascular fibrosis associated with intimal hyperplasia (arrow in B) as well as interstitial fibrosis (C). By comparison, 129S1 TAC mice had very little fibrosis (D and E) (B-E, magnification 20x, Bar = 50 μm). Percent interstitial fibrosis per mm^2 MT cardiac section is represented as average ± SE.

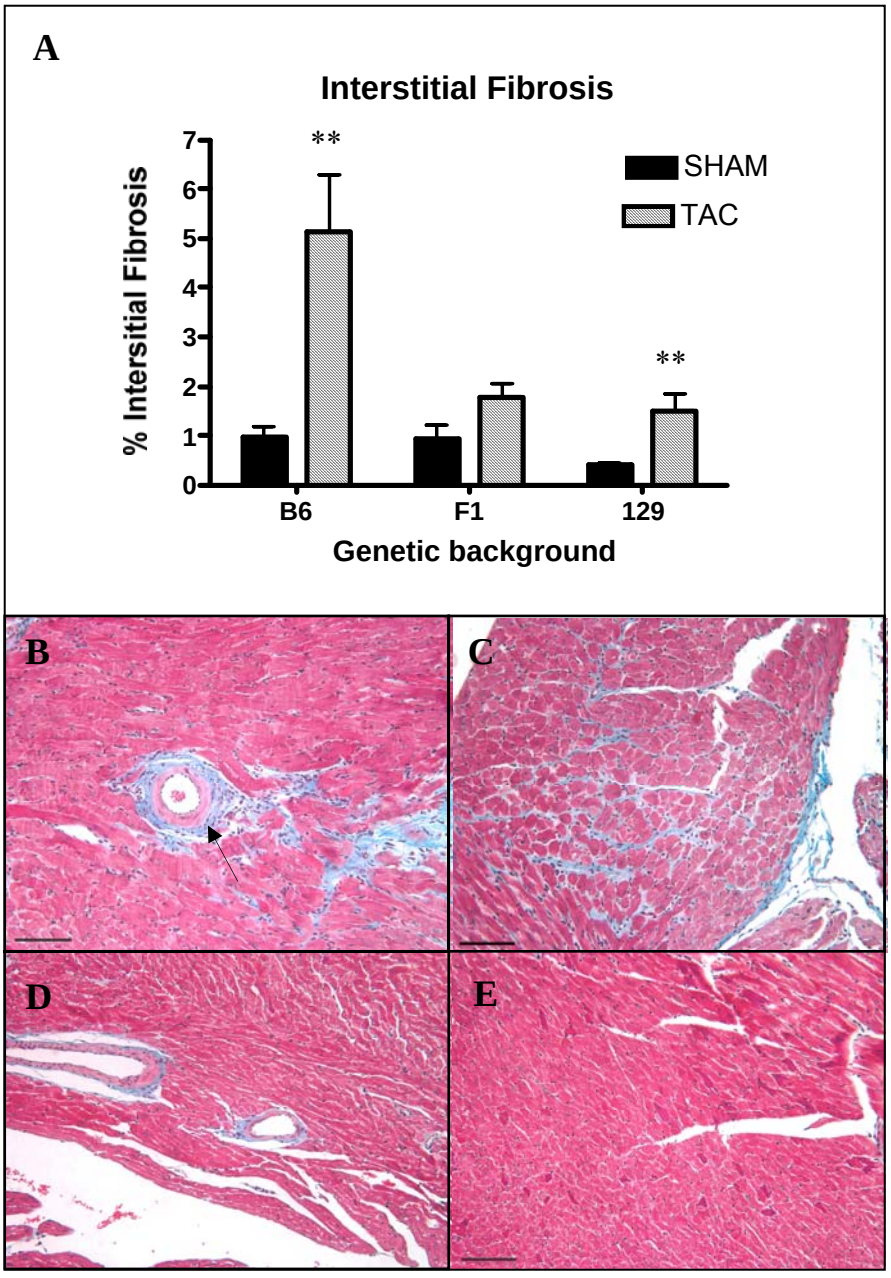

Figure 2-4. Inflammatory infiltrate is associated with fibrosis in B6 TAC hearts. (A and B) Staining for the pan macrophage/monocyte marker MOMA-2 revealed inflammatory infiltrate in regions of perivascular and interstitial fibrosis in B6 TAC hearts (A, brown staining at arrows), while little to no infiltrate was detected in fibrotic regions of F_1 (not shown) or 129 TAC hearts (B) (A and B, magnification 40x, Bar = 25 μm). (C) A low number of positively staining cells were detected in the hearts of all sham mice as well as F_1 and 129S1 TAC hearts. Mean cell count is per mm^2 of tissue and is represented as average ± SEM.

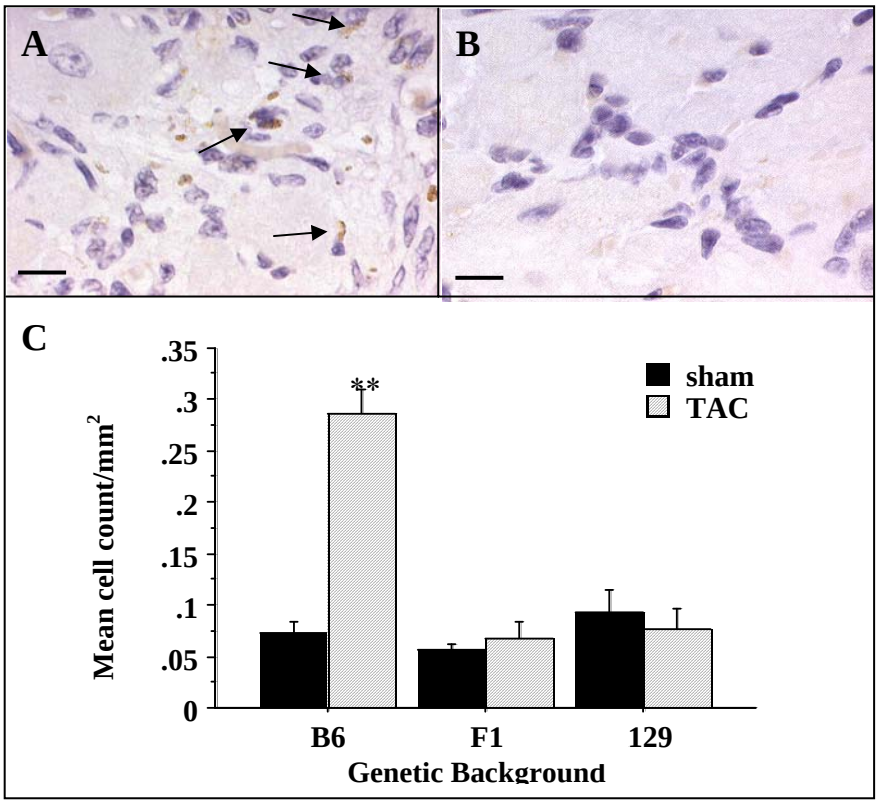

Figure 2-5. Comparison of relative expression of cardiac hypertrophy markers in LV by treatment and genetic background. (A-E) Expression of *Nppa* (ANP), *Nppb* (BNP) and *Myh7* (β-MHC) were all significantly increased in B6 and F1 TAC mice ($p < 0.05$ versus sham controls), while *Myh6* (α-MHC) and *Acadm* (MCAD) were significantly decreased in B6 TAC mice ($p < 0.05$ versus sham controls). Additionally there were significant differences in the gene expression of some markers (*Nppa, Nppb, Acadm*) among the sham groups. Fold change is relative to mean B6 sham values and is expressed as average ± SE.

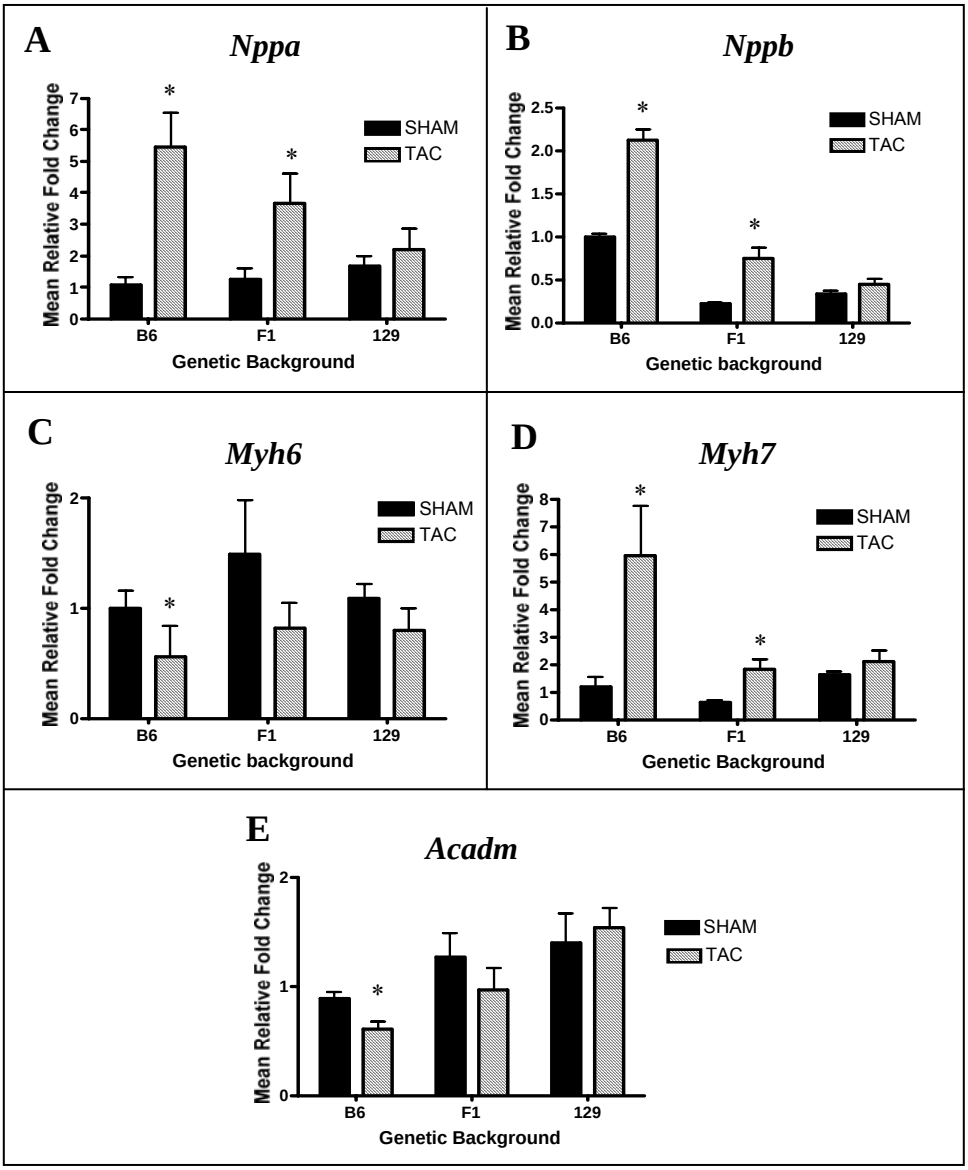

Figure 2-6. 129S1 genetic modifiers delay transition to decompensated heart failure. Temporal echocardiographic analysis of B6, F_1 and 129S1 TAC mice post-surgery. Percent change in (A) LVED,d, (B) LVED,s, (C) LVPWTh, d, (D) LVPWTh,S and (E) % FS over time. LVED,d, LV end diastolic diameter; LVED,s, LV end systolic diameter; LVPWTh, d, LV posterior wall thickness diastole; % FS, percent fractional shortening. Echocardiographic measurements are represented as average percent change over baseline ± SE. n = 3-5 mice per group. *$p < 0.05$ or **$p < 0.01$ versus sham controls.

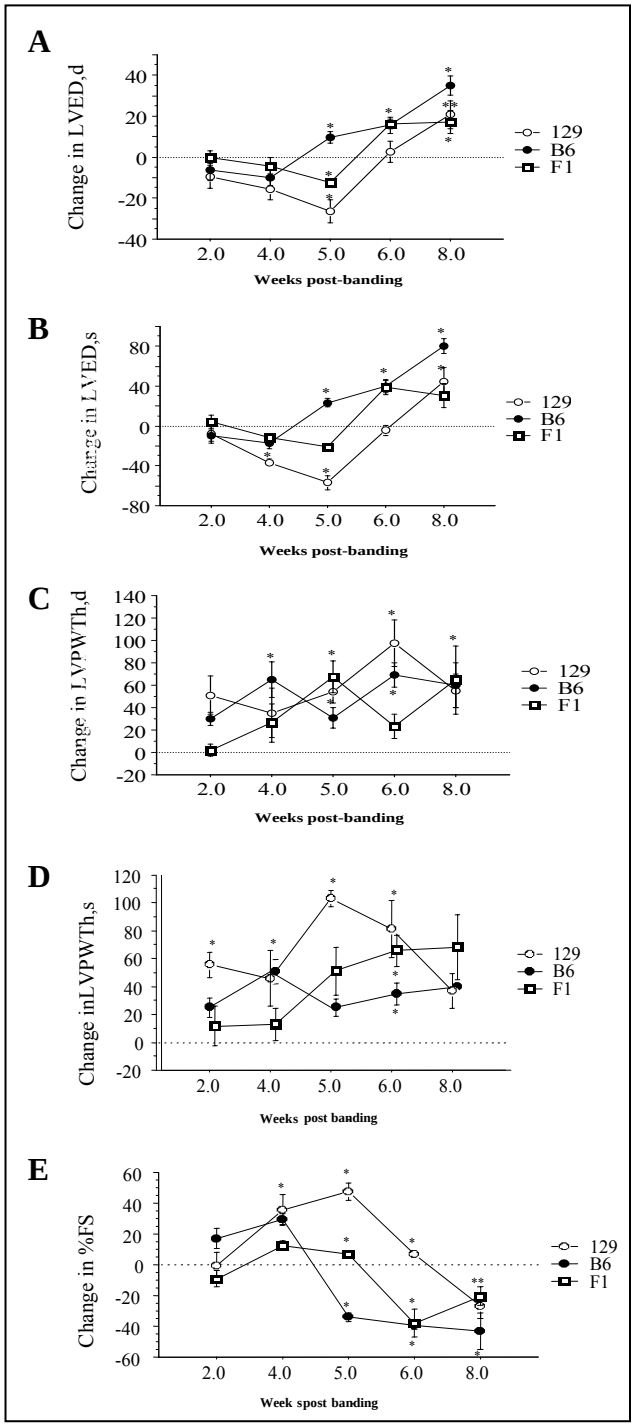

References

1. Spirito, P., et al., *The management of hypertrophic cardiomyopathy.* N Engl J Med, 1997. **336**(11): p. 775-85.

2. Maron, B.J., et al., *Hypertrophic cardiomyopathy. Interrelations of clinical manifestations, pathophysiology, and therapy (2).* N Engl J Med, 1987. **316**(14): p. 844-52.

3. Brown, D.W., W.H. Giles, and J.B. Croft, *Left ventricular hypertrophy as a predictor of coronary heart disease mortality and the effect of hypertension.* Am Heart J, 2000. **140**(6): p. 848-56.

4. Levy, D., et al., *The progression from hypertension to congestive heart failure.* Jama, 1996. **275**(20): p. 1557-62.

5. Haider, A.W., et al., *Increased left ventricular mass and hypertrophy are associated with increased risk for sudden death.* J Am Coll Cardiol, 1998. **32**(5): p. 1454-9.

6. Braunwald, E., *Harrison's Priniciples of Internal Medicine*. 14 ed. Disorders of the Cardivascular System, ed. B. Fauci, Isselbacher, Wilson, Martin, Kasper, Hauser, Longo. 1998, New York: McGraw-Hill.

7. Fields, L.E., et al., *The burden of adult hypertension in the United States 1999 to 2000: a rising tide.* Hypertension, 2004. **44**(4): p. 398-404.

8. Mathew, J., et al., *Reduction of cardiovascular risk by regression of electrocardiographic markers of left ventricular hypertrophy by the angiotensin-converting enzyme inhibitor ramipril.* Circulation, 2001. **104**(14): p. 1615-21.

9. Muiesan, M.L., et al., *Association of change in left ventricular mass with prognosis during long-term antihypertensive treatment.* J Hypertens, 1995. **13**(10): p. 1091-5.

10. Verdecchia, P., et al., *Prognostic significance of serial changes in left ventricular mass in essential hypertension.* Circulation, 1998. **97**(1): p. 48-54.

11. Ganau, A., et al., *Patterns of left ventricular hypertrophy and geometric remodeling in essential hypertension.* J Am Coll Cardiol, 1992. **19**(7): p. 1550-8.

12. Koren, M.J., et al., *Relation of left ventricular mass and geometry to morbidity and mortality in uncomplicated essential hypertension.* Ann Intern Med, 1991. **114**(5): p. 345-52.

13. Devereux, R.B., et al., *Left ventricular hypertrophy and geometric remodeling in hypertension: stimuli, functional consequences and prognostic implications.* J Hypertens Suppl, 1994. **12**(10): p. S117-27.

14. Mayet, J., et al., *Racial differences in cardiac structure and function in essential hypertension.* Bmj, 1994. **308**(6935): p. 1011-4.

15. Liebson, P.R., et al., *Echocardiographic correlates of left ventricular structure among 844 mildly hypertensive men and women in the Treatment of Mild Hypertension Study (TOMHS).* Circulation, 1993. **87**(2): p. 476-86.

16. Kizer, J.R., et al., *Differences in left ventricular structure between black and white hypertensive adults: the Hypertension Genetic Epidemiology Network study.* Hypertension, 2004. **43**(6): p. 1182-8.

17. Hammond, I.W., et al., *The prevalence and correlates of echocardiographic left ventricular hypertrophy among employed patients with uncomplicated hypertension.* J Am Coll Cardiol, 1986.

7(3): p. 639-50.

18. Cooper-DeHoff, R.M., et al., *Characteristics of contemporary patients with hypertension and coronary artery disease.* Clin Cardiol, 2004. **27**(10): p. 571-6.

19. Hallberg, P., et al., *B2 bradykinin receptor (B2BKR) polymorphism and change in left ventricular mass in response to antihypertensive treatment: results from the Swedish Irbesartan Left Ventricular Hypertrophy Investigation versus Atenolol (SILVHIA) trial.* J Hypertens, 2003. **21**(3): p. 621-4.

20. Tripodi, G., et al., *Haplotype analysis of carnitine transporters and left ventricular mass in human essential hypertension.* J Ren Nutr, 2005. **15**(1): p. 2-7.

21. Saeed, M., et al., *Association of angiotensin converting enzyme gene polymorphisms with left ventricular hypertrophy.* Hypertens Res, 2005. **28**(4): p. 345-9.

22. Manunta, P. and G. Tripodi, *Haplotype analysis in human hypertension.* J Hypertens, 2005. **23**(4): p. 711-2.

23. Lanzani, C., et al., *Role of the adducin family genes in human essential hypertension.* J Hypertens, 2005. **23**(3): p. 543-9.

24. De Castro, S., et al., *Effects of angiotensin-converting enzyme inhibition on left ventricular geometric patterns in patients with essential hypertension.* J Clin Pharmacol, 1996. **36**(12): p. 1141-8.

25. Baessler, A., et al., *Association of the Ghrelin receptor gene region with left ventricular hypertrophy in the general population: results of the MONICA/KORA Augsburg Echocardiographic Substudy.* Hypertension, 2006. **47**(5): p. 920-7.

26. Fu, Y., et al., *Relationship of bradykinin B2 receptor gene polymorphism with essential hypertension and left ventricular hypertrophy.* Hypertens Res, 2004. **27**(12): p. 933-8.

27. Tachibana, H., et al., *JNK1 is required to preserve cardiac function in the early response to pressure overload.* Biochem Biophys Res Commun, 2006. **343**(4): p. 1060-6.

28. Tarnavski, O., et al., *Mouse cardiac surgery: comprehensive techniques for the generation of mouse models of human diseases and their application for genomic studies.* Physiol Genomics, 2004. **16**(3): p. 349-60.

29. Hu, P., et al., *Minimally invasive aortic banding in mice: effects of altered cardiomyocyte insulin signaling during pressure overload.* Am J Physiol Heart Circ Physiol, 2003. **285**(3): p. H1261-9.

30. Rockman, H.A., et al., *Segregation of atrial-specific and inducible expression of an atrial natriuretic factor transgene in an in vivo murine model of cardiac hypertrophy.* Proc Natl Acad Sci U S A, 1991. **88**(18): p. 8277-81.

31. Liao, Y., et al., *Echocardiographic assessment of LV hypertrophy and function in aortic-banded mice: necropsy validation.* Am J Physiol Heart Circ Physiol, 2002. **282**(5): p. H1703-8.

32. Lygate, C.A., et al., *Serial high resolution 3D-MRI after aortic banding in mice: band internalization is a source of variability in the hypertrophic response.* Basic Res Cardiol, 2006. **101**(1): p. 8-16.

33. Sanna, B., et al., *Modulatory calcineurin-interacting proteins 1 and 2 function as calcineurin facilitators in vivo.* Proc Natl Acad Sci U S A, 2006. **103**(19): p. 7327-32.

34. Palazzesi, S., et al., *Pressure overload causes cardiac hypertrophy in beta1-adrenergic and beta2-adrenergic receptor double knockout mice.* J Hypertens, 2006. **24**(3): p. 563-71.

35. Song, K., et al., *The transcriptional coactivator CAMTA2 stimulates cardiac growth by opposing class II histone deacetylases.* Cell, 2006. **125**(3): p. 453-66.

36. Auerbach, W., et al., *Establishment and chimera analysis of 129/SvEv- and C57BL/6-derived mouse embryonic stem cell lines.* Biotechniques, 2000. **29**(5): p. 1024-8, 1030, 1032.

37. Bader, M., et al., *Transgenic animals in cardiovascular disease research.* Exp Physiol, 2000. **85**(6): p. 713-31.

38. Downing, G.J. and J.F. Battey, Jr., *Technical assessment of the first 20 years of research using mouse embryonic stem cell lines.* Stem Cells, 2004. **22**(7): p. 1168-80.

39. Deschepper, C.F., et al., *Characterization of blood pressure and morphological traits in cardiovascular-related organs in 13 different inbred mouse strains.* J Appl Physiol, 2004. **97**(1): p. 369-76.

40. Jones, G.L., et al., *A functional analysis of mouse models of cardiac disease through metabolic profiling.* J Biol Chem, 2005. **280**(9): p. 7530-9.

41. Gao, X.M., et al., *Mouse model of post-infarct ventricular rupture: time course, strain- and gender-dependency, tensile strength, and histopathology.* Cardiovasc Res, 2005. **65**(2): p. 469-77.

42. Wang, Q., et al., *Blood pressure, cardiac, and renal responses to salt and deoxycorticosterone acetate in mice: role of Renin genes.* J Am Soc Nephrol, 2002. **13**(6): p. 1509-16.

43. Manning, W.J., et al., *In vivo assessment of LV mass in mice using high-frequency cardiac ultrasound: necropsy validation.* Am J Physiol, 1994. **266**(4 Pt 2): p. H1672-5.

44. Baumgarten, G., et al., *Load-dependent and -independent regulation of proinflammatory cytokine and cytokine receptor gene expression in the adult mammalian heart.* Circulation, 2002. **105**(18): p. 2192-7.

45. Collins, K.A., C.E. Korcarz, and R.M. Lang, *Use of echocardiography for the phenotypic assessment of genetically altered mice.* Physiol Genomics, 2003. **13**(3): p. 227-39.

46. Svensson, E.C., et al., *A syndrome of tricuspid atresia in mice with a targeted mutation of the gene encoding Fog-2.* Nat Genet, 2000. **25**(3): p. 353-6.

47. Bonow, R.O., et al., *ACC/AHA Guidelines for the Management of Patients With Valvular Heart Disease. Executive Summary. A report of the American College of Cardiology/American Heart Association Task Force on Practice Guidelines (Committee on Management of Patients With Valvular Heart Disease).* J Heart Valve Dis, 1998. **7**(6): p. 672-707.

48. Zhang, W., et al., *Failure of calcineurin inhibitors to prevent pressure-overload left ventricular hypertrophy in rats.* Circ Res, 1999. **84**(6): p. 722-8.

49. Livak, K.J. and T.D. Schmittgen, *Analysis of relative gene expression data using real-time quantitative PCR and the 2(-Delta Delta C(T)) Method.* Methods, 2001. **25**(4): p. 402-8.

50. Schmitt, J.P., et al., *Consequences of pressure overload on sarcomere protein mutation-induced hypertrophic cardiomyopathy.* Circulation, 2003. **108**(9): p. 1133-8.

51. Jung-Ching Lin, J., et al., *Structure, Expression, and Function of a Novel Intercalated Disc Protein, Xin.* J Med Sci, 2005. **25**(5): p. 215-222.

52. Chaves, A.A., D.M. Weinstein, and J.A. Bauer, *Non-invasive echocardiographic studies in mice: influence of anesthetic regimen.* Life Sci, 2001. **69**(2): p. 213-22.

53. Chu, D.K., et al., *Comparing isoflurane with tribromoethanol anesthesia for echocardiographic phenotyping of transgenic mice.* J Am Assoc Lab Anim Sci, 2006. **45**(4): p. 8-13.

54. Kawahara, Y., et al., *Preferable anesthetic conditions for echocardiographic determination of murine cardiac function.* J Pharmacol Sci, 2005. **99**(1): p. 95-104.

55. Kiatchoosakun, S., D. Kirkpatrick, and B.D. Hoit, *Effects of tribromoethanol anesthesia on echocardiographic assessment of left ventricular function in mice.* Comp Med, 2001. **51**(1): p. 26-9.

56. Rottman, J.N., et al., *Temporal changes in ventricular function assessed echocardiographically in conscious and anesthetized mice.* J Am Soc Echocardiogr, 2003. **16**(11): p. 1150-7.

57. Schaefer, A., et al., *Effects of anesthesia on diastolic function in mice assessed by echocardiography.* Echocardiography, 2005. **22**(8): p. 665-70.

58. Weber, K.T. and C.G. Brilla, *Pathological hypertrophy and cardiac interstitium. Fibrosis and renin-angiotensin-aldosterone system.* Circulation, 1991. **83**(6): p. 1849-65.

59. Simpson, P.C., et al., *Transcription of early developmental isogenes in cardiac myocyte hypertrophy.* J Mol Cell Cardiol, 1989. **21 Suppl 5**: p. 79-89.

60. Cameron, V.A. and L.J. Ellmers, *Minireview: natriuretic peptides during development of the fetal heart and circulation.* Endocrinology, 2003. **144**(6): p. 2191-4.

61. Gao, X.M., et al., *Regression of pressure overload-induced left ventricular hypertrophy in mice.* Am J Physiol Heart Circ Physiol, 2005. **288**(6): p. H2702-7.

62. Barger, P.M. and D.P. Kelly, *Fatty acid utilization in the hypertrophied and failing heart: molecular regulatory mechanisms.* Am J Med Sci, 1999. **318**(1): p. 36-42.

63. Perrino, C., et al., *Intermittent pressure overload triggers hypertrophy-independent cardiac dysfunction and vascular rarefaction.* J Clin Invest, 2006. **116**(6): p. 1547-60.

64. Hartner, A., et al., *Strain differences in the development of hypertension and glomerular lesions induced by deoxycorticosterone acetate salt in mice.* Nephrol Dial Transplant, 2003. **18**(10): p. 1999-2004.

65. Lum, C., et al., *Cardiovascular and renal phenotype in mice with one or two renin genes.* Hypertension, 2004. **43**(1): p. 79-86.

66. Yang, T., et al., *Influence of genetic background and gender on hypertension and renal failure in COX-2-deficient mice.* Am J Physiol Renal Physiol, 2005. **288**(6): p. F1125-32.

67. Wheeler, F.C., et al., *QTL mapping in a mouse model of cardiomyopathy reveals an ancestral modifier allele affecting heart function and survival.* Mamm Genome, 2005. **16**(6): p. 414-23.

68. Le Corvoisier, P., et al., *Multiple quantitative trait loci modify the heart failure phenotype in murine cardiomyopathy.* Hum Mol Genet, 2003. **12**(23): p. 3097-107.

69. Le Corvoisier, P., et al., *Impact of genetic polymorphisms on heart failure prognosis.* Arch Mal Coeur Vaiss, 2003. **96**(3): p. 197-206.

70. Suzuki, M., et al., *Genetic modifier loci affecting survival and cardiac function in murine dilated*

cardiomyopathy. Circulation, 2002. **105**(15): p. 1824-9.

71. Conrady, A.O., et al., *Prospective study of the changes in left ventricular mass and geometry patterns in hypertensive patients During 5 years of follow-up.* Circ J, 2005. **69**(11): p. 1374-9.

CHAPTER 3

EPIDERMAL GROWTH FACTOR RECEPTOR IS REQUIRED TO PREVENT LEFT VENTRICULAR HYPERTROPHY, CARDIAC FAILURE AND CALCIFIC VALVULAR AORTIC STENOSIS IN C57BL/6J BUT NOT 129S1/SVIMJ MICE

Abstract

Mice homozygous for the hypomorphic *Egfr*^{wa2} allele of epidermal growth factor receptor have semilunar valve hyperplasia and aortic stenosis on a hybrid genetic background. Since previous studies demonstrated that genetic background significantly modifies other phenotypes associated with reduced or absent EGFR activity, we created C57BL/6J and 129S1/SvImJ-*Egfr*^{wa2} congenic lines to investigate the effect of genetic background on the development of aortic stenosis and cardiac function. *Egfr*$^{wa2/wa2}$ mice on both genetic backgrounds have obvious congenital valve defects at birth, with similar levels of aortic valve hyperplasia. However, by three months of age, C57BL/6J-*Egfr*$^{wa2/wa2}$ mice had significantly thicker aortic cusps and elevated transvalvular gradients compared to heterozygous controls and age-matched *Egfr*^{wa2} homozygous mice on either 129S1/SvImJ or B6.129 F_1 backgrounds. Additionally, only C57BL/6J-*Egfr*$^{wa2/wa2}$ mice developed severe left ventricular hypertrophy and progressive cardiac failure. Histological analysis revealed cellular changes in cardiac valves unique to C57BL/6J-*Egfr*$^{wa2/wa2}$ mice including increased cellular proliferation, ectopic cartilage formation, extensive calcification and inflammatory infiltrate, which mimic changes seen in human calcific aortic stenosis. Despite having congenital aortic stenosis, 129S1/SvImJ and B6.129 F_1-*Egfr*$^{wa2/wa2}$ mice had normal

lifespans, no evidence of left ventricular hypertrophy and maintained normal systolic function. These results suggest that a threshold exists for aortic valve function before a significant pressure gradient develops triggering a hypertrophic response and that the 129S1/SvImJ background dominantly protects against calcific aortic stenosis in *Egfr*^{wa2} mice.

Introduction

Valvular aortic stenosis (AS), in which calcification and fibrosis of the aortic valve leaflets obstruct left ventricular outflow, is the most common indication for valve replacement surgery in the US [1]. Since valvular calcific lesions progress slowly over several decades before causing clinically relevant AS, prevalence is highest in the elderly [2-5]. In the US, the number of persons greater than 65 years of age is projected to more than double by 2030; consequently, calcific AS is predicted to become an increasing health burden [6, 7]. The only treatment for severe calcific AS is valve replacement surgery as there are no medical treatments proven to prevent or delay the disease process in the aortic valve leaflets [1]. While several risk factors have been associated with increased prevalence and/or progression of AS, growing evidence suggests genetic factors also modify susceptibility to congenital and calcific valvular disease [8-15]. Moreover, genetic factors may predispose to both developmental defects such as bicuspid aortic valve and valvular calcification [16]. Even though the incidence of AS in increasing, there is a paucity of useful experimental models for development of AS caused by calcific valves, as most mouse models with valve defects arising from gene disruptions have a drastically shortened life span and/or do not have isolated valve defects [17-22].

Mice homozygous for the *Egfr*^{wa2} hypomorph mutation in the epidermal growth factor receptor (*Egfr*) gene develop semilunar valve thickening and AS on mixed genetic

backgrounds [23]. *Egfr*^{wa2} mutant mice are otherwise normal despite having up to a 90% reduction in EGFR tyrosine kinase activity [24]. Similar to *Egfr*^{wa2} homozygosity, deficiency for EGFR results in semilunar valve thickening on a mixed genetic background [23], but also results in genetic background-dependent pre- or peri-natal lethality [25, 26].

To elucidate whether genetic modifiers alter AS severity when EGFR signaling is perturbed, we created congenic lines by backcrossing the *Egfr*^{wa2} allele onto the commonly used C57BL/6J (B6) and 129S1/SvImJ (129S1) strains that have different responses to pressure-induced cardiac overload (see Chapter 2). All *Egfr*$^{wa2/wa2}$ mice have significantly thickened aortic valves compared to heterozygous littermates, yet they differ dramatically by genetic background in the severity of valvular abnormalities, development of left ventricular hypertrophy (LVH) and progression to cardiac failure. Phenotypic analysis of *Egfr*^{wa2} homozygous mice shows that the 129S1 strain harbors dominant and protective genetic modifiers that prevent progression to calcific aortic stenosis and cardiac failure in the context of reduced EGFR activity.

Materials and Methods

Generation of congenic lines

Stock B6EiC3H-a/A-*Egfr*^{wa2} *Wnt3a*^{vt} mice were obtained from The Jackson Laboratory (Bar Harbor, Maine). The *Egfr*^{wa2} allele was backcrossed to the 129S1 and B6 inbred strains. After ten generations, animals carrying the *Egfr*^{wa2} allele were freely incrossed. Segregation and loss of the *Wnt3a*^{vt} mutation, which resides approximately 20 cM distal to *Egfr* on chromosome 11 and which is maintained in *cis* with *Egfr*^{wa2} in the progenitor stocks, was verified by PCR genotyping. An F_1 population was created by outcrossing B6-*Egfr*$^{wa2/+}$

females to 129S1-*Egfr*$^{wa2/wa2}$ males. Homozygous pups were identified by their curly whisker phenotype and confirmed by PCR genotyping as previously described [27]. Adult *Egfr*^{wa2} homozygous mice and wild-type controls were housed and analyzed in same-sex littermate pairs to allow for paired statistical comparisons.

Cardiovascular and molecular phenotyping.

Echocardiography. Transthoracic echocardiography (TTE) was performed using a 30 mHz probe and the Vevo 660 Ultrasonograph (VisualSonics) as previously described (see Materials and Methods in Chapter 2). Doppler tracings were obtained at the level of the aortic root and mean maximum velocities were obtained over three cardiac cycles. Pressure gradients were calculated from the modified Bernoulli equation $P=4(v)^2$ where v= maximum transvalvular velocity in cm/s.

Blood pressure measurements. Systolic blood pressure was measured in conscious mice using a Blood Pressure Analysis tail cuff from Hatteras Systems, Inc (Apex, NC) [28].

Arterial cannulation and ventricular pressure measurements. Mice were anesthesized with 50-80 mg of pentobarbital, IP, and intubated. Mouse body temperature was monitored with a rectal probe and maintained at 37 ±1 degree C throughout the surgical procedure with a variable output halogen lamp. The mouse was positioned on a "mouse pad" (THM-100 board, Indus Instruments, Houston, Texas) that contains EKG electrodes and a built in surface mounted semi-conductor temperature sensor that distributes heat through surface mounted resistors providing control of body temperature. All procedures were done aseptically. Surgery was performed with the aid of a OPMI-DFC surgical stereomicroscope (Carl Zeiss, Dublin, California). An approximate 1 cm midline neck incision from the lower mandible to the sternum was made. The right common carotid artery was exposed and

isolated by blunt dissection of the thin layer around the trachea. A secure suture was placed around the distal end of the artery and a loose suture is placed around the proximal end of the artery. A small vascular clip was placed on the proximal end to minimize bleeding. A 1-2 mm incision near the distal end of the artery was made and the incision extended longitudinally. After removal of the clip, a 1.4 French catheter (Millar Instruments, Houston, Texas) was quickly advanced beyond the proximal suture. The catheter was then advanced retrograde down the ascending aorta and pressure readings were obtained. Since enlarged aortic valves prevented advancement of the catheter into the LV, a bilateral subcoastal incision was performed on the skin and extended into the abdominal cavity. The diaphragm was incised and the pericardium was removed. A small incision with a 11.0 scapel was made on the LV apex and a 1.4 French catheter was advanced beyond the proximal electrodes. The shape of the PV loops was used to determine the optimal placement of the catheter within the LV.

Histology. After the mice were weighed, the hearts, lungs, liver, and kidneys were dissected, rinsed in PBS and weighed individually. Hearts were cut in cross-section just below the level of the papillary muscle. For assessment of cardiomyocyte size and fibrosis, the top half of the heart was fixed in neutral buffered formalin and embedded in paraffin wax. Sections of 5 μm thickness were prepared at 200 μm intervals. The sections were stained with hematoxylin and eosin (H&E) for examination of gross appearance, while Masson's Trichrome (MT) or Periodic Acid-Schiff counterstained with hematoxylin (PAS-H) was employed in order to facilitate quantification of fibrosis, valve size, and cardiomyocyte size. Cardiomyocyte hypertrophy was assessed by measuring cross-sectional area of 100 cardiomyocytes per PAS-H stained section in ten randomly selected fields having nearly circular capillary profiles and

centered nuclei in the left ventricular free wall. Histological images were analyzed using Nova Prime 6.75.10 software (BioQuant Image Analysis, San Diego, California). For measurement of cardiac valve size, morphology and immunohistological analysis, serial sagittal sections were collected from at least four littermate pairs on each genetic background. Aortic cusp diameter was only measured from sections where the aortic outflow tract and aortic walls were clearly visible and in similar orientation. Immunostaining of the valves for demonstration of cellular proliferation and bone matrix protein expression was performed on paraffin-embedded tissues using a streptavidin-biotin method following manufacturer's instructions (DakoCytomation, Universal LSAB™+, AP, K0678, K0689, Carpentaria, California). Proliferating nuclear cell antigen (PCNA), a DNA polymerase, and phospho ERK1/2 were used as markers for cellular proliferation (Cell Signaling, Danvers, Massachusetts) while osteopontin was detected using anti-osteopontin (Abcam, Cambridge, Massachusetts). Alizarin Red S and Von Kossa's method were used as markers for calcification, (http://www.medlib.med.utah.edu/WebPath/HISTHTML/MANUALS; [29] while Movat's pentachrome stain was used to assess extracellular matrix (ECM) composition. DAPI and the pan rat anti-mouse monoclonal IgG macrophage/monocyte marker MCA519G (clone number MOMA-2) (Accurate Chemical, Westbury, New York) followed by a Cy3-labeled goat anti- rat secondary (Jackson ImmunoResearch, West Grove, Pennsylvania) was used to detect inflammatory cells within the aortic valves.

Gene expression. Total RNA was extracted from the lower half of the LV using TRIzol (Invitrogen, Carlsbad, California). After DNAse treatment, 500 ng of total RNA was reverse transcribed using the High Capacity cDNA Archive Kit (Applied Biosystems, Foster City , California). The expression of α-myosin heavy chain (*Myh6*), β-myosin heavy chain (*Myh7*),

atrial nautriuretic peptide (*Nppa*), brain nautriuretic peptide (*Nppb*), and medium chain acyl dehydrogenase (*Acadm*) was determined by real-time quantitaive PCR (qPCR) using Taqman Univeral Master Mix and Assays-on Demand primers and probes (Applied Biosystems, Foster City , California). β-actin (*Actb*) was used as an internal control. Results are represented as mean fold changes relative to *Egfr* $^{wa2/+}$ expression. Reactions were run on a Stratagene MX3000P machine with analysis software. Threshold cycles [30] were determined by an in-program algorithm that assigned a fluorescence baseline based on readings prior to exponential amplification. Fold change in expression was calculated using the $2^{-\delta\delta CT}$ method [31] using the gene *β*-actin as an endogenous control.

***In vivo* phosphorylation assays.** Neonatal pups (PD7) were injected subcutaneously with 5μg/g body weight of EGF (R&D Systems,Minneapolis, Minnesota) in PBS. After 10 min, liver and heart were harvested, frozen in liquid nitrogen, and stored at -80°C. The frozen tissues were sonicated in 5–10 volumes (5–10 ml/g tissue) of lysis buffer consisting of 20 mM HEPES, pH 7.4, 150 mM NaCl, 10% glycerol, 1% Triton X-100, 1 mM PMSF, 10 μg/ml of leupeptin, 10 μg/ml of aprotinin, 1 mM sodium vanadate, and 10 mM β-glycerophosphate at 4°C. The tissue lysates were cleared by centrifugation for 10 min at 4°C and protein concentrations were determined by the Bradford assay (Bio-Rad, Hercules, California). An equal amount of protein lysate (15 μg for liver or 30 μg for heart) was separated by denaturing 7.5% sodium dodecylsulfate polyacrylamide gel electrophoresis (SDS-PAGE) and transferred to PVDF membranes (Bio-Rad, Hercules, California). Protein blots were incubated overnight at 4°C with EGFR ab-17 polyclonal rabbit antibody (RB-1417-P1, LABVISION/Neomarker, Freemont, California), polyclonal rabbit phospho-EGFR (Tyr1086) antibody (36-9700, Zymed, San Fransico, California), or polyclonal rabbit

phospho-p44/42 MAP Kinase (Thr202/Tyr204) antibody (Cell Signaling, Danvers, Massachusetts) followed by incubation goat anti-rabbit horseradish peroxidase conjugated antibody (1858413, Pierce, Rockford, Illinois) and detected with an enhanced chemiluminesence system (AmershamPharmacia/GE Healthcare).

Characterization of congenital cardiac defects. Noon on the day that copulation plugs were observed was designated as 0.5 days post-coitus (dpc). Pregnant females were euthanized by CO2 asphyxiation and embryos were dissected from the uterine horns on the morning of 12.5 through 18.5 dpc into PBS. The placenta and extra-embryonic tissues were separated from the embryo by mechanical dissection and a tail biopsy was collected for DNA extraction to determine the genotype. Embryos were fixed in neutral buffered formalin for histological analysis and paraffin embedded. Sections of 5 μm thickness were deparaffinized, rehydrated in a graded series of ethanols, and counterstained with hematoxylin and eosin (H&E) for morphological characterization.

Statistical analysis. Data is presented as mean +/- standard deviation (SE). The nonparametric Wilcoxon rank sum test or the two sided student's t-test was used for statistical analysis, pairing data from littermates. The Kruskal-Wallis test or analysis of variance [20] was used to detect significance by genotype or genetic background. Statistical analyses were performed using StatView (SAS, Cary, NC). A $p < 0.05$ was considered statistically significant.

Results

Survival of mice with reduced EGFR activity. Although B6-*Egfr*$^{wa2/wa2}$ mice were born close to the expected Mendelian ratios from B6-*Egfr*$^{wa2/+}$ female by B6-*Egfr*$^{wa2/wa2}$ male matings (43%, n = 8 litters, 43 pups), at weaning less than 30% of surviving mice were

homozygous for the *Egfr*^{wa2} allele as compared to 44.44% and 46.15% from similar crosses on F1 and 129S1 backgrounds, respectively (n = 4 and 9 litters; 27 and 39 mice, respectively). Between weaning and six months of age, an additional 15% of B6-*Egfr*$^{wa2/wa2}$ mice died. Thus, by one year of age, approximately 50% of B6-*Egfr*$^{wa2/wa2}$ mice had died as compared to less than 10% of B6-*Egfr*$^{wa2/+}$ littermates (Figure 3-1 A; n = 50 mice of each genotype, $p < 0.001$). A pronounced sex difference in survival was observed as approximately 40% of B6-*Egfr*$^{wa2/wa2}$ male mice but only one female B6-*Egfr*$^{wa2/wa2}$ mouse (10%) died prior to three months of age. Sudden death was a common complication resulting from minor stressors such as handling or ear notching, and necropsies of these mice showed massive enlargement of their hearts (Figure 3-1 B) as well as increased liver and lung weights, all characteristics of congestive heart failure. Normalized for body weight, the B6-*Egfr*$^{wa2/wa2}$ heart and lung weights were significantly larger when compared to B6-*Egfr*$^{wa2/+}$ littermates (n = 16 sibling pairs, $p < 0.001$; Figure 3- 1C and Table 3-1). There were no significant differences in survival or normalized heart or lung weights in inbred 129S1 (n = 18 sibling pairs) or hybrid F1 (n = 9 sibling pairs) wildtype versus *Egfr*$^{wa2/wa2}$ mice even at 15 months of age.

EGFR expression and signaling activity. To determine whether differences in expression from the *Egfr*^{wa2} allele contributed to background-dependent lethality, lysates were prepared from liver and hearts of one week old *Egfr*$^{wa2/wa2}$ and *Egfr*$^{wa2/+}$ littermates. Western blot analyses demonstrated that EGFR of similar size is produced in the hearts and livers of controls and *Egfr*$^{wa2/wa2}$ mice (Figure 3- 2, A and B). Although there were strain- and organ-specific differences in total EGFR protein, no significant differences in EGFR protein levels were observed among *Egfr* $^{wa2/wa2}$ mice. To verify equivalent levels of EGFR signaling,

ligand-induced EGFR activity was measured in one-week-old pups by dosing with EGF (5 mg/g body weight) and quantifying the level of phosphorylated EGFR and ERK1/2 by western blot analyses. Similar to previous reports [26] phosphorylated EGFR was below the limits of detection in heart lysates of all mice, but was significantly decreased in liver lysates of *Egfr*$^{wa2/wa2}$ mice compared to their respective controls (ANOVA, $p < 0.01$). Phosphorylated ERK1/2 levels were also significantly decreased in heart lysates of *Egfr*$^{wa2/wa2}$ mice on all genetic backgrounds and in liver lysates of B6 and 129S1-*Egfr* $^{wa2/wa2}$ mice compared to heterozygous controls, consistent with depressed activation of downstream EGFR signaling pathways (ANOVA, $p < 0.01$). Quantitative PCR analysis of *Egfr* verified equivalent transcript levels in hearts of three-month-old *Egfr* $^{wa2/wa2}$ mice across all backgrounds, although *Egfr*$^{wa2/wa2}$ mice had consistently higher levels of *Egfr* transcripts than wildtype (Figure 3-2 C).

Pathological, molecular and functional effects. Since a large proportion of B6-*Egfr*$^{wa2/wa2}$ deaths occurred prior to weaning, we compared cardiac development at mid (13.5 dpc - 15.5 dpc) and late (18.5 dpc – postnatal day (PD) 1) gestational windows by genotype and genetic background. Consistent with previous reports, thickened semilunar valves were observed in *Egfr*$^{wa2/wa2}$ embryos on all genetic backgrounds from 15.5 dpc to PD1, highlighting a requirement for normal EGFR activity for valvular remodeling (Figure 3-3 A). However, additional congenital cardiac defects like decreased trabeculation, ventricular septal defects, thinned chamber walls and enlarged hearts, unique to B6-*Egfr*$^{wa2/wa2}$ mice, were detected at earlier time points (12.5 dpc - 13.5 dpc;) and likely contribute to the observed postnatal deaths (Figure 3-3 B).

Cardiomyocyte size, as measured by mean cross-sectional area, was enlarged by approximately two-fold in PD1 B6-*Egfr*$^{wa2/wa2}$ mice and by almost three-fold in adult B6-*Egfr*$^{wa2/wa2}$ mice as compared to heterozygous littermates (Figure 3-1 A; n = 8 sibling pairs, $p < 0.01$). By 12 weeks of age, B6-*Egfr*$^{wa2/wa2}$ mice demonstrated dilated left ventricles and thickened septal and chamber walls (Figure 3-1 B). No difference in cardiomyocyte size was detected among 129S1 or F1-*Egfr*$^{wa2/wa2}$ and heterozygous littermates, even at 15 months of age (data not shown). Hyperchromasia and karyomegaly, hallmarks of cardiac hypertrophy, were observed in histological sections from adult B6-*Egfr*$^{wa2/wa2}$ hearts (Figure 3-4 B). Additionally, multifocal lesions with vacuolar degeneration, inflammatory infiltrate, and necrosis were observed in the hearts of moribund B6-*Egfr*$^{wa2/wa2}$ mice. These pathological changes were accompanied by extensive interstitial fibrosis localized primarily to the apex and subendocardial regions of the heart (Figure 3-4 B). Consistent with previous reports [23], histological examination of other tissues that were severely affected in *Egfr* null mice (brain, liver, lung, kidney, gastrointestinal tract) revealed no significant morphological defects in *Egfr*$^{wa2/wa2}$ mice.

The re-expression of a fetal gene program, which occurs in response to a variety of stimuli, is a consistent and sensitive marker of cardiac hypertrophy in humans and laboratory animals. The expression of the atrial and brain nautriuretic peptide genes (*Nppb* and *Nppa*, the products of which induce vasodilation and sodium excretion) and the gene for the fetal isoform of myosin heavy chain (*Myh7*) were significantly or suggestively upregulated in B6-*Egfr*$^{wa2/wa2}$ left ventricles compared to wildtype (mean fold transcript increases in B6-*Egfr*$^{wa2/wa2}$ vs. *Egfr*$^{wa2/+}$ hearts: *Nppb,* 65 ± 7.5, $p < 0.07$, *Nppa*, 50 ± 2.5, $p < 0.05$, *Myh7*, 20 ± 2.5, $p < 0.05$; 4 sibling pairs; data not shown). Consistent with altered cardiac metabolism,

expression of the medium chain acyl dehydrogenase gene (*Acadm*) was reduced by approximately 50% in B6-*Egfr*$^{wa2/wa2}$ LV (data not shown). In agreement with histological measurements, there were no significant differences in expression of these markers in the LV among 129S1 or F1-*Egfr*$^{wa2/wa2}$ and heterozygous littermates.

Cardiovascular function was evaluated by transthoracic echocardiography (TTE) in three-to-five month old sex matched littermates on all three genetic backgrounds (Figure 3-3 C; Table 3-2). Compared to their sex matched B6-*Egfr*$^{wa2/+}$ littermates, B6-*Egfr*$^{wa2/wa2}$ mice had larger left ventricles and reduced fractional shortening (FS, a measure of ventricular systolic function) consistent with dilation of the LV and a thickened chamber wall. By contrast, 129S1-*Egfr*$^{wa2/wa2}$ mice had smaller left ventricular end diameter diastole (LVED,d) and left ventricular end diameter systole (LVED,s) measurements with thinner chamber walls compared to 129S1-*Egfr*$^{wa2/+}$ littermate controls, matching their proportionately smaller heart and body size; there was no significant difference in FS among 129S1 or F1-*Egfr*$^{wa2/wa2}$ and heterozygous littermates. Additionally, there were no significant differences by genetic background or genotype in systolic blood pressures as assessed by the tail cuff method (conscious mice) or by aortic catheterization (anesthetized mice) (Table 3-3), suggesting that differences in systolic pressures did not contribute to differences in cardiac hypertrophy. Taken together, histopathological and echocardiographic analysis indicated that B6-*Egfr*$^{wa2/wa2}$ mice displayed increased chamber size, myofiber hypertrophy, and decreased fractional shortening, signs of severe cardiac dysfunction.

Development of calcific aortic stenosis. Since analysis of congenic *Egfr*^{wa2} embryos suggested defects in cardiac valve remodeling, we suspected there also might be differences in postnatal valve function and degeneration, modulated by genetic modifiers of cardiac

valve homeostasis, function and subsequent severity of the AS leading to background-dependent differences in cardiac hypertrophy, dysfunction and survival. While aortic valve cusp thickness, estimated by cusp diameter, was significantly increased in *Egfr*^{wa2} homozygous mice compared to heterozygous controls on all three genetic backgrounds (Figure 3-4 A), B6-*Egfr*$^{wa2/wa2}$ mice had the thickest cusps (Figure 3-5 B; B6, n = 8 sibling pairs, $p < 0.001$; F1, n = 4 sibling pairs, $p < 0.01$; 129S1, n = 6 sibling pairs, $p < 0.01$). Moreover a positive linear relationship exists between aortic valve thickness and heart weight in B6-*Egfr*$^{wa2/wa2}$ mice (Figure 3-5 C, R^2=0.77), suggesting an inverse relationship between hypertrophy and aortic systolic opening. Inclusion of B6 *Egfr* $^{wa2/+}$ mice increased the correlation coefficient (R^2=0.91), however no such relationship was observed by genotype or genetic background in F_1 or 129S1 mice.

Doppler tracings taken at the level of the aortic root confirmed elevated average peak velocities in *Egfr*$^{wa2/wa2}$ mice compared to age and sex matched littermate controls (Figure 3-6 A; Table 3-2). However, aliasing, an artifact that occurs in pulsed wave Doppler peak velocities above the threshold for the VisualSonics instrument (*i.e.* greater than 4 m/s), was evident in tracings from many B6-*Egfr*$^{wa2/wa2}$ mice. Thus, the gradients calculated from peak Doppler velocities may under represent the true peak velocities in the most severely affected B6-*Egfr*$^{wa2/wa2}$ mice. Cardiac catheterization confirmed higher left ventricular end systolic pressures (PSP) in all *Egfr*$^{wa2/wa2}$ mice examined compared to littermate controls (Table 3-2). Although the catheter cannot simultaneously monitor LV and aortic PSP, peak-to-peak gradients could be calculated by measuring aortic PSP and then inserting the catheter into the LV to measure PSP. B6-*Egfr*^{wa2} mice consistently exhibited the largest pressure gradients, indicating severe AS. Transvalvular gradients in B6 *Egfr* $^{wa2/wa2}$ mice showed a positive

linear relationship with aortic valve thickness (Figure 3-6 B; $R^2 = 0.89$), suggesting that in this mouse model as in human patients, there may be a physiological threshold for AS which must be reached before significant pressure gradients and cardiac disease symptoms appear.

Further examination of the thickened aortic valves demonstrated distinct genetic background differences in cellular morphology and differentiation. Gross dissection revealed that the cardiac valves of severely affected B6-*Egfr*$^{wa2/wa2}$ mice had pronounced, dense pigmentation around the aortic and mitral valve cusps (Figure 3-7 A). Cardiac valves of B6-*Egfr*$^{wa2/+}$ mice had mild or no discoloration, while 129S1 and F1-*Egfr*^{wa2} mice of both genotypes were unaffected (data not shown). Because melanocytes have been reported in cardiac valves from wildtype B6 mice, we crossed B6-*Egfr*^{wa2} mice to albino B6-*Tyr*$^{c-2J}$ mice to verify the pigmentation was due to melanocytes. The cardiac valves of B6-*Tyr*$^{c-2J}$ *Egfr*$^{wa2/wa2}$ mice, although similarly thickened, were not discolored, demonstrating that the cardiac valves of B6-*Egfr*$^{wa2/wa2}$ mice have increased resident melanocyte populations.

Recent evidence from clinical and experimental models supports the hypothesis that calcific AS is an active disease process with many similarities to atherosclerosis [5, 14, 32-46]. Studies of diseased valves have shown cusp and leaflet thickening, inflammatory infiltrate, collagen fiber disorganization, increased valvular interstitial cell (VIC) proliferation, and calcification. Calcification contributes to lesion rigidity, worsening obstruction to left ventricular outflow and correlates clinically both with more rapid disease and worse outcomes [35]. Because histomorphological evidence of ectopic cartilage formation was seen in hematoxylin and eosin stained aortic valves of adult B6-*Egfr*$^{wa2/wa2}$ mice, we performed further immunohistochemical analysis using markers for cellular proliferation (PCNA, pERK1/2), extracellular matrix composition (ECM) composition

(Movat's pentachrome), macrophage infiltration (MOMA-2), calcification (Alizarin Red S and von Kossa), and mature osteoblasts (osteopontin). B6-*Egfr*$^{wa2/wa2}$ valves had evidence of cellular proliferation and MAPK activation (Figure 3-7 B and C) and altered ECM composition (Figure 3-8 A); the intense teal color with Movat's pentachrome that was unique to B6-*Egfr*$^{wa2/wa2}$ valves indicates close proximity of glycosaminoglycans and collagen. B6-*Egfr*$^{wa2/wa2}$ valves also contained osteoblasts, were calcified and had evidence of inflammatory infiltrate (Figure 3-8 B -D). A low level of positive staining for calcification was also observed in the cardiac valves of some B6-*Egfr*$^{wa2/+}$ while 129S1 and F1-*Egfr*$^{wa2/wa2}$ valves showed no evidence of positive staining for any markers (data not shown). Neither calcification nor altered ECM composition was detected in the valves of embryonic or neonatal B6-*Egfr*$^{wa2/wa2}$ mice (see Figure 3-3). Taken together, these data suggest that modifiers on the B6 genetic background sustain continued post-natal proliferation and differentiation of valvular interstitial cells residing in the cardiac valves. In the environment of congenitally malformed aortic valves, these differences become critical to cardiac function as what is already a grossly enlarged valve becomes stiff and dysfunctional in the B6-*Egfr*$^{wa2/wa2}$ mice

Discussion

Egfr^{wa2} mutant mice on a mixed genetic background have semilunar valve thickening and mild to moderate AS that is enhanced when combined with a mutation in *Ptpn11* [23]. Since previous studies established that phenotypes resulting from reduced or ablated EGFR activity are highly dependent upon genetic background [25, 47], we generated and examined B6 and 129S1-*Egfr*^{wa2} congenic lines and their F_1 hybrids. Similar to findings in other organ systems, genetic background significantly modifies the cardiovascular phenotype in the *Egfr*^{wa2} mouse

model of AS (Figure 3-9), although there are no detectable background-dependent differences in residual EGFR activity. B6-*Egfr*$^{wa2/wa2}$ mice have significantly decreased survival secondary to congestive heart failure. In contrast, mice homozygous for the *Egfr*^{wa2} mutation on the 129S1 inbred or F1 backgrounds have normal life spans and cardiac function with no histological or molecular evidence of LVH, implying the presence of dominant 129S1 protective modifiers. Although aortic valves are thickened in *Egfr*$^{wa/wa2}$ mice on all genetic backgrounds relative to littermate controls, aortic valves of adult B6-*Egfr*$^{wa2/wa2}$ mice are significantly more thickened as compared to *Egfr*^{wa2} homozygous mice on other genetic backgrounds. Moreover, aortic valve thickness is highly correlated with cardiac weight and physiologically significant pressure gradients in *Egfr*^{wa2} mutant mice. We also found degenerative cellular changes unique to B6-*Egfr*$^{wa2/wa2}$ cardiac valves, such as increased VIC proliferation and differentiation, altered ECM composition, calcification and inflammation.

In humans, significant hemodynamic or clinical changes are rare in AS until the valve orifice has narrowed to approximately one-third of normal [48, 49]. Studies using a hypercholesterolemic mouse model of AS showed that an almost identical threshold of decreased aortic valve orifice must be achieved before significant hemodynamically-induced transvalvular gradients and pathophysiological responses are detected in mice [50]. Our morphometric, immunohistochemical and hemodynamic analysis also support a threshold effect in the *Egfr*^{wa2} model of AS, whereby congenitally thickened aortic valves of B6-*Egfr*$^{wa2/wa2}$ mice become progressively larger and stiffer than those of 129S1 or F_1-*Egfr*$^{wa2/wa2}$ mice, leading to a critical reduction in systolic valve area, valve flexibility and elevated pressure gradients. Because 129S1 and F1-*Egfr*$^{wa2/wa2}$ valves do not reach the critical threshold, LV compensatory mechanisms are not triggered, even in aged mice. Thus, the

striking differences in *Egfr*-associated cardiac hypertrophy and mortality between genetic backgrounds are most likely secondary to genetic modifiers influencing cardiac valve development and homeostasis. Although delayed relative to B6, 129S1 mice will eventually develop LVH in the presences of elevated aortic pressure gradients induced by minimally invasive aortic banding (MIAB) (Chapter 2), further supporting that the dominant protective 129S1 modifier(s) prevent the degenerative valvular changes that lead to LVH and congestive heart failure. However, since 129S1-*Egfr*^{wa2wa2} mice have congenitally thickened semilunar valves and mild pressure gradients across the aortic valve (8-10 mmHg), yet do not develop LVH or cardiac dysfunction, 129S1 protective modifiers may also directly sustain normal cardiomyocyte development, survival and function.

Genetic studies using knockout mouse models established that endocardial outflow track cushion growth is largely controlled by the amount of BMP signaling, with diminished and excessive signaling correlating to hypo and hyperplastic cushions, respectively [51, 52]. Defective cardiac valvulogenesis in mice lacking *Dtr* (coding for the EGFR ligand HB-EGF), *Egfr* or *Adam17* (coding for a metalloprotease required to process mature EGFR ligands) results from abnormal valvular mesenchymal cell proliferation, while *Erbb3* deficient embryos have hypoplastic cushions completely lacking mesenchymal cells. Since the thickened valves of *Dtr* null embryos showed dramatic increases in activated BMP signaling effectors SMAD1/5/8 [17, 53] and since EGFR has been shown to downregulate BMP signaling by inactivating SMAD1 *in vitro*, Jackson et al. postulated that EGFR activation by TACE-derived soluble DTR normally limits BMP signaling during the transition from cushion formation/growth to valve remodeling [17]. Although we did not find overt genetic background-dependent differences in cardiac valve size from 15.5 dpc through PD1

Egfr$^{wa2/wa2}$ mice, modifiers may have affected the balance of these signaling pathways post-natally. Cellular changes in adult B6-*Egfr*$^{wa2/wa2}$ semilunar valves mimic those seen in degenerative aortic stenosis [36, 42, 43, 46, 54, 55], suggesting that EGFR activity is also required to repress abnormal growth and differentiation in mature aortic valves. Several mediators of BMP signaling like TGFβ1, BMP2 and BMP4 are detected in aortic valve lesions and promote differentiation of isolated valvular interstitial cells to osteoblast-like cells [56]; osteoblasts express EGFR, while EGF stimulates osteoblast proliferation *in vitro*. Additionally, primary osteoblast cultures isolated from *Egfr*$^{tm1Mag/tm1Mag}$ null mice have reduced proliferation, but increased differentiation and ability to form bone nodules relative to controls [57]. Thus, attenuation of EGFR signaling predisposes to congenital defects and promotes a calcifying cell phenotype in mature valves on a B6 background.

Accumulating evidence from epidemiologic, clinical and animal studies supports the hypothesis that calcific AS and atherosclerosis have common cardiovascular risk factors and pathological processes [34-36, 39, 44, 58, 59]. B6 and 129S1 inbred mouse strains are known to differ markedly in plasma HDL-cholesterol concentrations and susceptibility to atherosclerosis after high-fat diet consumption, with B6 mice having lower HDL levels and increased fatty streak aortic lesion formation [60]. Recently, it was shown that B6 mice chronically fed a high fat/high carbohydrate diet acquire aortic valve abnormalities, with decreased corrected valve orifice area, histological evidence of calcification and inflammation, and increased mean aortic outflow tract peak systolic velocities [61]. Since we detected similar pathological changes in the cardiac valves of adult B6-*Egfr*$^{wa2/wa2}$ mice and wild-type B6 mice subjected to surgically induced pressure overload (C.J.B and D.W.T, unpublished observations), we speculate that the B6 background is predisposed to valve

disease that can be triggered by a variety of insults. Moreover, the predisposition of B6 mice to atherosclerosis and calcific AS may be mediated by common mechanisms.

The B6 genetic background is also susceptible to developmental defects that probably contribute to early postnatal lethality in the presence of reduced EGFR activity. Decreased trabeculation, ventricular septal defects, thinned chamber walls and enlarged hearts were observed in B6-*Egfr*$^{wa2/wa2}$ embryos at 12.5 dpc, prior to detection of obvious valve defects. Similar but more severe cardiac phenotypes were reported with targeted disruption of the neuregulin 1 (*Nrg1*) gene or of either of the two neuregulin receptor genes (*Erbb*2 or *Erbb4*) resulting in death by mid-gestation [62-64]. *Nrg1*, *Erbb2* and *Erbb4* remain expressed in postnatal and adult ventricular myocytes, and signaling through the ERBB axis is crucial for adult cardiomyocyte survival and cardiac function [65-69]. Additionally, *Erbb2* and *Erbb4* are downregulated at both the message and protein levels in experimental and clinical studies of heart failure, supporting a role for disabled ERBB receptor signaling in the transition from compensatory hypertrophy to failure [70, 71]. EGFR has been biochemically linked to the ERBB signal axis through NRG1, which can bind to and activate EGFR heterodimers with ERBB3 and ERBB4.

Most models of aortic valve deformities caused by gene disruptions have a drastically shortened life span and/or do not have isolated valve defects [17-22]. Consequently, it has been difficult to conduct detailed phenotypic analysis. Herein, we have extensively phenotyped two *Egfr*^{wa2} congenic lines that are susceptible or resistant to valvular degeneration with subsequent development of LVH and cardiac failure, despite having similar congenital valvular disease. Humans with acquired or congenital AS have considerable variability in onset of symptoms, cardiac response and function, and disease

progression. A subset of patients with AS remain asymptomatic despite rapid disease development and have a heightened risk of sudden death. Thus far, the only reliable predictor for these high risk patients is age and the extent of valvular calcification [72]. The development of therapeutic approaches that will halt or retard valve calcification should be aided by the *Egfr*^{wa2} model of AS. Finally, many cancers are now being managed as chronic rather than terminal diseases, and since targeted inhibition of EGFR activity is becoming a widely used cancer therapeutic, our results suggest that a subset of patients with congenital valve defects or predisposed to valvular defects may be at risk for developing drug-induced valvulopathy with prolonged EGFR inhibition.

Figure 3-1. Survival curve, gross and histological comparison of hearts in B6 *Egfr* ^{wa2} littermates and comparison of normalized heart weights in *Egfr* ^{wa2} littermates. A. Survival curve of B6 *Egfr* ^{wa2} littermates (n=50 mice, $p<0.001$). B. Gross and histological comparison of hearts from three-month-old B6 *Egfr* ^{wa2} littermates. C. Comparison of normalized heart weights by genotype and genetic background in three-to-five month old *Egfr* ^{wa2} littermates (N= 16, 13 and 17 sibling pairs, ***$p<0.001$).

A.

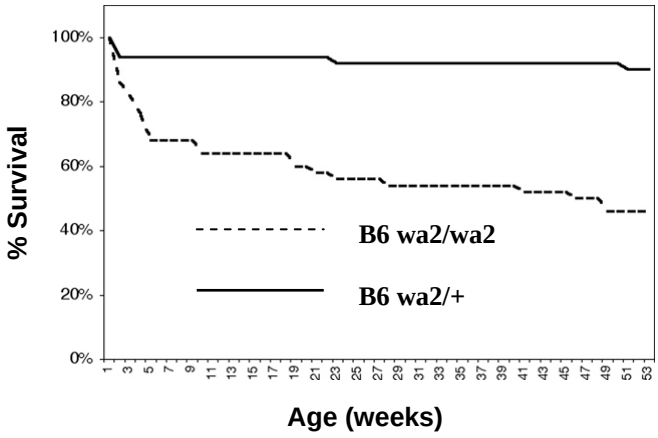

B.

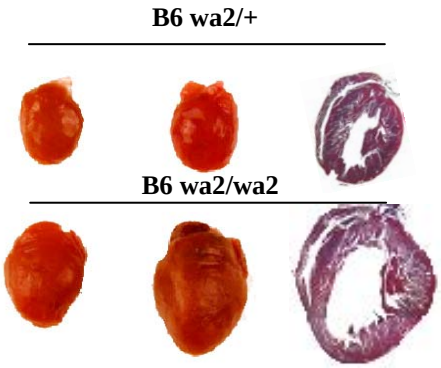

C.

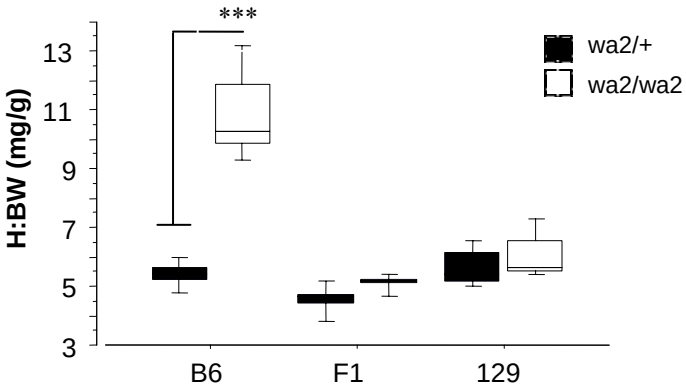

Table 3-1. Organ weights from three-to five month old *Egfr* ^{wa2} littermates. Comparison by genotype *$p<0.05$, **$p<0.01$,***$p<0.001$.

Genetic Background	B6		F1		129S1	
Genotype	wa2/+	wa2/wa2	wa2/+	wa2/wa2	wa2/+	wa2/wa2
N	16	16	9	9	18	18
BW (g)	26.45±0.96	26.80±1.11	24.94±0.72	25.24±0.90	27.17±1.17	23.14±1.04*
HW	141.83±3.50	330.15±24.36***	124.27±4.23	134.11±4.14	148.31±4.94	136.26±4.60
H:BW	5.42±0.16	12.33±0.82***	4.98±0.07	5.34±0.18	5.56±0.23	5.99±0.21
N	6	6	6	6	8	8
LuW	149.63±1.84	173.25±2.75***	141.4±15.34	157.67±3.43	141.96±8.62	129.4±3.5
LiW	1244.62±30.65	1354.08±63.45	971.00±20.42	1086.67±52.33	981.20±31.93	758.78±46.97.00**
Lu:BW	5.88±0.27	6.72±0.22*	5.44±0.58	5.47±0.40	5.33±0.50	6.02±0.31
Li:BW	48.61±0.91	52.57 ±1.54*	37.43±1.45	37.53±2.72	36.65±2.27	35.06±2.16

Figure 3-2. Western blot and densitometry analysis of total EGFR and phospho-ERK1/2 from B6 and 129S1 *Egfr* ^{wa2} littermates A. Western blot and densitometry analysis of total EGFR and phospho-ERK1/2 (heart lysates) from B6 and 129S1 *Egfr* ^{wa2} littermates. B. Western blot and densitometry analysis of total and phospho-EGFR and phospho-ERK1/2 (liver lysates) from B6 and 129S1 *Egfr* ^{wa2} littermates. All values are normalized to the β-actin loading control. Values represent the means from at least 3 samples. C. EGFR transcript levels in total RNA extracted from hearts of adult *Egfr* ^{wa2} littermates. Fold change is relative to B6 *Egfr* $^{wa2/+}$ samples. *$p<0.05$, **$p<0.01$ relative to *Egfr* $^{wa2/+}$ littermates.

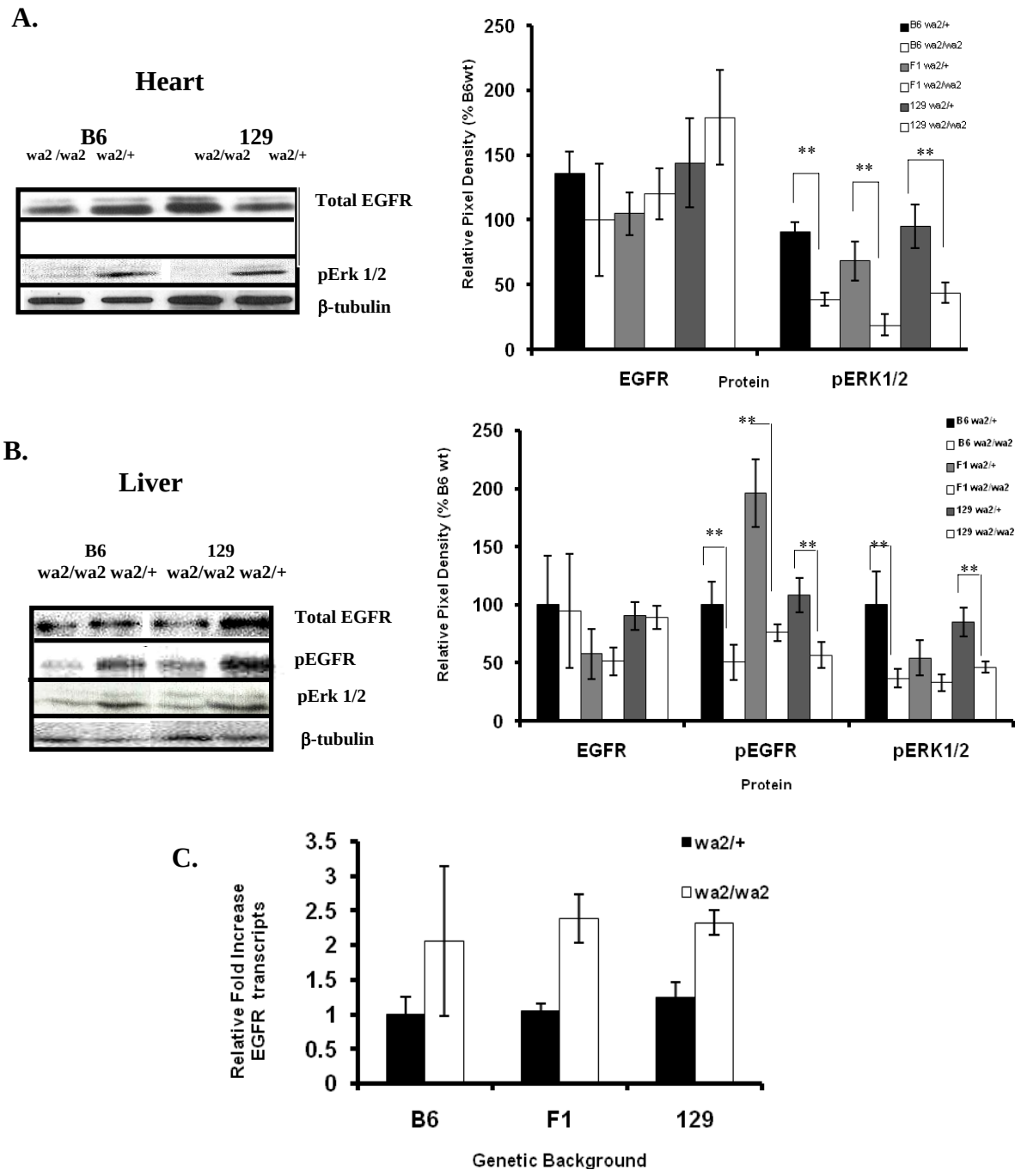

Figure 3-3. Comparison of congenital cardiac defects in B6 and 129 *Egfr* ^{wa2} embryos. A. Endocardial cushions which give rise to the cardiac valves are similar in size and ECM composition in B6 and 129 *Egfr* $^{wa2/wa2}$ 12.5-13.5 dpc embryos. Aortic valves from newborn *Egfr* $^{wa2/wa2}$ mice on both genetic backgrounds also appear similarly affected. B. Additional cardiac defects were detected in B6 *Egfr* $^{wa2/wa2}$ prior to valve defects which likely contribute to early post-natal lethality. A. Heart enlargement was detected as early as 12.5 dpc. Histological analysis of B6 *Egfr* $^{wa2/wa2}$ embryos demonstrated that both left and right ventricular chambers were dilated at this point in development, with some embryos manifesting additional defects such as thinned chamber walls, hypotrabeculation, and ventricular septal defects (VSDs). (A and B, B6 *Egfr* $^{wa2/wa2}$ compared to E and F, B6 *Egfr* $^{wa2/+}$). At E12.5 cardiac cushions were similar in size in *Egfr* $^{wa2/wa2}$ mice on all genetic backgrounds. By PD1, B6 *Egfr* $^{wa2/wa2}$ hearts had visibly enlarged cardiac chambers, with loosely packed cardiomyocytes, and increased apoptosis, particularly in the intraventricular septal wall (Figure C, D, and E, B6 *Egfr* $^{wa2/wa2}$ compared to B6 *Egfr* $^{wa2/+}$ G, H and I; VSD= ventral septal defect, AVC= cardiac cushions contributing to aortic valve).

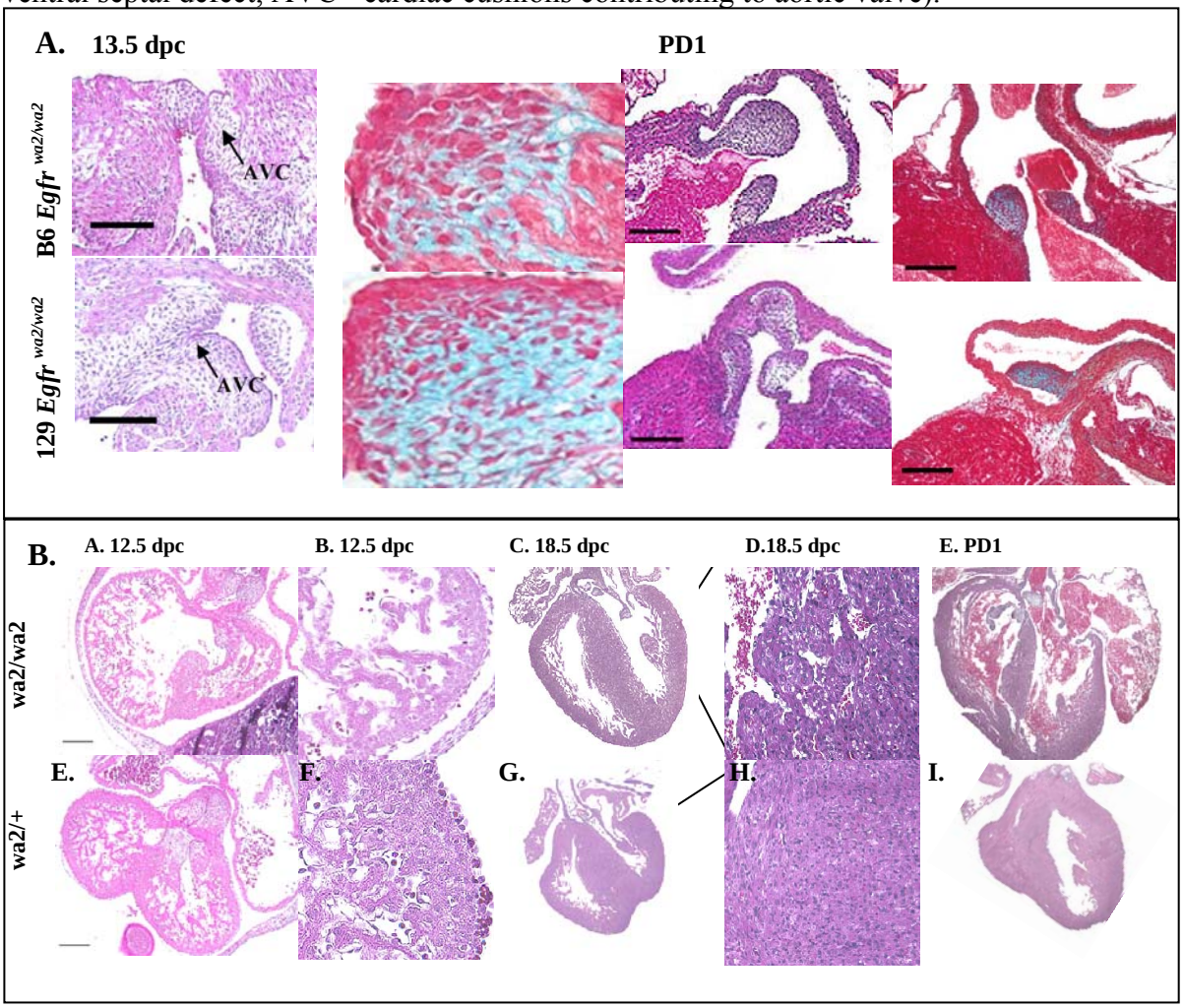

Figure 3-4. Comparison of cardiomyocyte size and cardiac fibrosis in B6 *Egfr* ^{wa2} littermates. A. Comparison of mean cardiomyocyte cross-sectional area in PD1 and 12 week-old B6 *Egfr* ^{wa2} littermates (N=3 and 8 sibling pairs, respectively, 300 cardiomyocytes measured per animal, $**p<0.01$). B. Representative Masson's trichrome stained histological slices from the LV free wall of B6 *Egfr* ^{wa2} littermates (20x magnification). C. Representative short-axis M-mode tracings from three month old B6 *Egf* ^{wa2} littermates**.**

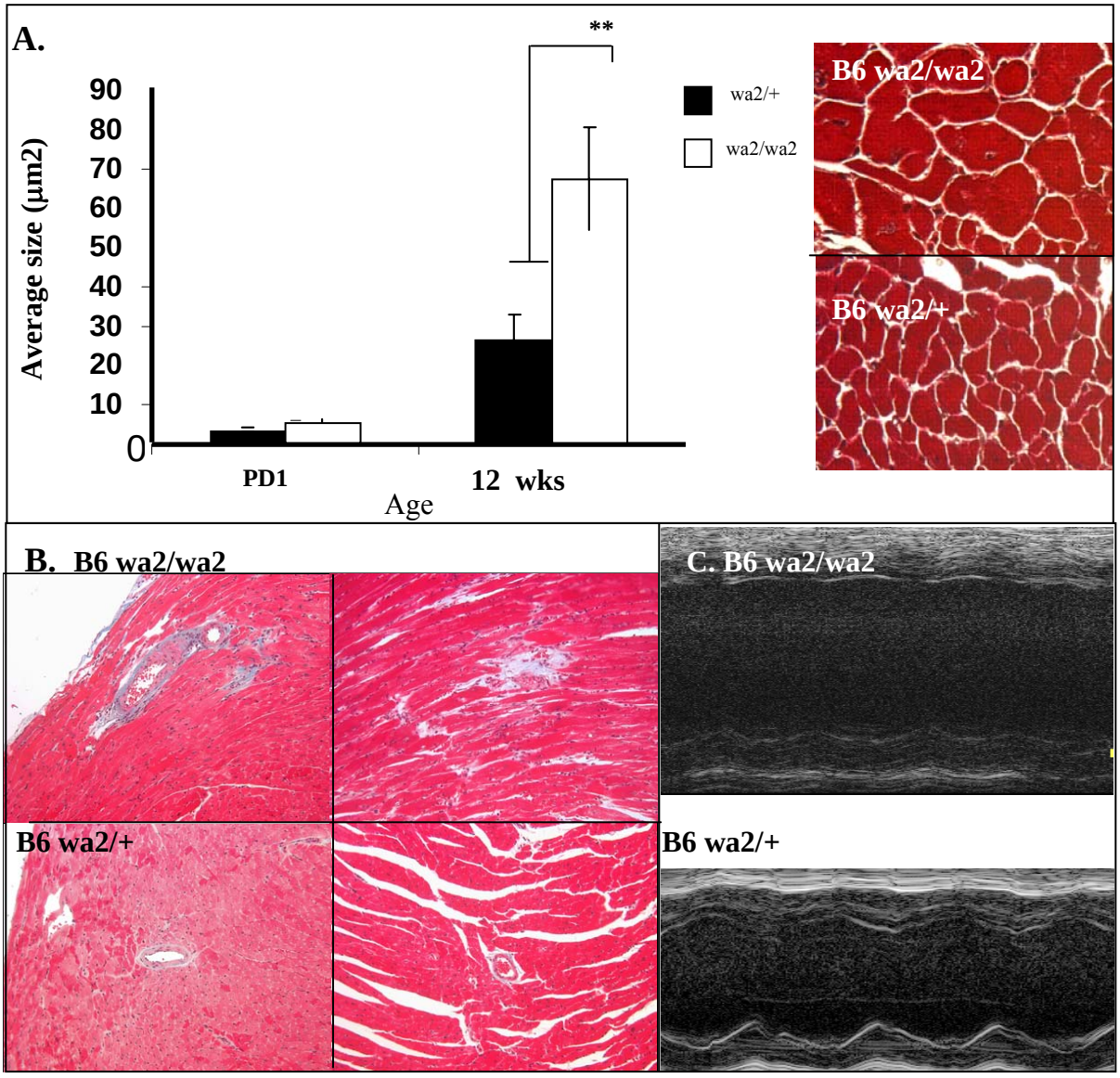

Table 3-2. Measurements of cardiac function from three-to five month old *Egfr* ^{wa2} littermates. Comparison by genotype *$p<0.05$, **$p<0.01$,***$p<0.001$.

Genetic Background	**B6**		**F1**		**129**	
Genotype	wa2/+	wa2/wa2	wa2/+	wa2/wa2	wa2/+	wa2/wa2
N	11	11	8	8	8	8
LVED, d (mm)	3.52±0.06	4.88±0.15***	3.79±0.07	3.73±0.05	3.72±0.05	3.31±0.09
LVED, s (mm)	2.11±0.08	3.43±0.15***	2.29±0.11	2.40±0.07	2.17±0.07	1.83±0.10
LVPWTh, d (mm)	0.97±0.07	1.52±0.09***	0.82±0.02	0.70±0.03*	0.84±0.04	0.74±0.05
LVPWTh, s (mm)	1.34±0.08	2.16±0.10***	1.09±0.02	1.02±0.05	1.19±0.04	1.14±0.08
% FS	40.23±1.70	29.32±1.50***	39.70±2.40	35.69±1.61	41.81±1.19	45.27±2.05
RWT	0.56±0.05	0.63±0.05	0.44±0.01	0.38±0.02*	0.45±0.02	0.47±0.04
HR (BPM)	437±14	430±9	461±15	425±12	470±17	445±13
N	5	5	4	4	4	4
Mean Peak AoVelocity (cm/s)	108±13	371±100*	103±8.1	180±11	98±16	184±44
N	5	15	4	4	7	12
Pressure gradient (mmHg) (catheterization)	-0.40±1.33	22.13±2.87**	3.5±3.01	11.35±5.54	-2.49±3.36	5.59±1.93*

Table 3-3. Blood pressure measurements from three-to five month old *Egfr* ^{wa2} littermates. No significant differences were detected in any parameters by genotype or genetic background.

Genetic Background	**B6**		**129**	
Genotype	wa2/+	wa2/wa2	wa2/+	wa2/wa2
N	7	4	8	8
SYS (mmHg)	119±9	125±7	125±11	133±30
DIAS (mmHg)	90±16	108±11	94±17	106±16
MAP (mmHg)	102±15	110±15	106±14	114±19
HR (BPM)	757±40	734±24	683±42	708±14

Figure 3-5. Comparison of aortic cusp thickness and correlation of aortic cusp thickness and heart weight in *Egfr* ^{wa2} littermates. A. Representative hemotoxylin and eosin stained sections of the thickest region of two cusps of the aortic valves from B6 and 129 *Egfr* ^{wa2} littermates. B. Comparison of mean aortic valve cusp diameter by genotype and genetic background. (**$p<0.01$, *** $p<0.001$) C. Correlation between heart weight and mean cusp thickness by genotype and genetic background.

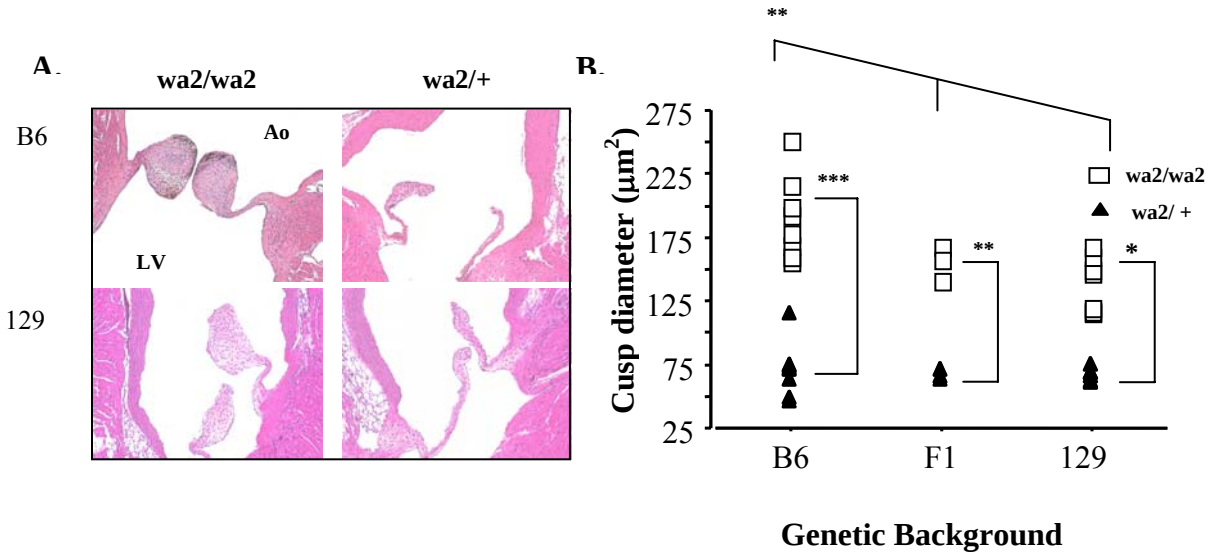

C.

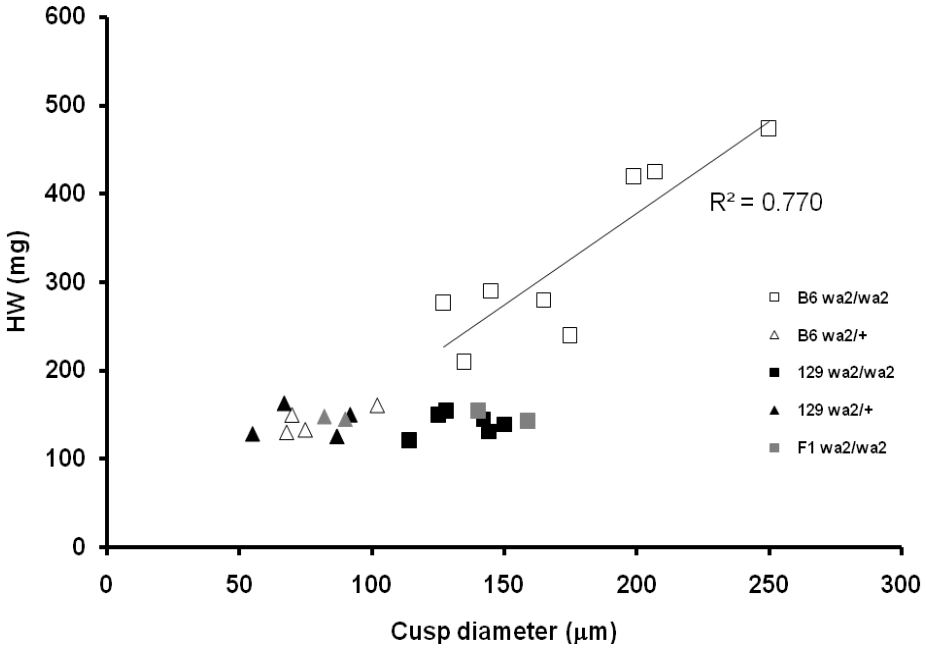

Figure 3-6. Representative Doppler tracings from B6 *Egfr* ^{wa2} littermates and correlation between pressure gradients and mean cusp thickness in *Egfr* ^{wa2}littermates A. Representative Doppler tracings from three-month-old B6 *Egfr* ^{wa2} littermates at the level of the aortic root. B. Correlation between peak systolic pressure (PSP) and mean aortic valve cusp diameter in B6 and 129 *Egfr* ^{wa2} littermates.

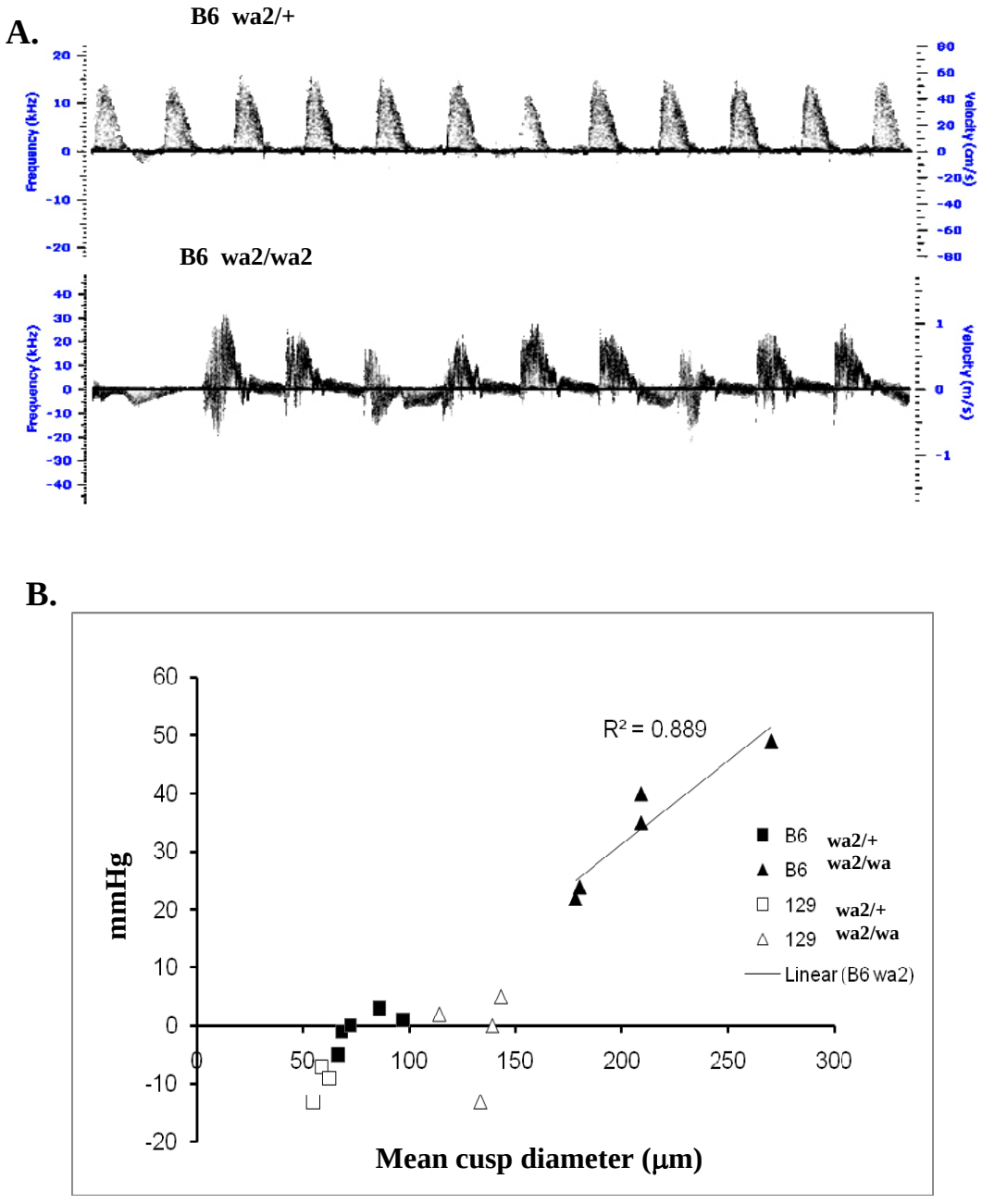

Figure 3-7. Histological comparison of markers for cellular proliferation in aortic cusps from B6 and 129S1 *Egfr* ^{wa2} littermates. A. Comparison of aortic and mitral valves at gross dissection between three-month-old *B6 Tyrc-2J Egfr* ^{wa2} littermates. Cells in the aortic valves of B6 *Egfr* $^{wa2/wa2}$ mice stain positive for PCNA (B) and pERK1/2 (C) (magnification= 20x and 40x, respectively).

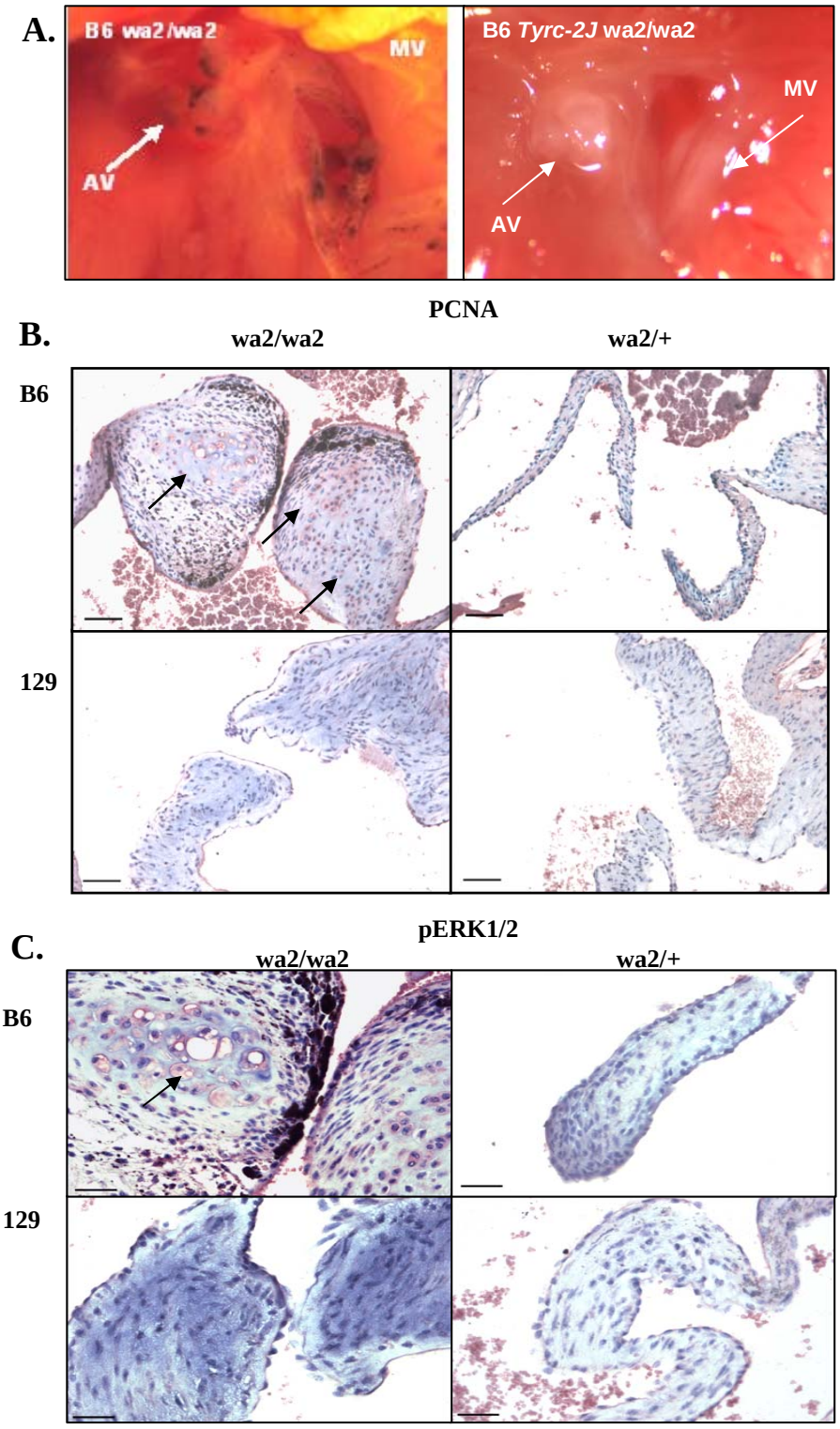

Figure 3-8. Histological comparison of markers for altered extracellular matrix composition, calcification and inflammation in aortic cusps from B6 and 129S1 *Egfr* ^{wa2} littermates. A. Movat's pentachrome stain reveals altered ECM composition in the aortic valves of *B6 Egfr* $^{wa2/wa2}$ mice compared to B6 *Egfr* $^{wa2/+}$ and 129 *Egfr* ^{wa2} mice (magnification= 10x (first panel) and 40x (second and third panels)). Arrows point to cells within the aortic valves of B6 *Egfr* $^{wa2/wa2}$ mice that stained positive for osteopontin (B, magnification=40x). Calcification (black staining) is detected in aortic valves of B6 *Egfr* ^{wa2} littermates (C, magnification=20x). D. Inflammatory cells are detected in the aortic valves of some B6 *Egfr* $^{wa2/wa2}$ mice (blue= DAPI stained nuclei, red= Cy3 labeled MOMA-2 positive cells, magnification= 20x).

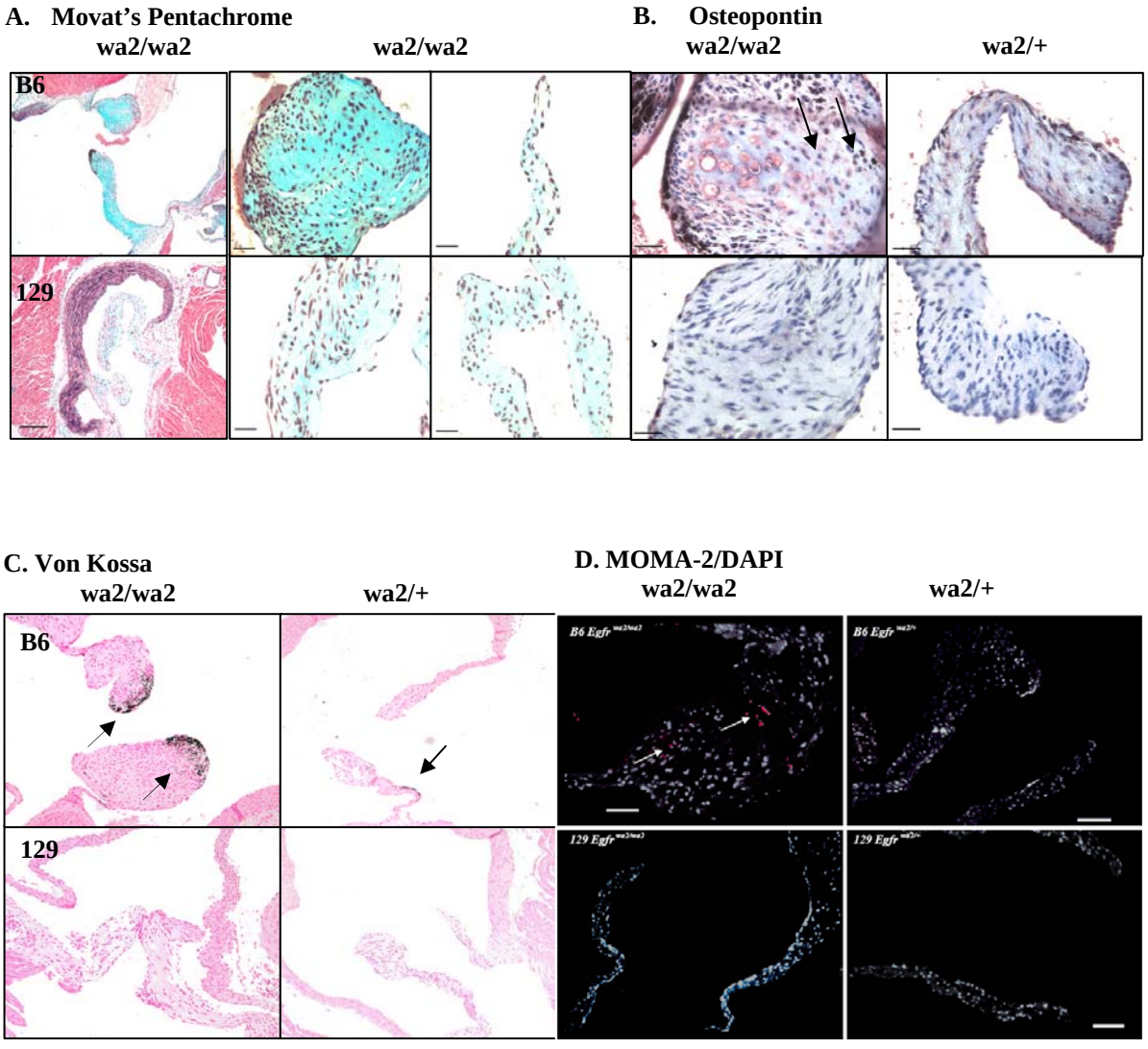

Figure 3-9. Timeline comparing observed cardiac phenotypes in B6 and 129S1 *Egfr* $^{wa2/wa2}$ mice.

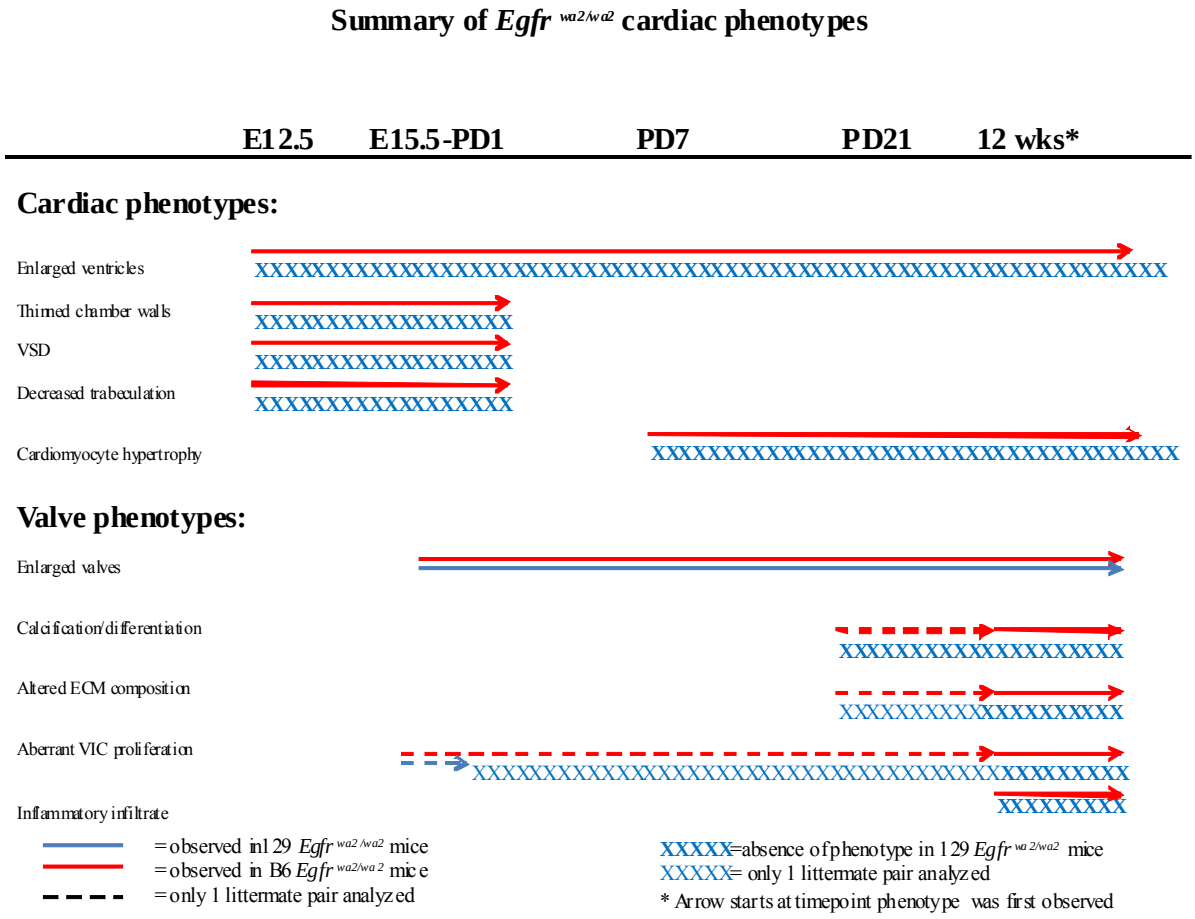

References

1. Bonow, R.O., et al., *ACC/AHA 2006 guidelines for the management of patients with valvular heart disease: a report of the American College of Cardiology/American Heart Association Task Force on Practice Guidelines (writing committee to revise the 1998 Guidelines for the Management of Patients With Valvular Heart Disease): developed in collaboration with the Society of Cardiovascular Anesthesiologists: endorsed by the Society for Cardiovascular Angiography and Interventions and the Society of Thoracic Surgeons.* Circulation, 2006. **114**(5): p. e84-231.

2. Alipour, M.S. and P.A. Shah, *Diagnosis of aortic stenosis in the elderly: role of echocardiography.* Am J Geriatr Cardiol, 2003. **12**(3): p. 201-6.

3. Iivanainen, A.M., et al., *Calcific degeneration of the aortic valve in old age: is the development of flow obstruction predictable?* J Intern Med, 1996. **239**(3): p. 269-73.

4. Iivanainen, A.M., et al., *Natural history of aortic valve stenosis of varying severity in the elderly.* Am J Cardiol, 1996. **78**(1): p. 97-101.

5. Peter, M., et al., *Progression of aortic stenosis. Role of age and concomitant coronary artery disease.* Chest, 1993. **103**(6): p. 1715-9.

6. *From the Centers for Disease Control and Prevention. Public health and aging: trends in aging--United States and worldwide.* Jama, 2003. **289**(11): p. 1371-3.

7. *Trends in aging--United States and worldwide.* MMWR Morb Mortal Wkly Rep, 2003. **52**(6): p. 101-4, 106.

8. Orlowska-Baranowska, E., et al., *Influence of ACE I/D genotypes on left ventricular hypertrophy in aortic stenosis: gender-related differences.* J Heart Valve Dis, 2004. **13**(4): p. 574-81.

9. Novaro, G.M., et al., *Association between apolipoprotein E alleles and calcific valvular heart disease.* Circulation, 2003. **108**(15): p. 1804-8.

10. Knez, I., et al., *Angiotensin-converting enzyme polymorphisms and their potential impact on left ventricular myocardial geometry after aortic valve surgery.* J Heart Valve Dis, 2003. **12**(6): p. 687-95.

11. Ortlepp, J.R., et al., *The vitamin D receptor genotype predisposes to the development of calcific aortic valve stenosis.* Heart, 2001. **85**(6): p. 635-8.

12. Junker, R., et al., *Infant methylenetetrahydrofolate reductase 677TT genotype is a risk factor for congenital heart disease.* Cardiovasc Res, 2001. **51**(2): p. 251-4.

13. Feit, L.R., *Genetics of congenital heart disease: strategies.* Adv Pediatr, 1998. **45**: p. 267-92.

14. Garg, V., *Molecular genetics of aortic valve disease.* Curr Opin Cardiol, 2006. **21**(3): p. 180-4.

15. Cripe, L., et al., *Bicuspid aortic valve is heritable.* J Am Coll Cardiol, 2004. **44**(1): p. 138-43.

16. Garg, V., et al., *Mutations in NOTCH1 cause aortic valve disease.* Nature, 2005. **437**(7056): p. 270-4.

17. Jackson, L.F., et al., *Defective valvulogenesis in HB-EGF and TACE-null mice is associated with aberrant BMP signaling.* Embo J, 2003. **22**(11): p. 2704-16.

18. Rivera-Feliciano, J., et al., *Development of heart valves requires Gata4 expression in endothelial-derived cells.* Development, 2006. **133**(18): p. 3607-18.

19. Kokubo, H., et al., *Targeted disruption of hesr2 results in atrioventricular valve anomalies that lead to heart dysfunction.* Circ Res, 2004. **95**(5): p. 540-7.

20. Zhou, H.M., et al., *Essential role for ADAM19 in cardiovascular morphogenesis.* Mol Cell Biol, 2004. **24**(1): p. 96-104.

21. Delot, E.C., et al., *BMP signaling is required for septation of the outflow tract of the mammalian heart.* Development, 2003. **130**(1): p. 209-20.

22. de la Pompa, J.L., et al., *Role of the NF-ATc transcription factor in morphogenesis of cardiac valves and septum.* Nature, 1998. **392**(6672): p. 182-6.

23. Chen, B., et al., *Mice mutant for Egfr and Shp2 have defective cardiac semilunar valvulogenesis.* Nat Genet, 2000. **24**(3): p. 296-9.

24. Luetteke, N.C., et al., *The mouse waved-2 phenotype results from a point mutation in the EGF receptor tyrosine kinase.* Genes Dev, 1994. **8**(4): p. 399-413.

25. Threadgill, D.W., et al., *Targeted disruption of mouse EGF receptor: effect of genetic background on mutant phenotype.* Science, 1995. **269**(5221): p. 230-4.

26. Sibilia, M. and E.F. Wagner, *Strain-dependent epithelial defects in mice lacking the EGF receptor.* Science, 1995. **269**(5221): p. 234-8.

27. Mrosovsky, N., et al., *Masking in waved-2 mice: EGF receptor control of locomotion questioned.* Chronobiol Int, 2005. **22**(6): p. 963-74.

28. Hagaman, J.R., et al., *An improved technique for tail-cuff blood pressure measurements with dark-tailed mice.* Contemp Top Lab Anim Sci, 2005. **44**(5): p. 43-6.

29. Carson, F.L., *Histotechnology: A self- Instructional text*. 1990, Chicago, Ill: ASCP Press. pp226-227.

30. Burris, H.A., 3rd, et al., *Phase I safety, pharmacokinetics, and clinical activity study of lapatinib (GW572016), a reversible dual inhibitor of epidermal growth factor receptor tyrosine kinases, in heavily pretreated patients with metastatic carcinomas.* J Clin Oncol, 2005. **23**(23): p. 5305-13.

31. Livak, K.J. and T.D. Schmittgen, *Analysis of relative gene expression data using real-time quantitative PCR and the 2(-Delta Delta C(T)) Method.* Methods, 2001. **25**(4): p. 402-8.

32. Satta, J., et al., *Progression of human aortic valve stenosis is associated with tenascin-C expression.* J Am Coll Cardiol, 2002. **39**(1): p. 96-101.

33. Cowell, S.J., et al., *Calcific aortic stenosis: same old story?* Age Ageing, 2004. **33**(6): p. 538-44.

34. Rajamannan, N.M., *Calcific aortic stenosis: a disease ready for prime time.* Circulation, 2006. **114**(19): p. 2007-9.

35. O'Brien, K.D., *Pathogenesis of calcific aortic valve disease: a disease process comes of age (and a good deal more).* Arterioscler Thromb Vasc Biol, 2006. **26**(8): p. 1721-8.

36. Caira, F.C., et al., *Human degenerative valve disease is associated with up-regulation of low-density lipoprotein receptor-related protein 5 receptor-mediated bone formation.* J Am Coll Cardiol, 2006. **47**(8): p. 1707-12.

37. Rajamannan, N.M., et al., *Atorvastatin inhibits calcification and enhances nitric oxide synthase production in the hypercholesterolaemic aortic valve.* Heart, 2005. **91**(6): p. 806-10.

38. Rajamannan, N.M., et al., *Calcified rheumatic valve neoangiogenesis is associated with vascular endothelial growth factor expression and osteoblast-like bone formation.* Circulation, 2005. **111**(24): p. 3296-301.

39. Rajamannan, N.M., *Calcific aortic stenosis: medical and surgical management in the elderly.* Curr Treat Options Cardiovasc Med, 2005. **7**(6): p. 437-42.

40. Makkena, B., et al., *Atorvastatin decreases cellular proliferation and bone matrix expression in the hypercholesterolemic mitral valve.* J Am Coll Cardiol, 2005. **45**(4): p. 631-3.

41. Agno, F.S., et al., *Aortic valve sclerosis is associated with preclinical cardiovascular disease in hypertensive adults: the Hypertension Genetic Epidemiology Network study.* J Hypertens, 2005. **23**(4): p. 867-73.

42. Rajamannan, N.M., *Is it time for medical therapy for aortic valve disease?* Expert Rev Cardiovasc Ther, 2004. **2**(6): p. 845-54.

43. Rajamannan, N.M., et al., *Human aortic valve calcification is associated with an osteoblast phenotype.* Circulation, 2003. **107**(17): p. 2181-4.

44. Rajamannan, N.M., B. Gersh, and R.O. Bonow, *Calcific aortic stenosis: from bench to the bedside--emerging clinical and cellular concepts.* Heart, 2003. **89**(7): p. 801-5.

45. Rajamannan, N.M., W.D. Edwards, and T.C. Spelsberg, *Hypercholesterolemic aortic-valve disease.* N Engl J Med, 2003. **349**(7): p. 717-8.

46. O'Brien, K.D., et al., *Osteopontin is expressed in human aortic valvular lesions.* Circulation, 1995. **92**(8): p. 2163-8.

47. Strunk, K.E., V. Amann, and D.W. Threadgill, *Phenotypic variation resulting from a deficiency of epidermal growth factor receptor in mice is caused by extensive genetic heterogeneity that can be genetically and molecularly partitioned.* Genetics, 2004. **167**(4): p. 1821-32.

48. Bonow, R.O., et al., *ACC/AHA Guidelines for the Management of Patients With Valvular Heart Disease. Executive Summary. A report of the American College of Cardiology/American Heart Association Task Force on Practice Guidelines (Committee on Management of Patients With Valvular Heart Disease).* J Heart Valve Dis, 1998. **7**(6): p. 672-707.

49. Braunwald, E., *Valvular heart disease.* . Harrison's Prinicples of Internal Medicine 14th edition. **Chapter 237** p. p 1318.

50. Weiss, R.M., et al., *Calcific aortic valve stenosis in old hypercholesterolemic mice.* Circulation, 2006. **114**(19): p. 2065-9.

51. Grazette, L.P., et al., *Inhibition of ErbB2 causes mitochondrial dysfunction in cardiomyocytes: implications for herceptin-induced cardiomyopathy.* J Am Coll Cardiol, 2004. **44**(11): p. 2231-8.

52. Delot, E.C., *Control of endocardial cushion and cardiac valve maturation by BMP signaling pathways.* Mol Genet Metab, 2003. **80**(1-2): p. 27-35.

53. Iwamoto, R., et al., *Heparin-binding EGF-like growth factor and ErbB signaling is essential for heart function.* Proc Natl Acad Sci U S A, 2003. **100**(6): p. 3221-6.

54. Rajamannan, N.M. and C.M. Otto, *Targeted therapy to prevent progression of calcific aortic stenosis.* Circulation, 2004. **110**(10): p. 1180-2.
55. Otto, C.M., et al., *Characterization of the early lesion of 'degenerative' valvular aortic stenosis. Histological and immunohistochemical studies.* Circulation, 1994. **90**(2): p. 844-53.
56. Mohler, E.R., 3rd, et al., *Identification and characterization of calcifying valve cells from human and canine aortic valves.* J Heart Valve Dis, 1999. **8**(3): p. 254-60.
57. Sibilia, M., et al., *Mice humanised for the EGF receptor display hypomorphic phenotypes in skin, bone and heart.* Development, 2003. **130**(19): p. 4515-25.
58. O'Brien, K.D., et al., *Apolipoproteins B, (a), and E accumulate in the morphologically early lesion of 'degenerative' valvular aortic stenosis.* Arterioscler Thromb Vasc Biol, 1996. **16**(4): p. 523-32.
59. Stewart, B.F., et al., *Clinical factors associated with calcific aortic valve disease. Cardiovascular Health Study.* J Am Coll Cardiol, 1997. **29**(3): p. 630-4.
60. Ishimori, N., et al., *Quantitative trait loci analysis for plasma HDL-cholesterol concentrations and atherosclerosis susceptibility between inbred mouse strains C57BL/6J and 129S1/SvImJ.* Arterioscler Thromb Vasc Biol, 2004. **24**(1): p. 161-6.
61. Drolet, M.C., et al., *A high fat/high carbohydrate diet induces aortic valve disease in C57BL/6J mice.* J Am Coll Cardiol, 2006. **47**(4): p. 850-5.
62. Lee, K.F., et al., *Requirement for neuregulin receptor erbB2 in neural and cardiac development.* Nature, 1995. **378**(6555): p. 394-8.
63. Carraway, K.L., 3rd, *Involvement of the neuregulins and their receptors in cardiac and neural development.* Bioessays, 1996. **18**(4): p. 263-6.
64. Meyer, D. and C. Birchmeier, *Multiple essential functions of neuregulin in development.* Nature, 1995. **378**(6555): p. 386-90.
65. Zhao, Y.Y., et al., *Neuregulins promote survival and growth of cardiac myocytes. Persistence of ErbB2 and ErbB4 expression in neonatal and adult ventricular myocytes.* J Biol Chem, 1998. **273**(17): p. 10261-9.
66. Crone, S.A., et al., *ErbB2 is essential in the prevention of dilated cardiomyopathy.* Nat Med, 2002. **8**(5): p. 459-65.
67. Ozcelik, C., et al., *Conditional mutation of the ErbB2 (HER2) receptor in cardiomyocytes leads to dilated cardiomyopathy.* Proc Natl Acad Sci U S A, 2002. **99**(13): p. 8880-5.
68. Fukazawa, R., et al., *Neuregulin-1 protects ventricular myocytes from anthracycline-induced apoptosis via erbB4-dependent activation of PI3-kinase/Akt.* J Mol Cell Cardiol, 2003. **35**(12): p. 1473-9.
69. Liu, F.F., et al., *Heterozygous knockout of neuregulin-1 gene in mice exacerbates doxorubicin-induced heart failure.* Am J Physiol Heart Circ Physiol, 2005. **289**(2): p. H660-6.
70. Rohrbach, S., et al., *Neuregulin in cardiac hypertrophy in rats with aortic stenosis. Differential expression of erbB2 and erbB4 receptors.* Circulation, 1999. **100**(4): p. 407-12.
71. Rohrbach, S., et al., *Neuregulin receptors erbB2 and erbB4 in failing human myocardium -- depressed expression and attenuated activation.* Basic Res Cardiol, 2005. **100**(3): p. 240-9.

72. O'Brien, K.E., C.L. O'Bryan, and R. Saad, *Predictors of outcome in asymptomatic aortic stenosis.* N Engl J Med, 2001. **344**(3): p. 227-8; author reply 228-9.

CHAPTER 4

CHRONIC REPRESSION OF EGFR ACTIVITY LEADS TO CARDIAC DYSFUNCTION IN C57BL/6J MICE

Abstract

Increased or constitutive signaling through EGFR/ERBB1 occurs in approximately one third of all human neoplasms and is associated with poor prognosis. EGFR targeted therapy using tyrosine kinase inhibitors (TKIs), which block receptor activity by binding to the ATP binding pocket of the kinase region, has impacted patient survival in several tumor types with oral administration. With these and other advances in drug discovery coupled with improvements in chemotherapy regimen and detection, the 10 year survivorship for many common cancers in the United States has substantially increased over the past two decades. Consequently, more individuals may be exposed to EGFR targeted therapies for longer duration. EGFR, as well as other ERBB family members, play key roles in cardiac development and homeostasis. However, the consequence of chronic suppression of EGFR activity on cardiac physiology is unknown. To address this question, we exposed 6-8 week old C57BL/6J (B6) mice to EKB-569, an irreversible TKI, or AG-1478, a reversible TKI, in chow for three months. Age and sex matched controls received the AIN-93G base diet. Body weight was monitored over the course of the experiment, while cardiac function was evaluated at baseline and prior to sacrifice. Heart, lung, liver and kidney weights were collected at necropsy. Cardiac fibrosis and apoptosis were assessed using the Masson's Trichrome and TUNEL assays while cardiomyocyte size was compared as an indicator of

cardiac hypertrophy. Real time PCR was used to evaluate gene expression of ERBB receptors and ligands (*Egfr*, *Erbb2*, *Egf*, *Nrg1*, and *Dtr*/*Hb-egf*), pro and anti-apoptotic genes (*Bcl2/1*, *Bax*, and *Bad*) and cardiac hypertrophy (*Nppa* and *Nppb*) in the LVs of AG-1478 exposed mice compared to controls. In B6 female mice, chronic dietary exposure to both TKIs depressed body weight gain and caused significant changes in LV wall thickness and cardiac function compared to controls. No significant differences were observed in heart weight or cardiomyocyte size by treatment. Histological analysis revealed increased numbers of TUNEL positive cells in the hearts of TKI-exposed B6 female mice; however this difference was only significant in EKB-569 exposed mice compared to controls. Consistent with histological results, LV apoptotic gene expression was altered, with significant downregulation of the anti-apoptotic gene *Bcl2/1*. Interestingly, there were no significant differences in any of these endpoints in AG-1478 exposed male mice compared to controls. However, the LVs of AG-1478 exposed male mice had significant upregulation of *Egf*, *Erbb2*, and *Nppb* over controls. Taken together, these data suggest that chronic dietary exposure to TKIs may result in pathological and physiological changes in the heart. Additionally, gender may influence susceptibility to TKI mediated toxicity.

Introduction

The EGFR (HER1) is the prototypical and first discovered member of the HER family of membrane receptors, which also includes ERBB2/HER2, ERBB3/HER3 and ERBB4/HER4. These receptors have a conserved molecular structure with an extracellular, cysteine-rich ligand-binding domain, a single alpha-helix transmembrane domain, and an intracellular domain with tyrosine kinase (TK) activity in the carboxy-terminal tail (except ERBB3) [1]. Ligand-binding induces EGFR homodimerization or heterodimerization with

other ERBB receptors and triggers tyrosine kinase catalytic activity. Subsequently, autophosphorylation or transphosphorylation of tyrosine residues in the carboxy-terminal tail produces phosphotyrosine sites where adaptor and docking molecules bind [2]. The net result of intracellular signaling cascades is altered transcription of key molecules involved in a wide range of cellular processes, including proliferation, differentiation, motility, survival, angiogenesis and invasion.

It has been estimated that increased or constitutive signaling through EGFR, occurs in approximately one third of all human neoplasms; moreover, aberrant signaling is associated with poor prognosis including non-responsiveness to traditional chemotherapy and decreased survival [3-5]. Since the EGFR was first proposed as a cancer drug target almost twenty years ago [6-8], advances in drug discovery have produced a plethora of inhibitors targeting specific regions of the receptor. In particular, tyrosine kinase inhibitors (TKIs), which block EGFR activity by competing with adenosine triphosphate (ATP) for binding to the receptor's kinase pocket, have impacted patient survival in several tumor types with oral administration [9]. Two EGFR TKIs, [Gefitinib/Iressa, (AstraZeneca, Wilmington, Delaware) and Erlotinib/Tarceva, (OSI Pharmaceuticals, Uniondale, New York)], have received regulatory approval for use in cancer patients while several others are being evaluated in ongoing clinical trials as mono or combinatorial therapies [10, 11]. With the enormous strides that have been made in cancer therapy, and the resultant increases in life expectancy after diagnoses, certain cancers are now perceived and treated as chronic, rather than terminal, disease [12-16]. Although the side effects of targeted therapies like TKIs are considered mild compared to traditional chemotherapeutics, patients may now be exposed to these drugs for

years rather than months. However, the long-term physiological consequences of suppressed EGFR activity are unknown.

A wealth of evidence has established that all four ERBB family members are essential to normal cardiovascular development [17-25]. A role for ERBB signaling in adult cardiac homeostasis is also emerging. Three of the four receptors (EGFR, ERBB2, and ERBB4) are detected in the adult human and rodent heart; among these ERBB4 appears to be the most abundant [26-29]. The expression and activity of ERBB2/4 receptors is depressed in clinical and experimentally induced heart failure [30-32] and signaling via NRG1/ERBB2/4 activation is critical for adult cardiomyocyte survival [26, 33-35]. The importance of this signaling pathway in normal cardiac physiology was not fully recognized until the unexpected and lethal cardiomyopathy reported in breast cancer clinical trials using trastuzmab (Herceptin, Genetech San Francisco, CA), a humanized monoclonal antibody targeting ERBB2 [35-38]. Subsequently, mouse models with ventricular specific deletion of ERBB2 or ERBB4 were found to recapitulate the cardiac phenotype observed in clinical trials [39-41]. More recently, signaling through EGFR also was shown to impact cardiomyocyte hypertrophy and survival as well as provide cardioprotection against stress-induced injury [42-46]. However, to date, no *in vivo* studies have specifically assessed the effects of chronically reduced EGFR activity (as might be expected with continuous drug exposure to TKIs) on adult cardiac function. To address this question, we used EKB-569 (6,7 disubstituted 4-anilinoquinoline-3-carbonitrile, Wyeth Pharmaceuticals, Collegeville, Pennsylvania) a selective irreversible TKI currently in clinical trials [47, 48], and AG-1478 (4-3-chloroamlino-6,7, dimethoxyquinazoline) a reversible TKI demonstrated to selectively

inhibit EGFR in various experimental systems [49-52], to assess the effects of chronic oral exposure to these drugs on cardiac function and pathology in C57BL/6J (B6) mice.

Materials and Methods

Animals and diet. B6 mice (6-8 weeks old) of both sexes were weighed, randomly distributed to treatment groups, and received either AIN-93G (Bioserve, Frenchtown, New York) control chow (controls, n=11 females and 4 males) or AIN chow containing the EGFR small molecule inhibitors EKB-569 (150 mg/kg of food, n=8, female) or AG-1478 (144 mg/kg of food, n=6 females and 4 males) equivalent to 20 and 19.2 mg/kg/mouse/day. Mice were housed together for the duration of the studies, and were maintained on these diets *ad libitum* for 90 days, then sacrificed (all protocols approved by institutional animal care and use committee). Body weights were measured at baseline and at approximately 15 days, 30 days, 60 days, and 90 days of treatment.

Pharmacologic Treatment of *Apc* $^{Min/+}$ mice. B6-*Apc*^{Min} mice were obtained from The Jackson Laboratory (Jackson Laboratories, Bar Harbor, Maine). Mice were genotyped for *Apc*^{Min} alleles as reported [53]. Starting at weaning, male and female *Apc* $^{Min/+}$ littermates were fed either AG-1478 or control diets as described above *ad libitum*. Animals euthanized at three months of age and gastrointestinal (GI) tracts were processed as described below.

Macroadenoma Counts. The GI tract from pylorus to rectum was removed. Small intestine was cut into thirds, and the caecum and colon were separated. Segments were gently flushed with PBS to remove fecal material, cut longitudinally, splayed flat on Whatmann 3MM paper, and fixed overnight at 4°C in 4% paraformaldeyhyde. Polyp counts and diameter measurements were made under a dissection microscope with an in-scope micrometer, allowing detection of polyps >0.3 mm in diameter.

Echocardiography. Transthoracic echocardiography (TTE) was performed at baseline and prior to sacrifice using a 30 mHz probe and the Vevo 660 Ultrasonograph (VisualSonics, Toronto, Canada). Mice were lightly anaesthetized with 1-1.5% isofluorane and a topical depilatory agent applied, before placing in the left lateral decubitus position under a heat lamp to maintain body temperature at 37°C. Heart rate was maintained between 450-500 BPM. Two dimensional short and long axis views of the left ventricle were obtained. M-mode tracings were recorded and used to determine LV end-diastolic diameter (LVED,d), LV end systolic diameter (LVED,s), LV posterior wall thickness diastole (LVPWThD) and LV posterior wall thickness systole (LVPWThS) over three cardiac cycles. LV fractional shortening was calculated using the formula % FS= (LVED,d-LVED,s)/(LVED,s).

Histology. At necropsy, hearts, lungs, liver, and kidneys were dissected from mice of each treatment group, rinsed in PBS and weighed. Hearts were cut in cross-section just below the level of the papillary muscle. For assessment of cardiomyocyte size, and fibrosis, the top half of the heart was formalin-fixed and embedded in paraffin. Sections (5 μm) were prepared at 200 μm intervals. The sections were stained with hematoxylin and eosin (H&E) for examination of gross appearance, while Masson's Trichrome (MT) was employed to facilitate visualization of fibrosis, aortic valve size and cardiomyocyte size. Cardiomyocyte hypertrophy was assessed by measuring cross-sectional area of 100 cardiomyocytes per PAS-H stained section in ten randomly selected fields having nearly circular capillary profiles and centered nuclei in the left ventricular free wall. Histological images were analyzed using Nova Prime 6.75.10 software (BioQuant Image Analysis, San Diego, California). For measurement of cardiac valve size and calcification, serial sagittal sections (5 μm) were collected from each treatment group. Von Kossa's method was used as a marker of

calcification.(http://www.medlib.med.utah.edu/WebPath/HISTHTML/MANUALS; [54]

Gene expression. Total RNA was extracted from the lower half of the LV using TRIzol (Invitrogen, Carlsbad, California). After DNAse treatment, 500 ng of total RNA was reverse transcribed using the High Capacity cDNA Archive Kit (Applied Biosystems, Foster City, California). The expression of classic hypertrophy markers [(atrial nautriuretic peptide (*Nppa*) and brain nautriuretic peptide (*Nppb*))], pro and anti-apoptotic members (*Bcl2/1*, *Bax* and *Bad*), and selected ERBB receptors and ligands (*Egf*, *Nrg1*, *Dtr/Hb-Egf*, *Erbb1* and *Erbb2*) was determined by real-time quantitative PCR (qPCR) using Taqman Univeral Master Mix and Assays-on Demand primers and probes (Applied Biosystems, Foster City, California). Results are represented as mean fold changes relative control groups. Reactions were run on a Stratagene MX3000P machine with analysis software. Threshold values (C_T) were determined by an in-program algorithm assigning a fluorescence baseline based on readings prior to exponential amplification. Fold change in expression was calculated using the $2^{-\Delta\Delta cT}$ method [55] using the gene β–actin as an endogenous control. Similar results were obtained using *GusB* as an endogenous control.

***In vivo* phosphorylation assays.** B6 mice maintained on the respective diets for approximately 90 days were injected subcutaneously with 5 μg/g body weight of EGF (R&D Systems, Minneapolis, Minnesota) in PBS. After 10 minutes, livers and hearts were harvested, frozen in liquid nitrogen, and stored at -80°C. The frozen tissues were sonicated in 5–10 volumes (5–10 ml/g tissue) of lysis buffer consisting of 20 mM HEPES, pH 7.4, 150 mM NaCl, 10% glycerol, 1% Triton X-100, 1 mM PMSF, 10 μg/ml of leupeptin, 10 μg/ml of aprotinin, 1 mM sodium vanadate, and 10 mM β-glycerophosphate at 4°C. The tissue lysates were cleared by centrifugation for 10 min at 4°C and protein concentrations were determined

by the Bradford assay (Bio-Rad, Hercules, California). An equal amount of protein lysate (15 μg, liver and 30 μg, heart) was separated by denaturing 7.5% sodium dodecylsulfate polyacrylamide gel electrophoresis (SDS-PAGE) and transferred to PVDF membranes (Bio-Rad, Hercules, California). Protein blots were incubated overnight at 4°C with EGFR ab-17 polyclonal rabbit antibody (RB-1417-P1, LABVISION/Neomarker, Freemont, California), polyclonal rabbit phospho-EGFR (Tyr1086) antibody (36-9700, Zymed, San Fransico, California), or polyclonal rabbit phospho-p44/42 MAP Kinase (Thr202/Tyr204) antibody (Cell Signaling, Danvers, Massachusetts) followed by incubation goat anti-rabbit horseradish peroxidase conjugated antibody (#1858413, Pierce, Rockford, Illinois) and detected with an enhanced chemiluminesence system (Amersham Pharmacia/GE Healthcare).

Statistical analysis. Data is presented as mean+/-SEM. Data from control groups was pooled where there was no significant difference between parameters. The Mann-Whitney or unpaired student's t-test was used to compare data between respective treatment and control groups. The Kruskal-Wallis test or analysis of variance (ANOVA) was used to detect significance by treatment. All was performed using the StatView (SAS, Cary, North Carolina) program. A $p<0.05$ is considered statistically significant.

Results

Dietary exposure to AG-1478 is biologically effective. Previous reports using the *Apc* $^{Min/+}$ mouse model of familial colorectal cancer demonstrated that dietary exposure to irreversible EGFR small molecule inhibitors EKB-785 or EKB-569 dramatically inhibited intestinal polyp formation [56, 57]. Although the reversible EGFR inhibitor AG-1478 has been used extensively and effectively with numerous *in vitro* and *in vivo* models of carcinogenesis, to

our knowledge it has not been used in this exposure regimen. To determine if dietary exposure to AG-1478 would elicit a significant biological response, recently weaned B6 *Apc* $^{Min/+}$ littermates were fed chow containing AG-1478 (144 mg/kg; equivalent to approximately 19.2 mg/kg/day, n=6) or base diet alone (n=6) *ad libitum* for 30 days after which their intestinal tracts were removed and the number of intestinal tumors counted under a dissecting microscope. AG-1478 was sufficient to reduce polyp number by 45% compared to controls (Table 4-1). This amount of protection was less than that reported for EKB-569 (at 20 mg/kg/day, 87% reduction in polyp number), but almost identical to protection by EKI-785 (at 40 mg/kg/day, 50% reduction in polyp number) under similar experimental conditions [56]. This preliminary experiment established the anti-tumor efficacy of AG-1478 in *Apc* $^{Min/+}$ mice, and demonstrated that dietary delivery was an effective route.

Dietary exposure to AG-1478 inhibits EGFR tyrosine kinase activity. Since pharmacokinetic studies in wild-type mice reported ^{3}H AG-1478 tissue distribution to be highest in liver, which also has the highest EGFR expression levels and phosphorylated protein content, we examined protein levels of EGFR, ERK1/2 and their phosphorylated forms in liver lysates from wild-type B6 mice fed either control or AG-1478 diets to confirm that EGFR activity was being suppressed [49]. Mice were injected with rhEGF (5μg/g BW) prior to sacrifice. As seen in Figure 4-1, AG-1478 treatment reduced phospho-EGFR and phospho ERK1/2 protein levels in livers from wild-type B6 mice although EGFR total protein was similar to controls (Figure 4-1).

Toxicology endpoints. Female wild-type B6 mice chronically exposed to small molecule EGFR inhibitors exhibited depressed weight gain over the course of the experiment compared to controls (Figure 4-2). After 90 days of treatment, EKB-569 treated mice had lost

almost 6% of their starting body weight while their respective controls gained approximately 16% over baseline body weights. Although AG-1478 and respective control groups gained weight over the course of the experiment, drug treatment retarded weight gain (37.89±1.25 controls, versus 29.08±7.20 AG-1478). Altered body weight suggested alterations in feeding behavior, energy expenditure or mild toxicity at these drug concentrations; however, there were no signs of dehydration, lethargy or ataxia in any treatment groups.

There were no significant differences in wet heart, liver, or kidney weight by treatment groups. (Table 4-2 and data not shown). However, EKB-569 treated mice had increased wet lung weights (147.85±6.30 control versus 184.30±10.80 EKB-569, $p<0.05$), which remained significant when normalized for body weight (6.94±0.48 control versus 9.67±0.28 EKB-569, $p<0.05$). Since interstitial lung disease has been reported in a subset of patients treated with the EGFR small molecule inhibitor gefitinib [58], we used MTC stain to visually inspect changes in collagen production in lungs from these mice. However, histological analysis did not reveal any obvious differences by treatment group.

Cardiovascular function. Chronic dietary exposure to EGFR small molecule inhibitors led to significantly altered cardiac function (assessed by TTE) although the severity varied by drug formula (Table 4-3). Both EGFR inhibitors caused increased left ventricular end diastolic and systolic dimensions and reduced contractility (as estimated by percent fractional shortening, %FS) compared to baseline values or control values, with EKB-569 having the greatest effect on LV wall thickness. Consistent with echocardiographic data, H&E stained cross sections taken at the level of the papillary muscle also showed morphological evidence of LV and septal wall thinning (Figure 4-3 A).

Cardiopathology and LV gene expression changes. Because significant alterations were seen in cardiac function with drug treatment, we conducted histological analysis of cardiac sections to investigate pathological endpoints such as cardiomyocyte hypertrophy, fibrosis, and apoptosis. Consistent with heart weight data, there were no significant differences in mean cardiomyocyte area or in gene expression of the classic hypertrophy markers natriuretic peptide precursors A and B (*Nppa*, *Nppb)* in the LV by treatment (data not shown). There were also no significant differences in LV gene expression of selected *Erbb* family members and ligands (*Erbb1*, *Erbb2*, epidermal growth factor (*Egf)*, neuregulin 1 (*Nrg1)*, diphtheria toxin receptor/ heparin-binding EGF-like growth factor (*Dtr/Hbegf)*, data not shown). Interstitial fibrosis, as demonstrated by Masson's Trichrome stain, was observed in the LV walls of 25% (2/8) EKB-569 and 50% (3/6) of AG-1478 treated mice. Mild fibrosis was also observed in 20% (2/10) of controls (representative slices shown in Figure 4-3 A)**.** Interestingly, both inhibitors increased the number of TUNEL-positive cardiac cells (Figure 4-3 B and C) with apoptotic cells located in the LV walls, LV papillary muscle, and left atria (20.98±5.40 EKB-569 versus 16.64±3.87 AG-1478, and 6.43±1.95 Control, TUNEL positive cells/cm^2*, $p<0.07$*). Consistent with TUNEL assay, altered expression of apoptotic genes was observed in the LV of inhibitor-treated mice relative to controls (Figure 4-3 D). Specifically, expression of the anti-apoptotic gene *Bcl2/1* was suppressed by approximately 50% (*$p<0.05$*) while pro-apoptotic genes *Bad* and *Bax* were non-significantly upregulated and downregulated, respectively.

Since earlier evidence suggested that EGFR activity is critical for normal semilunar valve development [18], we investigated the effects of chronic exposure to EGFR inhibitors on morphological and histological changes in cardiac valves. Results from the initial cohort

using EKB-569 suggested that reduced EGFR activity might trigger excessive ECM production and calcification in adult valves. All EKB-569 treated mice (8/8) but less than half of the control mice (3/8) had evidence of cardiac valve calcification by von Kossa stain (examples shown in Figure 4-4 A), however, all B6 female mice from respective control and AG-1478 groups had some evidence of calcification. Interestingly, there was a significant dietary effect on mean valve thickness (AG-1478 (n=6) 0.15±0.01 μm versus EKB-569 (n=5) 0.12±0.014μm versus Control (n=6) 0.95±0.02 μm, ANOVA $p<0.04$, Figure 4-4 B). For comparison, mean valve thickness for 16 week-old B6 male mice maintained on normal chow (NC) is also shown. Since the synthetic AIN-93G diet has higher fat content than regular chow (11% AIN-93G versus 5% NC) and B6 mice are known to be prone to valvulopathy induced by high fat diet [59], it is possible that the effects of the small molecule inhibitors on valvular pathology were confounded by dietary fat content. Thus, we are unable to draw conclusions about a correlation between chronic suppression of EGFR activity and valvulopathy.

Gender specific effects of AG-1478. It is well established that gender dramatically influences physiological and pathological responses to xenobiotics. To determine if chronic EGFR inhibition affected males differently than females, a smaller cohort of 6-8 week old male B6 mice were fed AG-1478 or control diets (n=4 per group) under identical conditions. Male mice had no significant differences in body weight gain, organ weights or cardiovascular function after 90 days of treatment, nor significant differences in cardiac pathology (no evidence of fibrosis, cellular necrosis, or increased apoptosis). Aortic valves appeared to be enlarged with AG-1478 treatment, but this did not reach significance (Figure 4-5 A). There were no significant changes in cardiac expression of apoptotic genes (*Bcl2/1*,

Bax or *Bad*) by treatment groups. However, the hypertrophy marker *Nppb* was upregulated in the hearts of AG-1478 treated male mice, despite the fact that mean cardiomyocyte area was smaller. *Erbb2* and *Egf* transcripts were also upregulated compared to controls (Figure 4-5 B).

Discussion

To our knowledge, this is the first study to extensively evaluate cardiac function and pathology with chronic oral exposure to EGFR TKIs in healthy adult mice. Consistent with earlier reports using TKIs EKB-569 or EKI-785 [56], we demonstrated that dietary delivery of EGFR small molecule inhibitor AG-1478 effectively repressed EGFR-kinase activity and tumorigenesis *in vivo*. Employing AG-1478 and EKB-569, potent TKIs from different chemical classes, we found marked changes in weight gain and cardiac function in B6 female mice with chronic dietary exposure. Drug exposure also resulted in pathological changes in the heart. Most notably, the number of TUNEL positive cells was increased by approximately three-fold in the hearts of AG-1478 treated female B6 mice over controls, and was supported molecularly by significantly decreased expression of the anti-apoptotic gene *Bcl2/1* in cardiac tissue from these animals compared to controls. We also found some histological evidence of pathological changes in cardiac valves of TKI-exposed mice, however, additional studies with larger numbers are needed to rule out possible confounding effects of the synthetic base diet.

Results of our studies also imply that EKB-569 may be more toxic than AG-1478 in female mice. EKB-569 exposure resulted in body weight loss, compared to suppression of body weight gain with AG-1478 treatment. Interestingly, reports from Phase I clinical trials reported anorexia in ~ 20% of patients receiving intermittent doses of EKB-569 [48].

Although AG-1478 caused greater depression in systolic function, hearts from EKB-569 treated mice had thinner LV walls and significantly more TUNEL positive cells per square centimeter compared to controls. Despite milder changes in cardiac contractility, wet lung weights were significantly increased with EKB-569 exposure. Although we did not see evidence of increased fibrosis or pulmonary congestion, it is important to note that interstitial lung disease has been reported in a subset of patients receiving gefinitib in non-small cell lung cancer clinical trials [60-62].

Although our observations are limited by small numbers, gender may influence response to TKIs, as we saw no differences in physiological and pathological parameters by treatment in male B6 mice that were significantly different in inhibitor-treated B6 female mice as compared to controls. We detected no significant differences by gender or treatment in cardiac EGFR expression, however, sexual dimorphism in basal EGF levels has been reported with male mice having higher protein levels in salivary glands [63] and higher transcript levels in pituitary glands [64] compared to females. Since we found that *Egf, Erbb2,* and *Nppb* transcripts were upregulated in the LV of male, but not female, AG-1478 exposed mice relative to respective controls, it is possible that incr**e**ased expression of these genes in the heart, coupled with higher circulating ligand levels, may compensate for reduced EGFR activity and contribute to the observed gender-specific effects.

Differences between mode of inhibition, potency and selectivity between the two TKIs used in our experimental regimen may account for the discrepancy in toxicity. EKB-569 is an irreversible inhibitor, forming a covalent bond with the Cys 773 residue within the EGFR catalytic domain, while AG-1478 is a competitive inhibitor of ATP binding [47]. With irreversible inhibition, normal levels of EGFR activity are only recovered after gene

transcription and translation. Recent findings suggest irreversible inhibitors may prevent the acquired resistance seen in non-small cell lung cancer patients treated with competitive inhibitors such as gefitinib and erlontinib [65, 66]. While these properties are promising for cancer therapy, irreversible TKIs may adversely affect cardiomyocyte function and survival, since EGFR transcript levels are normally very low in the adult mouse and human heart. The AG-1478 diet resulted in an approximately 45% reduction in polyp number, while at approximately the same concentration in identical base chow, EKB-569 caused about 87% reduction in polyp number in the *Apc* ^{Min} mouse model [56]. A single oral dose of EKB-569 (10 mg/kg) was previously reported to rapidly inhibit EGFR kinase activity by 90% while multiple oral doses of AG-1478 (126 μM/kg) decreased phosphorylation of EGFR and ERK1/2 by approximately 60% and 50%, respectively, in xenograft studies [49]. This data suggests that EKB-569 is more potent than AG-1478 in these systems.

Since ERBB2/HER2 and EGFR have a high sequence homology in their catalytic domains [67-69], it is not surprising that many TKIs suppress activity of both receptors. In cell free systems, AG-1478 showed higher selectivity for EGFR over ERBB2/HER2 (IC_{50}, 3 nM EGFR versus >100 μM ERBB2/HER2) than EKB-569 ($IC_{50,}$ 0.08 μM EGFR versus 1.23 μM for ERBB2/HER2) [9] [70]. In cell based assays using human carcinoma cell lines which overexpress EGFR (A431) or ERBB2/HER2 (SKBR3), the IC_{50} for EKB-569 was 0.03 μg/mL and 0.007 μg/mL, respectively, consistent with effective inhibition of both receptors. Mice with myocardium-specific gene targeting reducing myocardial *Erbb2* expression by 70% had a significant increase in cardiomyocyte apoptosis with anthracycline exposure [39]. Moreover, gene therapy with over-expression of *Bcl2/1* partially rescued the dilated cardiomyopathy in these mice. Recent data also demonstrated similarly depressed

Bcl2/1 expression, cardiomyocyte apoptosis, and mitochondrial dysfunction in isolated cardiomyocytes with exposure to the anti-ERBB2 drug Herceptin (Trastumizab)[71]. Given the well documented roles of ERBB2 and ERBB4 signaling in cardiomyocyte survival, it is possible that greater cardiac cell death and LV dilatation observed with EKB-569 exposure reflects greater inhibition of ERBB2 and/or ERBB4 signaling, or other off-target effects.

Consistent with growing literature underscoring the cardioprotective roles of ERBB signaling *in vitro* and *in vivo*, our studies suggest that prolonged exposure to TKIs targeting EGFR may compromise cardiac function. Recent analysis documents a major increase in the 10 year survivorship for many common cancers in the US compared to the late 1980's, thus more individuals may be exposed to TKIs and other chemotherapeutics for a longer duration [72]. Although overall, the side-effects of targeted therapies such as the TKIs are well-tolerated compared to older chemotherapeutic drugs, these studies imply that, as with Herceptin therapy, cardiovascular function should be monitored with chronic exposure to these drugs.

Table 4-1. Dietary exposure to AG1478 significantly reduces polyp count in *Apc*$^{Min/+}$ mice. $^{**}p<0.01$

Diet	N^a	Polyp count	% control
AG1478	6	23.7±5.8**	55.4%
Control	6	53.1±14.8	100%

Figure 4-1. Immunoblot analysis of liver lysates from wild-type B6 mice exposed to the EGFR small molecule inhibitor AG-1478 in AIN 93G diet (AG-1478) or AIN 93G diet (Control) for three months. Mice were dosed with recombinant EGF (5 μg/kg) 10 minutes prior to sacrifice.

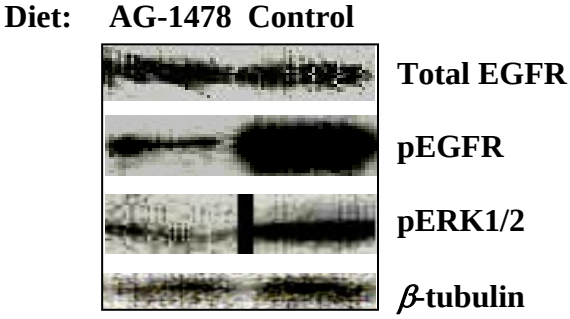

Figure 4- 2. Effects of dietary exposure to EGFR inhibitors on weight gain in B6 female mice**.** EKB-569 (A) or AG-1478 (B) exposure repressed weight gain in B6 female mice compared to controls. *$p<0.05$,**$p<0.01$, ***$p<0.001$

A. EKB-569 Body weight

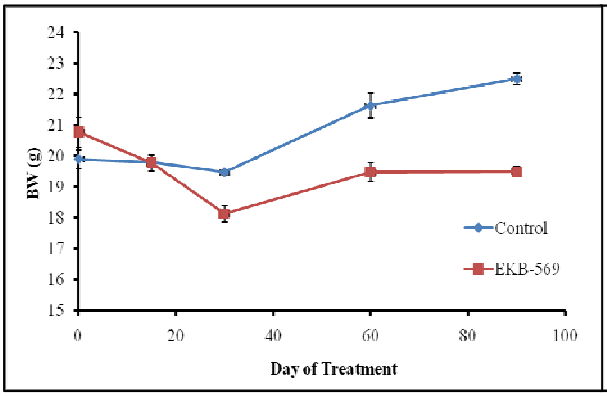

A EKB-569 Percent Increase in BW over baseline

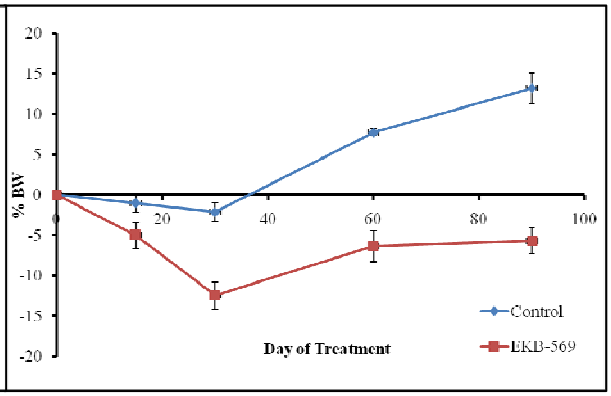

B. AG-1478 Body weight

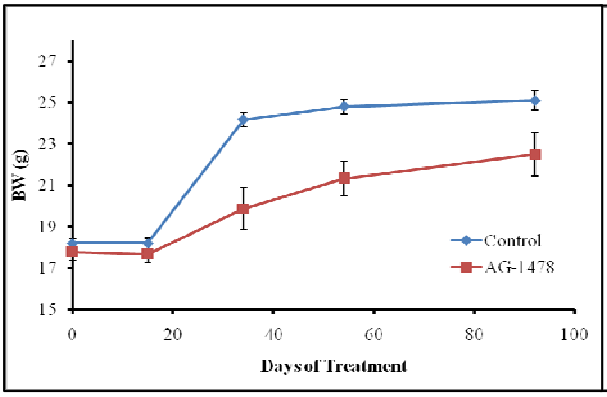

B. AG-1478 Percent Increase in BW over baseline

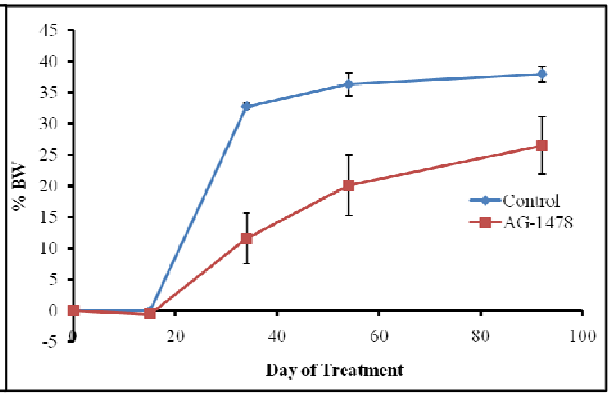

Table 4- 2. Organ and body weights of EGFR inhibitor exposed mice compared to controls. *$*p<0.05$,$**p<0.01$* compared to respective controls. BW, body weight, HW, heart weight, LuW, lung weight, H:BW, normalized heart weight, Lu:BW, normalized lung weight.

Treatment	N	BW (g)	HW [73]	LuW [73]	H:BW (mg:g)	Lu:BW (mg:g)
Control	8	22.04±0.40	121.93±6.0	147.85±10.80	5.74±0.31	6.94±0.48
EKB-569	8	19.65±0.21**	112.61±5.73	184.25±10.85*	5.64±0.26	9.67±0.28*
Control	3	24.67±0.33	155.3±10.33	174.00±14.60	6.31±0.47	7.05±0.57
AG-1478	5	22.50±1.05	141.20±12.08	172.29±13.55	6.30±0.53	7.78±0.86

Table 4-3. Echocardiographic parameters measured at baseline and after approximately 90 days on respective diets. *$p<0.05$, Inhibitor versus Baseline**$p<0.01$, Inhibitor versus Baseline £ $p<0.05$; Inhibitor versus Control, ¥ $p<0.01$; Inhibitor versus Control, δ $p<0.05$; EKB-569 versus AG-1478. LVED,d, left ventricular end diastolic diameter, LVPWTh,d, left ventricular posterior diastolic wall thickness, %FS, Percent fractional shortening, HR, heart rate.

Treatment	N	LVED,d	LVPWTh,d	%FS	HR
Baseline	16	3.40±0.07	0.70±0.08	39.80±2.38	455±20
Control	6	3.35±0.08	0.81±0.07	42.42±5.53	467±15
EKB-569	5	**3.58±0.05**$^{*,£}$	**0.59±0.03**$^{£δ}$	**36.24±2.10**$^{£}$	444±30
AG-1478	5	**3.60±0.27**$^{£}$	0.75±0.13	**29.34±2.56**$^{¥}$	452±12
ANOVA	p<	0.05	0.01	ns	ns

Figure 4-3. Pathological changes in the hearts of B6 mice chronically exposed to EGFR inhibitors. LV wall thinning and interstitial fibrosis (A) and increased apoptosis (B) were observed in the hearts of TKI exposed mice. C. Gene expression of proapoptotic and anti-apoptotic genes. *$p<0.05$

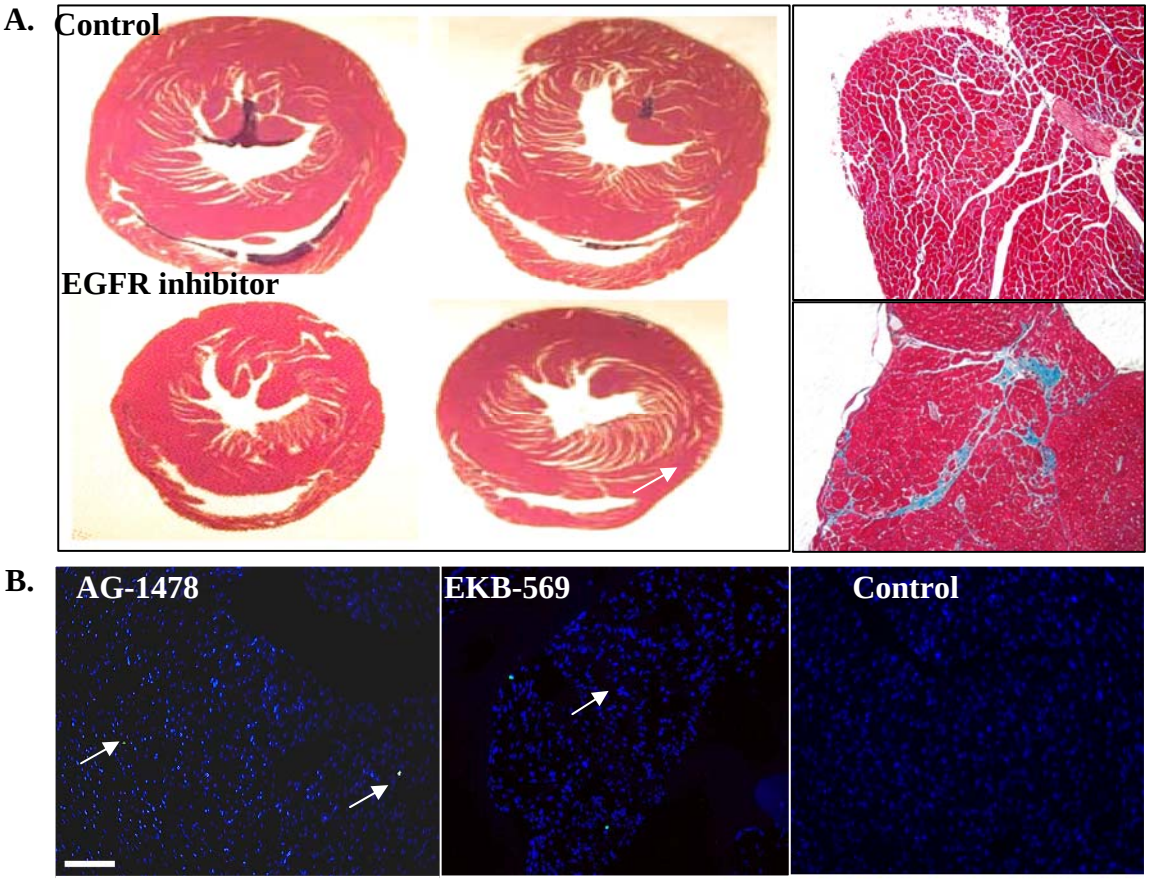

Figure 4-4. Valvular changes in the hearts of EGFR inhibitor-exposed B6 mice compared to mice fed normal chow. Valvular changes, such as calcification (detected by von Kossa stain, A) and increased aortic cusp thickness (B) were observed in the hearts of EGFR inhibitor-exposed B6 mice compared to mice fed normal chow (NC) or control (AIN-93G) chow. Arrows in A indicate positive staining for calcium deposition. NC= normal chow, **p<0.05.* Bar= 100 μm.

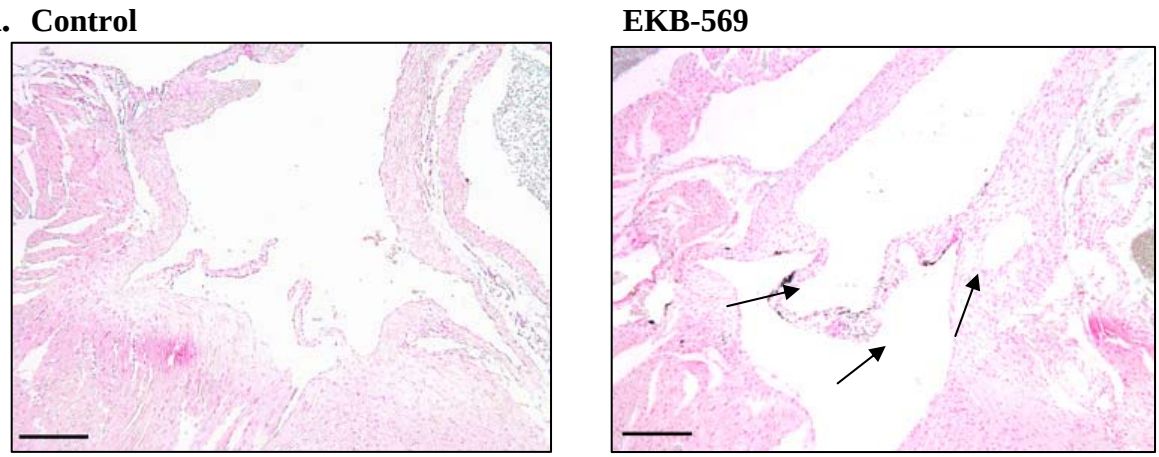

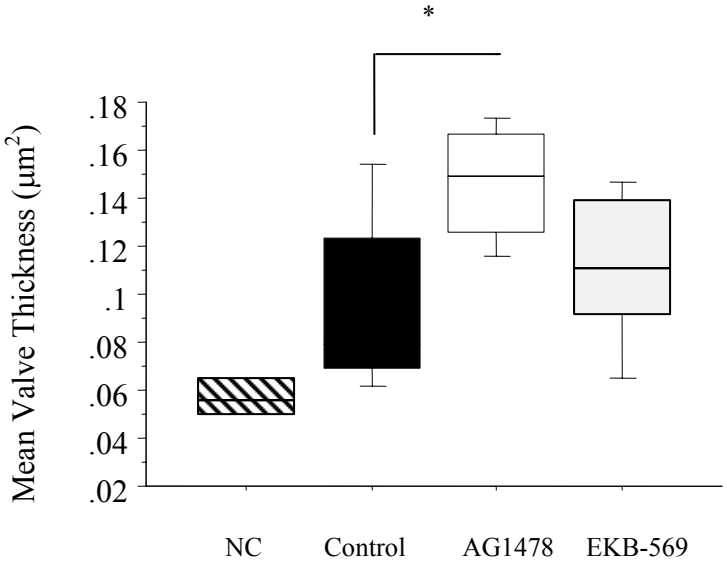

Figure 4-5. Mean thickness of aortic valves and relative fold changes in gene expression in the LV of B6 male mice chronically exposed to AG-1478 compared to controls. A. Mean thickness of aortic valves of B6 wild type mice fed normal chow (NC) control chow (AIN-93G) or AG1478 chow. B. Relative fold changes in gene expression in the LV of B6 male mice chronically exposed to AG-1478 compared to controls. *Nppa* =nautriuretic peptide precursor A, *Nppb*= Natriuretic peptide precursor B, *Egf*=epidermal growth factor *Erbb2*= erythroblastic leukemia viral oncogene homolog 2, neuro/glioblastoma derived oncogene homolog (avian), *Dtr/Hb-egf*= Diptheria toxin receptor/ heparin-binding epidermal growth factor. *$p<0.05$, **$p<0.01$.

A.

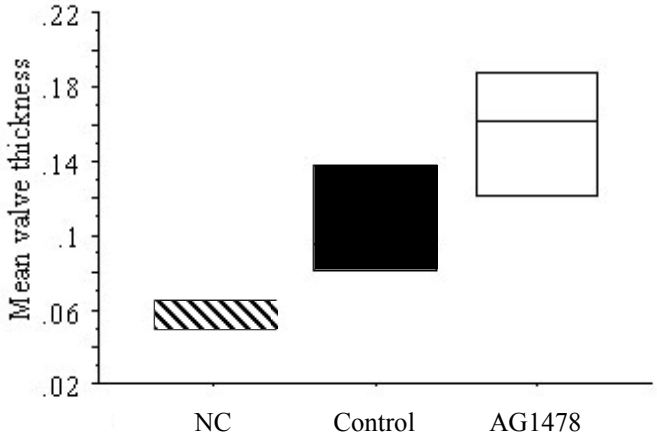

B.

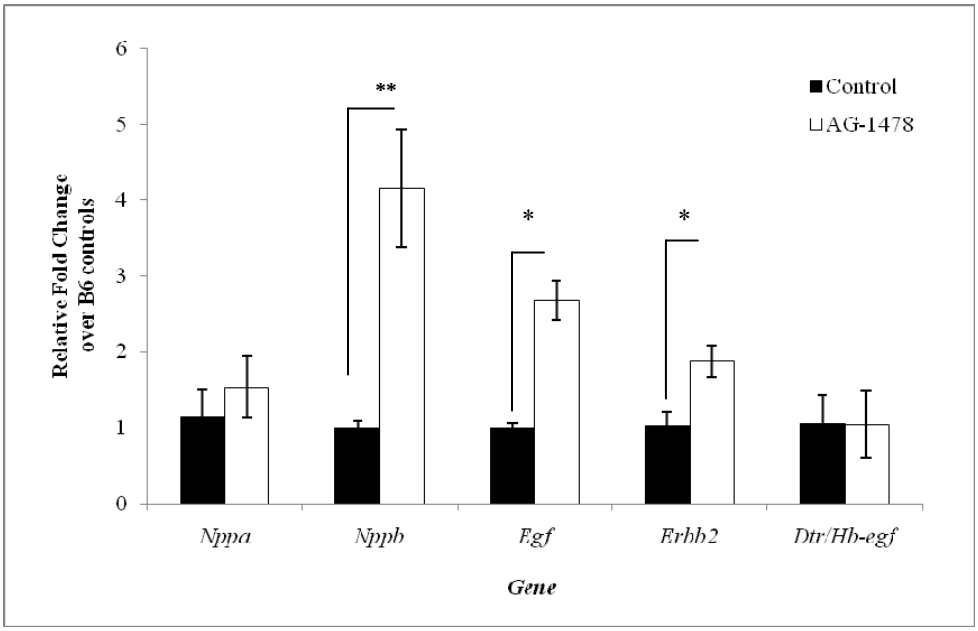

References

1. Wells, A., *EGF receptor.* Int J Biochem Cell Biol, 1999. **31**(6): p. 637-43.

2. Schlessinger, J., *Cell signaling by receptor tyrosine kinases.* Cell, 2000. **103**(2): p. 211-25.

3. Salomon, D.S., et al., *Epidermal growth factor-related peptides and their receptors in human malignancies.* Crit Rev Oncol Hematol, 1995. **19**(3): p. 183-232.

4. Woodburn, J.R., *The epidermal growth factor receptor and its inhibition in cancer therapy.* Pharmacol Ther, 1999. **82**(2-3): p. 241-50.

5. Nicholson, R.I., J.M. Gee, and M.E. Harper, *EGFR and cancer prognosis.* Eur J Cancer, 2001. **37 Suppl 4**: p. S9-15.

6. Gill, G.N., et al., *Monoclonal anti-epidermal growth factor receptor antibodies which are inhibitors of epidermal growth factor binding and antagonists of epidermal growth factor binding and antagonists of epidermal growth factor-stimulated tyrosine protein kinase activity.* J Biol Chem, 1984. **259**(12): p. 7755-60.

7. Masui, H., et al., *Growth inhibition of human tumor cells in athymic mice by anti-epidermal growth factor receptor monoclonal antibodies.* Cancer Res, 1984. **44**(3): p. 1002-7.

8. Sato, J.D., et al., *Biological effects in vitro of monoclonal antibodies to human epidermal growth factor receptors.* Mol Biol Med, 1983. **1**(5): p. 511-29.

9. Jimeno, A. and M. Hidalgo, *Pharmacogenomics of epidermal growth factor receptor (EGFR) tyrosine kinase inhibitors.* Biochim Biophys Acta, 2006. **1766**(2): p. 217-29.

10. Marshall, J., *Clinical implications of the mechanism of epidermal growth factor receptor inhibitors.* Cancer, 2006. **107**(6): p. 1207-18.

11. Steeghs, N., J.W. Nortier, and H. Gelderblom, *Small molecule tyrosine kinase inhibitors in the treatment of solid tumors: an update of recent developments.* Ann Surg Oncol, 2007. **14**(2): p. 942-53.

12. Disis, M.L. and S. Rivkin, *Future directions in the management of ovarian cancer.* Hematol Oncol Clin North Am, 2003. **17**(4): p. 1075-85.

13. Snyderman, N., *Cancer is no longer a death sentence.* http://www.msnbc.msn.com/id/17760785/, 2007.

14. Michener, C.M. and J.L. Belinson, *Modern management of recurrent ovarian carcinoma. A systematic approach to a chronic disease.* Oncology (Williston Park), 2005. **19**(10): p. 1277-85; discussion 1285, 1288, 1293.

15. Markman, M., *Viewing ovarian cancer as a "chronic disease": what exactly does this mean?* Gynecol Oncol, 2006. **100**(2): p. 229-30.

16. Burton, A.W., et al., *Chronic pain in the cancer survivor: a new frontier.* Pain Med, 2007. **8**(2): p. 189-98.

17. Lee, K.F., et al., *Requirement for neuregulin receptor erbB2 in neural and cardiac development.* Nature, 1995. **378**(6555): p. 394-8.

18. Chen, B., et al., *Mice mutant for Egfr and Shp2 have defective cardiac semilunar valvulogenesis.* Nat Genet, 2000. **24**(3): p. 296-9.

19. Iwamoto, R. and E. Mekada, *ErbB and HB-EGF signaling in heart development and function.* Cell Struct Funct, 2006. **31**(1): p. 1-14.

20. Iwamoto, R., et al., *Heparin-binding EGF-like growth factor and ErbB signaling is essential for heart function.* Proc Natl Acad Sci U S A, 2003. **100**(6): p. 3221-6.

21. Jackson, L.F., et al., *Defective valvulogenesis in HB-EGF and TACE-null mice is associated with aberrant BMP signaling.* Embo J, 2003. **22**(11): p. 2704-16.

22. Negro, A., B.K. Brar, and K.F. Lee, *Essential roles of Her2/erbB2 in cardiac development and function.* Recent Prog Horm Res, 2004. **59**: p. 1-12.

23. Erickson, S.L., et al., *ErbB3 is required for normal cerebellar and cardiac development: a comparison with ErbB2-and heregulin-deficient mice.* Development, 1997. **124**(24): p. 4999-5011.

24. Gassmann, M., et al., *Aberrant neural and cardiac development in mice lacking the ErbB4 neuregulin receptor.* Nature, 1995. **378**(6555): p. 390-4.

25. Goishi, K., et al., *Inhibition of zebrafish epidermal growth factor receptor activity results in cardiovascular defects.* Mech Dev, 2003. **120**(7): p. 811-22.

26. Zhao, Y.Y., et al., *Neuregulins promote survival and growth of cardiac myocytes. Persistence of ErbB2 and ErbB4 expression in neonatal and adult ventricular myocytes.* J Biol Chem, 1998. **273**(17): p. 10261-9.

27. Zhao, Y.Y., et al., *Neuregulin signaling in the heart. Dynamic targeting of erbB4 to caveolar microdomains in cardiac myocytes.* Circ Res, 1999. **84**(12): p. 1380-7.

28. Srinivasan, R., et al., *Expression of the c-erbB-4/HER4 protein and mRNA in normal human fetal and adult tissues and in a survey of nine solid tumour types.* J Pathol, 1998. **185**(3): p. 236-45.

29. Fuchs, I.B., et al., *Analysis of HER2 and HER4 in human myocardium to clarify the cardiotoxicity of trastuzumab (Herceptin).* Breast Cancer Res Treat, 2003. **82**(1): p. 23-8.

30. Uray, I.P., et al., *Left ventricular unloading alters receptor tyrosine kinase expression in the failing human heart.* J Heart Lung Transplant, 2002. **21**(7): p. 771-82.

31. Rohrbach, S., et al., *Neuregulin receptors erbB2 and erbB4 in failing human myocardium -- depressed expression and attenuated activation.* Basic Res Cardiol, 2005. **100**(3): p. 240-9.

32. Rohrbach, S., et al., *Neuregulin in cardiac hypertrophy in rats with aortic stenosis. Differential expression of erbB2 and erbB4 receptors.* Circulation, 1999. **100**(4): p. 407-12.

33. Liu, X., et al., *Neuregulin-1/erbB-activation improves cardiac function and survival in models of ischemic, dilated, and viral cardiomyopathy.* J Am Coll Cardiol, 2006. **48**(7): p. 1438-47.

34. Fukazawa, R., et al., *Neuregulin-1 protects ventricular myocytes from anthracycline-induced apoptosis via erbB4-dependent activation of PI3-kinase/Akt.* J Mol Cell Cardiol, 2003. **35**(12): p. 1473-9.

35. Schneider, J.W., A.Y. Chang, and T.P. Rocco, *Cardiotoxicity in signal transduction therapeutics: erbB2 antibodies and the heart.* Semin Oncol, 2001. **28**(5 Suppl 16): p. 18-26.

36. Schneider, J.W., A.Y. Chang, and A. Garratt, *Trastuzumab cardiotoxicity: Speculations regarding pathophysiology and targets for further study.* Semin Oncol, 2002. **29**(3 Suppl 11): p. 22-8.

37. Ewer, M.S., et al., *Cardiotoxicity in patients receiving transtuzumab (Herceptin): primary toxicity, synergistic or sequential stress, or surveillance artifact?* Semin Oncol, 1999. **26**(4 Suppl 12): p. 96-101.

38. Schaller, G., et al., *Therapy of metastatic breast cancer with humanized antibodies against the HER2 receptor protein.* J Cancer Res Clin Oncol, 1999. **125**(8-9): p. 520-4.

39. Crone, S.A., et al., *ErbB2 is essential in the prevention of dilated cardiomyopathy.* Nat Med, 2002. **8**(5): p. 459-65.

40. Ozcelik, C., et al., *Conditional mutation of the ErbB2 (HER2) receptor in cardiomyocytes leads to dilated cardiomyopathy.* Proc Natl Acad Sci U S A, 2002. **99**(13): p. 8880-5.

41. Garcia-Rivello, H., et al., *Dilated cardiomyopathy in Erb-b4-deficient ventricular muscle.* Am J Physiol Heart Circ Physiol, 2005. **289**(3): p. H1153-60.

42. Zhai, P., et al., *An angiotensin II type 1 receptor mutant lacking epidermal growth factor receptor transactivation does not induce angiotensin II-mediated cardiac hypertrophy.* Circ Res, 2006. **99**(5): p. 528-36.

43. Howes, A.L., et al., *Galphaq expression activates EGFR and induces Akt mediated cardiomyocyte survival: dissociation from Galphaq mediated hypertrophy.* J Mol Cell Cardiol, 2006. **40**(5): p. 597-604.

44. Chan, H.W., et al., *Effect of dominant-negative epidermal growth factor receptors on cardiomyocyte hypertrophy.* J Recept Signal Transduct Res, 2006. **26**(5-6): p. 659-77.

45. Chan, H.W., et al., *Tackling the EGFR in pathological tissue remodelling.* Pulm Pharmacol Ther, 2006. **19**(1): p. 74-8.

46. Pareja, M., et al., *Activated epidermal growth factor receptor (ErbB1) protects the heart against stress-induced injury in mice.* Am J Physiol Regul Integr Comp Physiol, 2003. **285**(2): p. R455-62.

47. Wissner, A., et al., *Synthesis and structure-activity relationships of 6,7-disubstituted 4-anilinoquinoline-3-carbonitriles. The design of an orally active, irreversible inhibitor of the tyrosine kinase activity of the epidermal growth factor receptor (EGFR) and the human epidermal growth factor receptor-2 (HER-2).* J Med Chem, 2003. **46**(1): p. 49-63.

48. Erlichman, C., et al., *Phase I study of EKB-569, an irreversible inhibitor of the epidermal growth factor receptor, in patients with advanced solid tumors.* J Clin Oncol, 2006. **24**(15): p. 2252-60.

49. Ellis, A.G., et al., *Preclinical analysis of the analinoquinazoline AG1478, a specific small molecule inhibitor of EGF receptor tyrosine kinase.* Biochem Pharmacol, 2006. **71**(10): p. 1422-34.

50. Partik, G., et al., *Inhibition of epidermal-growth-factor-receptor-dependent signalling by tyrphostins A25 and AG1478 blocks growth and induces apoptosis in colorectal tumor cells in vitro.* J Cancer Res Clin Oncol, 1999. **125**(7): p. 379-88.

51. Lenferink, A.E., et al., *Blockade of the epidermal growth factor receptor tyrosine kinase suppresses tumorigenesis in MMTV/Neu + MMTV/TGF-alpha bigenic mice.* Proc Natl Acad Sci U S A, 2000. **97**(17): p. 9609-14.

52. Zhu, X.F., et al., *EGFR tyrosine kinase inhibitor AG1478 inhibits cell proliferation and arrests cell cycle in nasopharyngeal carcinoma cells.* Cancer Lett, 2001. **169**(1): p. 27-32.

53. Dietrich, W.F., et al., *Genetic identification of Mom-1, a major modifier locus affecting Min-induced intestinal neoplasia in the mouse.* Cell, 1993. **75**(4): p. 631-9.

54. Carson, F.L., *Histotechnology: A self- Instructional text*. 1990, Chicago, Ill: ASCP Press. pp226-227.

55. Livak, K.J. and T.D. Schmittgen, *Analysis of relative gene expression data using real-time quantitative PCR and the 2(-Delta Delta C(T)) Method.* Methods, 2001. **25**(4): p. 402-8.

56. Torrance, C.J., et al., *Combinatorial chemoprevention of intestinal neoplasia.* Nat Med, 2000. **6**(9): p. 1024-8.

57. Roberts, R.B., et al., *Importance of epidermal growth factor receptor signaling in establishment of adenomas and maintenance of carcinomas during intestinal tumorigenesis.* Proc Natl Acad Sci U S A, 2002. **99**(3): p. 1521-6.

58. Rabinowits, G., et al., *Fatal pulmonary toxicity in a patient treated with gefitinib for non-small cell lung cancer after previous hemolytic-uremic syndrome due to gemcitabine.* Anticancer Drugs, 2003. **14**(8): p. 665-8.

59. Drolet, M.C., et al., *A high fat/high carbohydrate diet induces aortic valve disease in C57BL/6J mice.* J Am Coll Cardiol, 2006. **47**(4): p. 850-5.

60. Yamamoto, N., et al., *Phase I dose-finding and pharmacokinetic study of the oral epidermal growth factor receptor tyrosine kinase inhibitor Ro50-8231 (erlotinib) in Japanese patients with solid tumors.* Cancer Chemother Pharmacol, 2007.

61. Yoneda, K.Y., et al., *Interstitial lung disease associated with epidermal growth factor receptor tyrosine kinase inhibitor therapy in non-small-cell lung carcinoma.* Clin Lung Cancer, 2006. **8 Suppl 1**: p. S31-5.

62. Cersosimo, R.J., *Gefitinib: an adverse effects profile.* Expert Opin Drug Saf, 2006. **5**(3): p. 469-79.

63. Stern, L.E., et al., *Salivary epidermal growth factor and intestinal adaptation in male and female mice.* Am J Physiol Gastrointest Liver Physiol, 2000. **278**(6): p. G871-7.

64. Lazar, L.M. and M. Blum, *Regional distribution and developmental expression of epidermal growth factor and transforming growth factor-alpha mRNA in mouse brain by a quantitative nuclease protection assay.* J Neurosci, 1992. **12**(5): p. 1688-97.

65. Kwak, E.L., et al., *Irreversible inhibitors of the EGF receptor may circumvent acquired resistance to gefitinib.* Proc Natl Acad Sci U S A, 2005. **102**(21): p. 7665-70.

66. Baselga, J., *Is there a role for the irreversible epidermal growth factor receptor inhibitor EKB-569 in the treatment of cancer? A mutation-driven question.* J Clin Oncol, 2006. **24**(15): p. 2225-6.

67. Coussens, L., et al., *Tyrosine kinase receptor with extensive homology to EGF receptor shares chromosomal location with neu oncogene.* Science, 1985. **230**(4730): p. 1132-9.

68. Arteaga, C.L., *The epidermal growth factor receptor: from mutant oncogene in nonhuman cancers to therapeutic target in human neoplasia.* J Clin Oncol, 2001. **19**(18 Suppl): p. 32S-40S.

69. Yamamoto, T., et al., *Similarity of protein encoded by the human c-erb-B-2 gene to epidermal growth factor receptor.* Nature, 1986. **319**(6050): p. 230-4.

70. Levitzki, A. and A. Gazit, *Tyrosine kinase inhibition: an approach to drug development.* Science, 1995. **267**(5205): p. 1782-8.

71. Grazette, L.P., et al., *Inhibition of ErbB2 causes mitochondrial dysfunction in cardiomyocytes: implications for herceptin-induced cardiomyopathy.* J Am Coll Cardiol, 2004. **44**(11): p. 2231-8.

72. Brenner, H. and V. Arndt, *Recent increase in cancer survival according to age: higher survival in all age groups, but widening age gradient.* Cancer Causes Control, 2004. **15**(9): p. 903-10.

73. Browe, D.M. and C.M. Baumgarten, *EGFR kinase regulates volume-sensitive chloride current elicited by integrin stretch via PI-3K and NADPH oxidase in ventricular myocytes.* J Gen Physiol, 2006. **127**(3): p. 237-51.

CHAPTER 5

GENETIC MODIFIER LOCUS AFFECTING LEFT VENTRICULAR HYPERTROPHY IN THE *EGFR* ^{WA2} MOUSE MODEL OF AORTIC STENOSIS

Abstract

Left ventricular hypertrophy (LVH), or increased left ventricle (LV) mass, is recognized as an independent risk factor for cardiac-related morbidity and mortality. LVH is most commonly caused by cardiovascular diseases which chronically elevate afterload, such as aortic stenosis (AS). Increasing evidence suggests heritable components significantly modulate the development and severity of AS-related cardiac hypertrophy. One approach to identify genes which modify disease outcome is to use mouse models that show distinct genetic variation of the disease phenotype. Mice homozygous for a hypomorphic mutation in the epidermal growth factor receptor gene (*Egfr* ^{wa2}) were discovered to have congenitally enlarged aortic valves with mild AS on a mixed genetic background. By backcrossing the *Egfr* ^{wa2} allele onto the C57BL/6J or 129S1/SvImJ inbred strains, we discovered significant strain and sex dependent variation in LVH and progression to heart failure, with male B6-*Egfr* $^{wa2/wa2}$ mice having the most severe cardiac phenotype. Using these two inbred strains, we created an F_2-*Egfr* $^{wa2/wa2}$ population to employ this genetically sensitized mouse model to map modifiers of LVH. Linkage analysis of F_2-*Egfr* $^{wa2/wa2}$ progeny identified one significant locus on chromosome 9 in males (LOD score ~4.82, $p<0.05$) and one suggestive locus on chromosome 16 in females (LOD score ~4.14, $p<0.63$) linked to heart weight. By applying

haplotype analysis, we were able to narrow the critical intervals for each locus. Identification of genetic modifiers using the *Egfr* ^{wa2} disease model may provide novel mechanistic insights into the pathogenesis and progression of AS and LVH. Moreover, these studies are particularly timely, since therapies targeting the EGFR have been proposed as novel treatments for LVH and hypertension.

Introduction

Left ventricular hypertrophy (LVH), or increased left ventricle (LV) mass, is associated with many cardiovascular disorders and is recognized as an independent risk factor for cardiac-related morbidity and mortality [1-5]. Although it can be associated with mechanical stress, growth factors, catecholamines, cytokines and primary genetic abnormalities, LVH is most commonly caused by chronically elevated afterload, which increases LV stroke work. Aortic stenosis (AS) and essential hypertension (EH) are two prevalent cardiovascular diseases that induce LVH secondary to increased afterload. Clinical presentation, onset of symptoms, disease progression and mortality associated with these diseases is highly variable [6-22]. Although several clinical risk factors have been elucidated, increasing evidence from clinical and experimental studies suggests heritable components significantly modulate the development and severity of AS and EH-related LVH, as well as LVH regression with therapy [11, 14, 23-28]. Thus, elucidating genetic factors underlying the pathogenesis of LVH is pivotal to the successful clinical management of these common cardiovascular diseases.

Surgical transverse aortic constriction (TAC) is an accepted experimental model for human cardiac response to chronic pressure overload, since it causes chronic LV pressure

overload, progressive LVH remodeling and subsequent cardiac failure in mice [29-34]. Recently, we reported that C57BL/6J (B6)TAC mice had decreased survival, LVH, significant pathological cardiac remodeling and earlier progression to heart failure compared to 129S1/SvImJ (129S1) or F_1 (B6x129S1) TAC mice (see Chapter 2). Since all mice shared similar environmental conditions, this strongly suggested that genetic background significantly modified the cardiac response to increased afterload. However this model is not ideal for genetic mapping studies, since the degree of constriction, and thus induced load, can fluctuate [35, 36] and technical expertise is required for consistent results. Therefore, to dissect quantitative trait locus (QTL) that modify the hypertrophic response, we took advantage of a genetic model of pressure-overload induced LVH.

The *waved-2* allele (*Egfr* ^{wa2}) encodes a single base pair mutation in the epidermal growth factor receptor (*Egfr/Erbb1*) gene, resulting in an up to 90% reduction in receptor activity [37]. When maintained on a mixed genetic background, *Egfr* $^{wa2/wa2}$ mice had hyperplastic aortic valves and mild to moderate AS, but otherwise were viable and fertile, with minor coat and eye phenotypes [38]. However, when this mutation was backcrossed onto the B6 and 129S1 genetic backgrounds, significant strain-dependent variability was detected in cardiac phenotypes. While both B6 and 129S1-*Egfr* $^{wa2/wa2}$ mice had similar congenital valve defects (consistent with previous reports), only B6-*Egfr* $^{wa2/wa2}$ had significant cardiac hypertrophy, congestive heart failure and severe AS. Since F_1-*Egfr* $^{wa2/wa2}$ (B6-*Egfr* $^{wa2/+}$ X 129S1-*Egfr* $^{wa2/wa2}$) offspring were protected from cardiac hypertrophy and had normal lifespans, we hypothesized that 129S1 genetic modifiers were protective and dominant to B6 modifiers in the cardiac response to chronic pressure overload. Therefore,

we created an F_2-*Egfr* $^{wa2/wa2}$ population in order to map genes modifying the development of LVH.

Materials and Methods

Generation of congenic lines. Stock B6EiC3H-a/A-*Egfr*^{wa2} *Wnt 3a*^{vt} mice were obtained from The Jackson Laboratory (Bar Harbor, Maine). The *Egfr*^{wa2} allele was backcrossed to the inbred strains 129S1/SvImJ (129S1) and C57BL/6J (B6). Greater than ten backcross generations were performed by crossing *Egfr*^{wa2} allele carriers at each generation to the respective inbred strain. After ten generations, animals carrying the *Egfr*^{wa2} allele were freely intercrossed. Segregation and loss of the *Wnt3a*^{vt} mutation, which resides approximately 20 cM distal to *Egfr* on chromosome 11 and which is maintained in *cis* with *Egfr*^{wa2} in the progenitor stocks, was verified by PCR genotyping. The F_1-*Egfr* $^{wa2/wa2}$ population was created by outcrossing B6-*Egfr*$^{wa2/+}$ females to 129S1-*Egfr*$^{wa2/wa2}$ males. Heterozygous mice were identified by PCR genotyping, while homozygous mice were identified by their curly whisker phenotype , with confirmation by PCR [39]. Four male and four female F_1 *Egfr* $^{wa2/wa2}$ mice were randomly intercrossed to generate 190 F_2 offspring. An additional 32 N_2 mice were generated by crossing F_1-*Egfr* $^{wa2/wa2}$ females to B6-*Egfr* $^{wa2/wa2}$ males. All crosses involved females between the ages of 2-10 months and males between the ages of 2-12 months. Since significant post-natal lethality had been observed in the B6-*Egfr* $^{wa2/wa2}$ mice (described in Chapter 3) cages were checked daily for the presence of newborn pups and litter size was recorded.

Phenotyping. A total of 190 F_2-*Egfr* $^{wa2/wa2}$ mice were sacrificed at three months of age. Body weights and gross heart weights were recorded at this time. Tail and liver biopsies were flash frozen in liquid nitrogen for future analyses.

Genome-wide Scan. A whole genome scan was performed on fifty-six progeny from the F_2 (F_1xF_1) intercross, chosen because their phenotypic values were greater than 0.5 standard deviations from the mean. Genomic DNA was prepared from mouse tails by using the PUREGENE Purification Kit for cells and tissue (Gentra Systems, Minneapolis, Minnesota). Genotyping was performed by the Mouse SNP Genotyping Service of the Mutation Mapping and Developmental Analysis Project (MMDAP; Brigham and Women's Hospital, Harvard Medical School), using Sequenom MassARRAY technology employing 482 informative SNPs between B6 and 129S1 inbred strains markers [40]. All physical positions of markers are based on the Ensembl v31 of the NCBI m33 mouse genome assembly. Table 5-1 lists the informative markers and their physical and genetic positions, with marker coverage spanning 19 autosomes. Markers were excluded on the basis of: (1) failure to recognize the three possible genotypes in B6, 129S1 and F_1 controls (2) the presence of impossible genotypes and (3) genotypes that created impossible recombinations between closely linked markers. On average, markers were spaced every 3.4 cM (range 0-27cM).

Linkage analysis. Genetic distances of informative SNPs included in this analysis were inferred using closely linked microsatellite markers for which the genetic distance from the centromere was determined previously [41]. We used heart weight (HW), normalized heart weight (H:BW), and body weight (BW) as the phenotypes for QTL mapping. Similar results were obtained when average HW or H:BW was used. Since HW and H:BW were not

normally distributed, these values were log transformed prior to analysis. Linkage analyses were performed using a parametric model within the R/qtl software program [42].

Haplotype analysis. The haplotypes of regions within a 1.5 LOD interval surrounding each QTL were compared using The Jackson Laboratory's Mouse Phenome Database SNP collection (http://www.jax.org/phenome/snp.html). All SNPs are mapped to NCBI mouse genome build 36.1 reference assembly (C57BL/6J). The C57BL/6J strain was used as the reference strain compared to 129S1/SvImJ strain.

Results

Cardiac hypertrophy in *Egfr* $^{wa2/wa2}$ mice is modified by genetic background. Distinct strain-dependent differences were found in heart and body weights by three-months of age in *Egfr* $^{wa2/wa2}$ mice. As seen in Figure 5-1 A, heart weight (HW) was significantly increased in B6 compared to F_1 and 129S1-*Egfr* $^{wa2/wa2}$ mice (284.50±22.63 mg B6, 138.00±4.71 mg F_1, 130.27±5.62 mg 129S1, *p<0.0001*) and B6-*Egfr* $^{wa2/+}$ littermates (see Chapter 3). Reduced EGFR activity also led to variable decreases in body weight (BW) in adult homozygous mice compared to heterozygous littermates. For example, three month-old 129S1-*Egfr* $^{wa2/wa2}$ mice weighed approximately 15% less than heterozygous littermates, compared to only a 3.8% and 4.6% decreased body weight in F_1 and B6-*Egfr* $^{wa2/wa2}$ mice relative to respective littermate controls. Despite the variable BW (Figure 5-1 B, $p<0.01$), normalized HW did not differ between F_1 and 129S1-*Egfr* $^{wa2/wa2}$ mice but remained higher in B6-*Egfr* $^{wa2/wa2}$ mice (11.28±0.75 mg:g B6, 5.38±0.15 mg:g F_1, 6.52±0.49 mg:g 129S1, *p<0.0001*, Figure 5-1 C). These data demonstrated that the severity of the cardiac phenotype was strongly dependent on genetic background, since environmental conditions were similar. Due to the distinct

strain-dependent differences, coupled with ease of measurement, we chose heart and body weights as our phenotypic endpoints for subsequent analyses.

Sexual dimorphism exists in the temporal development of cardiac hypertrophy and heart failure in B6-*Egfr* $^{wa2/wa2}$mice. While the hearts of B6-*Egfr* $^{wa2/wa2}$ mice of both genders were consistently heavier than those of B6-*Egfr* $^{wa2/+}$ littermates at all timepoints analyzed, comparison of B6-*Egfr* $^{wa2/wa2}$ heart weights by gender and age revealed sexual dimorphism in survival and temporal development of severe cardiac hypertrophy. By three months of age, approximately 40% of B6-*Egfr*$^{wa2/wa2}$ of male mice but only one female B6-*Egfr*$^{wa2/wa2}$ mouse (10%) (n=43 *Egfr* ^{wa2} littermates) died, most likely from congestive heart failure. Although there were no significant differences by gender in heart or lung weights in surviving three-month-old B6-*Egfr* $^{wa2/wa2}$ littermates, by 4-5 months the hearts of B6-*Egfr* $^{wa2/wa2}$ male mice were significantly larger than those of female B6-*Egfr* $^{wa2/wa2}$ mice (Figure 5-1 D and Table 5-2). Despite increased mortality in B6-*Egfr* $^{wa2/wa2}$ male mice, cardiac function as assessed by echocardiography was more severely depressed in female B6-*Egfr* $^{wa2/wa2}$ mice (25.75±2.93 %FS B6-*Egfr* $^{wa2/wa2}$ females, 31.35±1.26 % FS B6-*Egfr* $^{wa2/wa2}$ males, Table 5-3). However, these differences may have reflected the exclusion of the most severely affected males from echocardiography studies due to significant mortality.

Sexual dimorphism was also noted with other cardiovascular endpoints. For example mean arterial pressure (MAP) (data not shown), mean aortic peak velocity, and average peak systolic pressure gradients were all lower in B6-*Egfr* $^{wa2/wa2}$ female mice compared to B6-*Egfr* $^{wa2/wa2}$ male mice (Table 5-3). Although these differences did not reach significance, these data suggested that B6-*Egfr* $^{wa2/wa2}$ female mice experienced lower afterload compared to B6-*Egfr* $^{wa2/wa2}$ male mice. By 9 months of age, the hearts of B6-*Egfr* $^{wa2/wa2}$ female mice

were significantly larger hearts than B6-*Egfr* $^{wa2/wa2}$ male mice of all ages (Figure 5-1 D), suggesting either females survived longer with hypertrophy or there was a temporal delay in the development of severe hypertrophy. Consistent with previous findings in surgical models of pressure overload in B6 mice[43], these data suggested that female sex conferred a protective effect for cardiac hypertrophy and heart failure secondary to congenitally-induced pressure overload.

Cardiac phenotype of F_2 *Egfr* $^{wa2/wa2}$ progeny. To further assess the effects of genetic background on cardiac hypertrophy, we intercrossed F_1-*Egfr* $^{wa2/wa2}$ mice to generate F_2-*Egfr* $^{wa2/wa2}$ progeny. Because B6-*Egfr* $^{wa2/wa2}$ homozygous females exhibited variable lactation defects, while B6-*Egfr* $^{wa2/wa2}$ male mice had early mortality, F_1 progeny were derived by crossing B6-*Egfr* $^{wa2/+}$ dams to 129S1-*Egfr* $^{wa2/wa2}$ sires. Since F_1-*Egfr* $^{wa2/wa2}$ female mice successfully supported large litters, F_1-*Egfr* $^{wa2/wa2}$ mice were subsequently intercrossed to produce 190 F_2 offspring. At necropsy (three months of age), both sexes were equally represented in our F_2 panel (48.5% female, 51.5% male), ruling out obvious gender bias in survival. However, there was evidence of sexual dimorphism in the cardiac phenotypes of these mice. A histogram of total distribution of gross HW from our F_2 panel is depicted in Figure 5- 2 A, while scatterplots comparing HW by gender in parental, F_1 and F_2-*Egfr* $^{wa2/wa2}$ mice is shown in Figure 5-2 B. Arrows demark the heaviest heart weight from 129S1-*Egfr* $^{wa2/wa2}$ mice (180 mg, blue arrow) and the lightest heart weight from the B6-*Egfr* $^{wa2/wa2}$ mice (220 mg, red arrow) as reference points. As expected, mean HW of B6 parental mice was significantly higher than all other groups (Figure 5-2 B, ANOVA $p<0.0001$), consistent with the hypothesis of dominant 129S1 protective modifiers of cardiac hypertrophy. Approximately 18% of the F_2 panel had a HW > 220 mg, yet within this subset of severely

affected mice, over 75% were male mice. Similar results were obtained when using H:BW as the phenotypic endpoint (data not shown). Since by three months of age, the hearts of both male and female B6-*Egfr* $^{wa2/wa2}$ mice are enlarged, we concluded that protective 129S1 genetic modifiers must have interacted strongly with female gender in the F_2 population.

Body weight was normally distributed (Figure 5- 2 C), but showed greater variability than in parental *Egfr* ^{wa2} lines or F_1 progeny (Figure 5- 2 D). In male mice, BW differed significantly by genetic backgrounds, with the highest mean BW in F_2 mice (29±4g F_2 *Egfr* $^{wa2/wa2}$ versus 27 ±0.25g B6-*Egfr* $^{wa2/wa2}$ versus 28±3g F_1-*Egfr* $^{wa2/wa2}$ versus 24 ±4g 129S1 *Egfr* $^{wa2/wa2}$, $p<0.005$). The mean BW of F_2 female mice fell within the BW range of parental and F_1 female mice. Normalized HW showed a distribution similar to HW (data not shown); moreover, there was little correlation between HW and BW (Figure 5-2 E, R^2=0.10).

Comparison of echocardiographic parameters, heart weights and histological sections in three-month-old F2-*Egfr* $^{wa2/wa2}$ littermates revealed remarkable variation in cardiac hypertrophy, aortic valve size, fibrosis, and cardiac function (Table 5-4, and Figure 5-3). Since these mice were age and sex-matched littermates, sharing the same cage and uterine environment, this highlights the significant contribution of genetic modifiers to phenotypic expression. Among these littermates, the most severely affected mouse (# 61) had the heaviest heart weight, depressed systolic function, enlarged LV chamber, affected valves, and cardiac fibrosis, replicating the phenotype of the B6-*Egfr* $^{wa2/wa2}$ parental line. Interestingly, mouse #60 had normal aortic valves. Since aortic valves were consistently enlarged in B6 and 129S1-*Egfr* $^{wa2/wa2}$ congenic lines and F_1 *Egfr* $^{wa2/wa2}$ offspring, this suggests that some combination of B6 and 129S1 genetic modifiers was able to compensate for reduced EGFR activity during valvular development.

Mapping modifiers of cardiac hypertrophy. To map the genes that modify cardiac hypertrophy, progeny from the F_2 intercross were used in a genome-wide scan for linkage. Four hundred and eighty two (482) informative SNPs were chosen with an average spacing of 3.4 cM to detect QTLs linked to HW, H:BW and BW. For the F_2 intercross, the initial genome screen included 56 progeny chosen from the extreme high and low ends of the heart weight distribution curve (>0.5 STD). No markers reached suggestive or significant thresholds when the entire cohort was analyzed using HW, H:BW or BW as the phenotypic endpoint. However, when gender was used as a covariate, two loci were suggestively linked to heart weight (Figure 5-4, marker 9.033.451 on chromosome 9, and marker rs3686531, chromosome 16, $p<0.63$). By partitioning the panel by sex, we determined that the QTL on chromosome 9 was significantly associated with male heart weight ($p<0.05$), while the marker on chromosome 16 was suggestively associated with female heart weight ($p<0.63$, summarized in Table 5-4). An additional marker on chromosome 12 (rs3686531, $p<0.63$) was suggestively linked to male heart weight. Two markers in male mice were also suggestively linked to BW (rs8254399, chromosome 9 and rs1348167, chromosome 12, $p<0.63$).

An overlay of single marker association tests for all three endpoints in male F_2 progeny (Figure 5-5 A) demonstrated that QTLs for HW and H:BW were identical, but did not overlap BW QTLs. To show a relationship between phenotype and genotype, log HW was plotted against genotype at the marker at the chromosome 9 and chromosome 12 loci that had the highest LOD score (marker 9.033.451 and marker rs3686531, Figures 5-5 B and C respectively). A homozygous B6 genotype (B6/B6) at the chromosome 9 locus was more often associated with a higher HW than a heterozygous (B6/129S1) or homozygous

(129S1/129S1) genotype in male mice. Conversely, the locus on chromosome 12 appeared to contain 129S1 susceptibility modifier(s), as a homozygous 129S1 genotype (129S1/129S1) was more often associated with a higher HW. When single marker association tests were repeated on the male cohort using BW as a covariate, the LOD score on for the QTL on chromosome 9 increased to 6.39 ($p<0.01$), and an additional QTL on chromosome 1 was identified (gnf01.132.831, LOD 3.23, $p<0.63$) suggesting BW dependent effects for these loci (Figure 5-6). Two markers in F_2 male mice were also independently linked to BW (Figure 5-7). Interestingly, a homozygous 129S1 genotype was more often associated with higher BW in F_2 male mice at both loci, an unexpected result given the significantly lower BW in male 129S1 *Egfr* $^{wa2/wa2}$ mice relative to heterozygous controls and B6 and F_1 *Egfr* $^{wa2/wa2}$ male mice. An overlay of single marker association tests in the female cohort is shown in Figure 5-8 A, identifying a single QTL on chromosome 16. To show a relationship between phenotype and genotype, log HW was plotted against genotype at the marker at the chromosome 16 locus that had the highest LOD score (marker 4220927, Figure 5-8 B). A homozygous B6 genotype (B6/B6) at the chromosome 16 locus was more often associated with a higher heart weight than a heterozygous (B6/129S1) or homozygous (129S1/129S1) genotype in female mice. The LOD score for the QTL on chromosome 16 showed little difference when analyzed using BW as a covariate, suggesting BW independent effects (Table 5-5). The discovery that disparate loci modulate the same phenotype (cardiac hypertrophy) in male and female F_2 mice supports the observed sexual dimorphism in the cardiac phenotype.

In order to identify additional QTLs whose effects might have been masked by dominant modifier loci, we performed covariate scans (using the QTL on chromosome 9 and

the QTL on chromosome 16) on the entire mapping panel. Additional modifiers of heart weight were identified on chromosome 1 (rs3711079, LOD 7.32, *p<0.05*), chromosome 15 (rs13482485, LOD 4.72, *p<0.63*) and chromosome 19 (rs1348389, LOD 5.37, *p<0.63*).

SNPs density and polymorphism for C57BL/6J versus 129S1/SvImJ strains within candidate QTL regions. Polymorphisms (the difference in genome sequences in each strain) can be used to map QTL regions because these variations correlate with phenotypic traits [44, 45]. Using the SNP collection from the Jackson Laboratory Mouse Phenome database (MPD), which contains ~10 million SNP locations, we compared haplotypes between C57BL/6J and 129S1/SvImJ genomes in regions near QTLs identified on chromosome 9 and 16 linked to cardiac hypertrophy. Regions spanning a 1.5 LOD score confidence interval around each locus are depicted in Figure 9. For the region near the chromosome 9 QTL (A) there is a major region (spanning approximately 4 Mb) with high SNP diversity between B6 and 129S1. The marker with the highest LOD score (9.0233.451, LOD 4.49) is located at 32.67 Mb, approximately at the start of this highly variable region. Approximately thirteen genes map to this region, all of which have SNPs that differ between B6 and 129S1 strains within non-coding regions. Four of these genes have known SNP variation within coding regions: kin of IRRE like 3 (*Kirrel3*), ST3 beta-galactoside alpha-2,3-sialyltransferase 4 (*St3gal4*), CAM-related/down-regulated by oncogenes (*Cdon*), STT3, subunit of the oligosaccharyltransferase complex, homolog A (*Stt3a*), and fasciculation and elongation protein zeta 1(zygin I) (*Fez1*).

There are two regions surrounding the QTL located on chromosome 16 with high SNP variability, spanning 5 or 6 Mb (Figure 5-8 B). The marker with the highest LOD score

on chromosome 16 (rs4220927, LOD 4.14) is located at 95.31 Mb, falling within the more proximal high variability SNP region. Approximately thirty-one known genes are mapped to this region. All but five have SNP variation within the non-coding regions of the gene, while fifteen have variation within the coding regions. However, since other genes within this region may have SNP variation that has not been detected, examined or reported at this time, we cannot exclude gene candidates based on haplotype comparison.

Discussion

Using a genetically sensitized disease model, we identified modifier loci located on chromosomes 9 and 16 associated with cardiac hypertrophy arising from chronic pressure overload. Interestingly, these loci individually modulated the hypertrophic response in male (chromosome 9 QTL) or female (chromosome 16 QTL) F_2-*Egfr* $^{wa2/wa2}$ mice, consistent with sexual dimorphism in the cardiac phenotypes of the F_2 progeny and B6 parental congenic line. The phenotype/genotype relationships (Figures 5-5 B and 5-8 B) also supported our hypothesis that the 129S1 inbred strain contributed a dominant resistance allele to the cardiac hypertrophy phenotype in this model.

Since collectively these modifiers did not account for 100% of the phenotypic variance, by holding these loci constant, we detected three additional modifiers of heart weight on chromosomes 1, 15 and 19. Because the observed effects are continuous, we assume that the interaction of additional modifiers with weaker effects may be at work but fall below the threshold for detection. It should also be noted that there was considerable variation of the cardiac phenotype within the parental B6-*Egfr* $^{wa2/wa2}$mice, suggesting that

subtle environmental effects, experimental error, and/or stochastic events also contribute to the variance.

Comparison of the B6 and 129S1 haplotypes revealed one region of high SNP variability within the 1.5 CI for the chromosome 9 QTL, and two regions of high SNP variability within the 1.5 CI for the chromosome 16 QTL. Within these highly variable regions, there are a large number of genes that are reported to influence EGFR activity, inflammation, or cardiac development based on literature review. We anticipate that inclusion of the entire F_2-*Egfr* $^{wa2/wa2}$ mapping panel, allowing detection of additional recombination events within these regions, will further refine the loci. Future studies include comparative analysis of cardiac gene expression and protein levels in B6 and 129S1-*Egfr* $^{wa2/wa2}$ mice, which we expect will narrow the list of potential candidate genes.

It is unclear if the major modifiers identified herein influence resistance to aortic valve disease or altered cardiomyocyte response to chronic pressure overload. Aortic leaflet size was highly correlated with heart weight and peak systolic pressure gradients in B6-*Egfr* $^{wa2/wa2}$ mice. Additionally, pathological changes unique to the B6-*Egfr* $^{wa2/wa2}$ aortic valves, coupled with progressively elevated peak aortic velocities, mimicked calcific degenerative aortic stenosis. In the etiology of this common valvular disease, calcification and other pathological changes gradually restrict systolic valve opening, and symptoms and LVH rarely occur until valve opening is decreased by seventy-five percent [46, 47]. Since the cardiac valves of F_2-*Egfr* $^{wa2/wa2}$ littermates varied in size, dominant 129S1 modifiers may have curtailed cardiac valve overgrowth in some mice, and in this manner prevented the pathophysiological responses observed in the B6 congenic mice. In this scenario, other

129S1 modifiers would have played a supportive role by buttressing cardiac function with increased afterload.

A limitation of this study is that we have not assessed EGFR activity, protein, or transcript levels in the hearts of F_2-*Egfr* $^{wa2/wa2}$ mice. However, previous experiments demonstrated that EGFR protein and transcript levels, and ligand-induced EGFR and ERK1/2 activity did not significantly differ by genetic background in the hearts and livers of *Egfr* $^{wa2/wa2}$ mice (see Chapter 3). All 56 mice selected for genotyping had characteristic curly coats and whiskers, and typed identically at markers in close proximity (~3Mb) to the *Egfr waved-2* locus, confirming maintenance of a homozygous state in the F_2 progeny. Thus, alterations in EGFR activity or expression would be due to a *trans* rather than a *cis* effect.

GPCR agonist-induced transactivation of EGFR has recently been linked to pathological processes underlying common cardiovascular diseases, including cardiac hypertrophy, vascular smooth muscle proliferation, fibrosis and vasoconstriction [48-54]. Consequently, blocking EGFR transactivation (via metalloproteinase inhibition, preventing conversion of EGF ligands into their active form) is proposed as a novel therapy for the treatment of hypertension and LVH [55] [56]. However, EGFR activity also provides significant cardioprotection against the detrimental effects of sustained beta-adrenergic stimulation and acute stress [57, 58]. Along with our studies, these data suggest that continuous pharmaceutical inhibition of EGFR in cardiac syndromes with increased afterload may exacerbate disease in some individuals; moreover the severity may be gender-dependent. Identification of genetic modifiers using the *Egfr* ^{wa2} model may help to further define the role of EGFR in the pathogenesis of common cardiac diseases.

Table 5-1. Informative markers used for SNP genotyping.

rs13475709	1	6.65693
rs3703103	1	10.0838
rs3655978	1	13.5322
rs13475735	1	15.1699
rs3711079	1	22.1371
rs3711203	1	28.944
rs13475794	1	32.3685
01.035.266	1	34.7676
rs3706514	1	38.7405
rs3677272	1	40.8222
rs13475845	1	45.3732
rs13475881	1	58.6336
rs6322485	1	63.4978
rs6293581	1	64.9845
rs3697638	1	68.0919
mCV22884877	1	77.8988
rs13475955	1	83.5477
01.087.139	1	86.8537
rs13475960	1	89.115
rs13475985	1	92.8572
rs13476005	1	98.2719
CEL-1_102831225	1	102.816
gnf01.107.327	1	107.388
rs13476049	1	110.137
01.118.639	1	115.842
rs13476079	1	119.241
rs13476086	1	122.097
gnf01.124.355	1	124.564
gnf01.126.387	1	126.608
rs13459051	1	130.755
gnf01.132.831	1	133.12
rs6194543	1	155.704
rs3661305	1	161.482
UT_1_175.440616	1	171.553
rs13476259	1	177.236
rs13476288	1	185.763
rs13476300	1	189.831
01.193.155	1	192.148
rs3680350	2	3.88002
rs6331390	2	5.89134
rs13476334	2	7.31452
rs3719255	2	10.6948
rs3699934	2	36.109

rs13476448	2	39.8218
rs3658919	2	54.1598
rs3672719	2	58.1903
rs13476535	2	61.6873
rs6367022	2	73.9189
rs3694656	2	97.0492
rs3674361	2	99.9858
rs3143810	2	103.135
rs6318808	2	109.841
02.113.755	2	112.066
rs13476739	2	121.108
rs8251635	2	125.043
rs13476765	2	128.215
rs4223510	2	131.595
rs13476785	2	134.502
02.140.785	2	138.844
UT_2_156.443943	2	155.56
rs3691210	2	157.736
rs3664408	2	161.121
rs3712766	2	165.751
rs3714936	2	168.88
rs3668691	2	172.482
rs8238755	2	174.163
rs6187766	2	180.024
rs6402916	2	182.308
rs6345660	3	16.8672
rs3677150	3	20.7694
rs6373308	3	26.0093
rs13477048	3	32.895
rs3714497	3	39.71
rs13477144	3	61.4248
rs3722255	3	63.4826
rs3674810	3	68.2438
rs6351657	3	72.7604
rs3686804	3	79.4384
rs3699123	3	82.5009
rs3670634	3	87.3056
03.090.273	3	89.2967
rs3708085	3	93.1366
rs3671622	3	102.176
rs6188615	3	104.812
rs13477320	3	108.837
rs6406405	3	112.047
rs3718783	3	120.545
rs13477384	3	124.645
03.131.780	3	130.962
rs13477421	3	134.033
rs13477451	3	140.604
rs6258013	3	142.785

rs3710548	3	146.168
gnf03.151.421	3	147.861
rs3656403	3	153.818
03.157.668	3	156.856
04.003.476	4	3.47653
rs13477542	4	6.63814
rs13477549	4	8.73086
rs13477554	4	9.87607
rs13477566	4	13.031
04.017.889	4	18.2352
gnf04.018.158	4	21.4202
rs13477612	4	24.7825
04.032.692	4	32.8548
rs3702229	4	39.295
rs13477681	4	46.1892
rs13477699	4	50.6966
04.060.127	4	62.1567
rs3023981	4	69.5328
rs13477785	4	75.5327
rs3700579	4	83.343
rs3707373	4	86.3369
rs13477832	4	88.5409
rs4136370	4	90.7473
rs3663299	4	93.825
rs3705454	4	98.3418
04.106.358	4	107.736
rs3659850	4	110.671
rs13477920	4	113.677
gnf04.117.102	4	120.837
gnf04.119.329	4	123.444
rs3661158	4	129.375
rs3680937	4	133.631
rs4136314	4	144.458
rs6230717	4	146.889
rs3697097	4	149.387
rs3696703	4	154.215
rs6245801	5	7.49898
rs3714258	5	11.8519
rs13478120	5	17.3349
05.020.074	5	20.9777
rs13478142	5	22.6867
rs13478151	5	25.2363
rs6196732	5	32.3251
rs3703261	5	38.9604
rs3656439	5	44.1853
rs3023045	5	49.9486
CEL-5_52953963	5	53.6994
rs6339023	5	57.5404
rs3090667	5	59.5946

rs6187409	5	62.1651
rs3656989	5	65.5703
rs6409508	5	72.5031
rs3153753	5	76.0782
rs13478349	5	79.8294
rs3678577	5	84.5716
rs3667067	5	88.1744
rs13478390	5	91.3025
CEL-5_93945748	5	95.8521
rs6245715	5	97.1918
rs3721248	5	100.573
rs13478476	5	114.813
rs3653889	5	118.742
rs13478500	5	122.809
rs3711495	5	125.381
rs13478536	5	131.492
rs3711751	5	135.889
rs13478605	6	4.41233
rs13478612	6	6.51136
CEL-6_10519419	6	10.7529
rs13478640	6	15.7343
06.016.811	6	16.9081
06.026.095	6	26.1231
rs13478687	6	29.8932
rs3678887	6	32.2382
rs3696518	6	43.9976
rs3718512	6	50.3202
rs13478758	6	53.0796
CEL-6_56528034	6	56.5317
rs3710429	6	75.5541
rs13478845	6	79.0147
rs3152159	6	82.7691
06.086.443	6	86.0185
rs3671004	6	88.7749
rs3683775	6	91.328
gnf06.093.201	6	94.3935
UT_6_102.533298	6	100.958
rs3722170	6	104.979
gnf06.106.186	6	107.467
rs3723352	6	111.513
mCV24115224	6	114.667
rs3716551	6	118.495
UT_6_123.37228	6	121.704
rs3688358	6	131.701
rs6400392	6	139.362
rs3705112	6	144.206
rs13479087	6	145.872
07.003.727	7	3.9089
rs13479119	7	8.88062

CEL-7_6264134	7	10.9586
rs6361142	7	15.3037
rs3726684	7	16.7142
rs3724397	7	20.9873
rs3156053	7	25.2359
rs13479186	7	31.2881
rs3720735	7	33.6747
rs8255275	7	42.3432
rs3680765	7	45.6178
rs13479251	7	48.6384
rs3663313	7	52.3752
rs3719301	7	60.1547
07.056.991	7	64.7128
rs3683475	7	66.4322
rs3716002	7	69.978
rs3671471	7	72.289
rs3700384	7	76.504
07.074.764	7	82.2714
rs3658777	7	85.551
07.080.264	7	87.8297
rs3717027	7	99.9414
rs3711721	7	103.122
rs3726501	7	107.744
rs13479471	7	111.049
rs6277857	7	114.275
rs6322316	7	116.616
rs3682038	7	122.437
07.121.767	7	129.276
rs3663988	7	135.733
rs13479567	7	140.273
CEL-8_7689226	8	7.66771
rs6343961	8	14.4544
08.020.650	8	20.578
gnf08.021.719	8	22.0073
rs3702973	8	25.198
rs13479678	8	29.4664
rs13479702	8	34.9055
rs13479731	8	41.9157
rs13479741	8	45.879
rs13479748	8	48.2907
CEL-8_51734273	8	51.3331
rs13479784	8	57.1494
08.068.088	8	66.5381
rs3722665	8	71.0682
rs13479840	8	73.9517
rs3667484	8	82.005
rs3724111	8	86.4835
rs13479916	8	90.0343
mCV23424042	8	101.132

rs6180306	8	105.241
gnf08.109.993	8	107.369
gnf08.119.598	8	116.994
rs13480019	8	120.28
rs3693295	8	121.589
rs3667341	8	127.183
09.016.217	9	16.2174
09.019.168	9	19.1827
rs6181976	9	23.8556
rs13480120	9	30.3768
09.033.451	9	32.6568
rs13480142	9	37.066
rs13480151	9	40.0571
rs13480192	9	51.9285
rs6206488	9	54.9415
09.059.359	9	57.2807
rs6358810	9	60.5322
rs3664533	9	65.8425
09.068.487	9	68.2968
rs3721056	9	71.0668
rs6292345	9	75.3386
09.081.324	9	81.0607
rs13480312	9	83.8923
rs3698443	9	87.1572
rs3693091	9	90.0332
rs3657346	9	102.885
rs6375364	9	106.149
09.114.032	9	113.607
rs6320810	9	114.807
rs8254399	9	123.748
10.003.693	10	6.5385
rs3664101	10	9.30896
rs3678286	10	17.7465
rs13459119	10	20.0503
rs3679120	10	22.678
rs13480579	10	35.978
rs13480605	10	45.6246
rs3696307	10	53.5612
rs6326263	10	69.3636
rs13480652	10	74.2681
rs13480657	10	76.3677
rs6331511	10	92.8158
10.097.478	10	97.5105
rs13480736	10	102.486
rs13480757	10	107.823
CEL-10_113177617	10	112.906
rs13480777	10	115.64
mCV25429984	10	118.721
rs3680343	10	126.385

rs3676330	10	127.712
rs13480836	11	3.5062
rs13480853	11	7.36709
gnf11.006.472	11	8.98622
rs13480871	11	11.5095
rs13480881	11	14.3308
rs13480889	11	17.4168
rs3708339	11	21.8094
rs4139111	11	37.2544
rs6317915	11	40.37
rs13480996	11	43.5097
rs13481011	11	46.8852
rs3698063	11	54.2785
rs3024185	11	63.1785
rs3694522	11	70.7883
rs3701609	11	73.3452
rs3705751	11	75.7884
rs13481126	11	83.3534
gnf11.093.966	11	87.4335
rs3697441	11	89.6498
rs13481185	11	99.8439
rs3723163	11	104.089
rs3669823	11	108.073
13.084.759i	11	110.713
11.114.529	11	113.765
rs13481245	11	115.719
rs3661724	11	117.795
12.003.413	12	3.46528
rs13481285	12	6.96789
rs3717933	12	11.1401
rs13481308	12	13.3891
rs3717860	12	22.5655
rs13481355	12	24.4093
rs13481367	12	26.8325
rs13481380	12	29.937
C12.033.955	12	33.3512
rs13481412	12	39.4976
rs3671614	12	44.9341
rs13481452	12	50.1111
rs3705833	12	55.8877
rs13481500	12	62.4094
rs6383133	12	67.1023
CEL-12_66272019	12	68.9488
rs3655558	12	72.6811
mCV23169261	12	74.9238
CEL-12_85059563	12	87.9484
rs13481601	12	94.2983
rs3666004	12	96.9617
CEL-12_108727612	12	111.45

rs3023711	12	113.911
rs3686531	12	117.516
rs3695486	13	4.04572
rs13481672	13	5.284
rs13481680	13	8.30161
rs6348604	13	14.7799
rs6345767	13	18.7634
rs8267056	13	23.0666
rs3710348	13	30.6389
gnf13.035.637	13	36.9378
rs13481775	13	39.6243
rs13481788	13	43.0729
gnf13.045.330	13	46.7262
rs3683883	13	54.1935
rs3690198	13	59.8269
rs6220659	13	62.0257
rs13481863	13	66.1198
rs3680075	13	71.2797
rs3679222	13	74.4116
rs13481908	13	79.1053
CEL-13_85525049	13	85.9409
rs13481944	13	90.0658
rs4229988	13	92.581
rs3090371	13	99.8353
rs13481998	13	104.265
rs6316705	13	113.107
rs6397687	13	116.6
rs3710916	14	5.82962
rs13482048	14	6.8277
rs6352512	14	9.0142
gnf14.007.267	14	12.4077
rs6339205	14	14.9744
rs3687889	14	17.3472
rs6175633	14	19.8518
rs3682880	14	23.0124
rs13482117	14	26.9072
rs13482132	14	31.7632
rs3689402	14	41.0937
14.040.618	14	44.5906
rs13482177	14	45.9768
rs13482191	14	49.5132
rs3699179	14	56.6365
rs3719672	14	62.387
rs4230463	14	65.2486
rs13482259	14	71.3111
rs3665356	14	73.2453
rs6379772	14	93.9578
rs6179144	14	95.6553
rs4230545	14	98.9074

rs3678059	14	100.841
rs4139535	14	103.989
rs13482374	14	105.949
rs3671398	14	111.44
CEL-14_110783830	14	112.865
rs13459176	15	3.10499
rs13482423	15	8.7464
CEL-15_15919629	15	16.0696
rs3696823	15	19.1654
rs3714169	15	21.871
rs13482485	15	25.5535
rs13482507	15	31.5535
rs8267917	15	33.3591
15.037.853	15	37.9183
rs4230714	15	44.4202
rs4222076	15	54.8993
rs13482602	15	61.4964
rs6213684	15	67.9314
rs3696311	15	71.2359
rs3682805	15	78.2732
rs3721372	15	80.4901
CEL-15_83750824	15	83.4774
rs3707587	15	88.1807
rs13482722	15	94.854
rs13482738	15	99.7796
16.005.872	16	6.05262
rs4158165	16	7.31967
rs4161857	16	11.0539
rs4165081	16	19.4331
rs4167574	16	29.3403
rs4179715	16	44.1695
rs4184315	16	48.4268
rs3682166	16	57.2872
rs3693190	16	65.2716
rs4201385	16	72.141
rs4205586	16	75.6071
rs3703235	16	78.5948
rs4211772	16	84.1393
rs4213876	16	87.154
rs4215932	16	88.9837
rs4220927	16	95.3101
rs3696981	16	97.7769
rs3721166	17	3.24696
rs13482893	17	13.979
rs6384940	17	27.2417
17.037.607	17	36.0121
rs3702604	17	38.9955
rs13482994	17	41.5491
rs3709891	17	47.1107

rs6191282	17	50.2134
rs3714819	17	53.5104
rs4231558	17	55.2074
17.059.952	17	59.747
rs13483068	17	62.2362
rs3727008	17	66.0056
rs6155172	17	69.9337
rs6280326	17	72.0723
rs3656948	17	74.7631
rs3718983	17	77.5827
rs13483133	17	81.3665
rs6336971	17	85.0605
rs3698948	17	87.0856
rs6313030	17	88.8606
rs6312389	18	6.80617
rs3660245	18	9.47735
gnf18.010.030	18	13.1482
rs6358426	18	16.775
rs6303064	18	19.9716
rs13483251	18	23.1631
rs3662641	18	25.8729
rs3723870	18	33.9455
rs13483314	18	40.3204
rs13483326	18	43.1267
CEL-18_46082735	18	46.0159
rs3722312	18	52.7245
rs13483368	18	54.8335
rs3705107	18	57.8132
CEL-18_60377359	18	60.251
rs13483398	18	63.4765
18.067.071	18	67.0452
rs13483427	18	70.8616
rs3715003	18	79.0183
18.081.133	18	81.0613
rs13483561	19	20.8292
rs6291559	19	27.2732
rs13483591	19	30.514
rs6185741	19	38.5364
rs3655407	19	40.1534
rs13483643	19	45.2086
rs3023496	19	48.0383
rs13483662	19	50.7111
gnf19.052.359	19	53.0789
rs3654713	19	54.9332
rs13483689	19	57.3624
19.060.549	19	60.6807

Table 5-2. Organ weights of three-to-five month old *Egfr* ^{wa2} littermates. BW, body weight; HW, heart weight; H:BW, normalized heart weight, LuW, lung weight; LiW, liver weight; Lu:BW, normalized lung weight; Li:BW, normalized liver weight. Comparison by genotype to sex matched littermates*$p<0.05$ **, $p<0.01$***,$p<0.001$.

	B6				**F_1**				**129S1**			
	wa2/+		wa2/wa2		wa2/+		wa2/wa2		wa2/+		wa2/wa2	
Sex	F	M	F	M	F	M	F	M	F	M	F	M
N	6	10	6	10	8	5	8	5	10	7	10	7
BW (g)	26.2±1.3	30.6±0.9	24.7±0.5	29±1.4	24.6±0.9	27.8±0.7	24.7±0.7	27.6±1.0	25.0±1.2	30.3±1.9	20.9±1.0*	26.5±1.9
HW	135.4±3.9	153.5±6.5	261.0±9.7***	339.8±29.2***	112.6±1.3	131.4±8.4	167.5±27.9*	169.8±26.1	143.9±6.2	155.3±8.1	124.8±5.1	154.8±6.4
H:BW	5.5±0.2	5.04±0.19	10.1±0.5**	11.3±0.9***	4.6±0.2	4.7±0.3	6.8±1.1	6.2±1.0	5.8±0.3	5.2±0.3	6.1±0.3	5.9±0.3
N	3	3	3	3	4	4	4	4	3	3	3	3
LuW	149.3±1.9	149.8±0.3	174.0±2.0*	170.5±2.2*	130.3±9.9	158.0±40	155.3±12.8	162.5±2.5	146.6±15	135.0±5.0	142.00±4.0	128.07±4.37
LiW	1150.3±22.1	1283.4±15.7	1322.0±148.0	1372.3±145.6	969.7±33.8	973.0±27.0	1141.8±60.8*	976.5±26.5	967.7±56.3	1001.5±1.5	836.0±29.0	658.5±45.7*
Lu:BW	6.2±0.3	5.5±0.1	6.9±0.4*	6.4±0.3*	5.2±0.1	5.8±1.8	5.6±0.6	5.3±0.1	5.9±0.6	4.4±0.2	7.2±0.4	5.8±0.2
Li:BW	47.9±1.6	47.4±1.6	52.8±3.7	51.7 ±3.5	40.0±1.9	35.1±1.0	40.4±3.1	31.7±1.1	39.3±2.8	32.6±0.1	42.4±0.4	29.8±1.8

Table 5-3. Echocardiographic parameters in three-to five month old *Egfr* ^{wa2} littermates. LVED,d, left ventricular end diastolic diameter; LVED,s, left end systolic diameter; LVPW,d, left ventricular posterior diastolic wall thickness; LVPW,s, left ventricular systolic wall thickness; % FS, percent fractional shortening; RWT, relative wall thickness; HW, heart rate; AoVelocity, peak systolic velocity. Comparison by genotype to sex matched littermates *$p<0.05$,**$p<0.01$, ***$p<0.001$

	B6				**F_1**				**129S1**			
Genotype	wa2/+		wa2/wa2		wa2/+		wa2/wa2		wa2/+		wa2/wa2	
Sex	F	M	F	M	F	M	F	M	F	M	F	M
N	7	5	7	5	4	4	4	4	8	10	8	10
LVED, d (mm)	3.48±0.07	3.60±0.05	5.25±0.20***	4.67±0.17***	3.72±0.12	3.85±0.05	3.76±0.05	3.70±0.11	3.69±0.11	3.74±0.05	3.16±0.11**	3.52±0.09
LVED, s (mm)	2.08±0.11	2.16±0.10	3.82±0.30**	3.20±0.10**	2.33±0.13	2.25±0.21	2.55±0.02	2.25±0.09	2.16±0.14	2.18±0.07	1.76±0.15	2.01±0.10
LVPW, d (mm)	0.90±0.06	1.14±0.17	1.56±0.16*	1.50±0.09*	0.84±0.04	0.81±0.03	0.63±0.02*	0.77±0.03	0.86±0.04	0.83±0.05	0.79±0.07	0.67±0.03
LVPW, s (mm)	1.27±0.06	1.52±0.20	2.12±0.18**	2.17±0.14**	1.12±0.02	1.06±0.02	0.93±0.01*	1.11±0.06	1.27±0.03	1.13±0.06	1.24±0.10	0.88±0.12
% FS	40.30±2.31	40.05±2.45	25.75±2.93*	31.35±1.26**	37.59±1.55	41.77±4.63	34.06±1.24	39.32±1.33	41.76±2.45	41.84±1.32	45.10±2.96	42.79±2.78
RWT	0.52±0.05	0.64±0.10	0.60±0.08	0.65±0.05	0.45±0.23	0.42±0.01	0.34±0.01*	0.42±0.02	0.47±0.03	0.44±0.03	0.52±0/06	0.38±0.01
HR (BPM)	437±14	450±11	475±20	430±9	461±15	425±12	470±17	445±13	434±10	460±17	449±9	465±9
N	4	4	4	4	2	2	2	2	4	4	4	3
Mean Peak AoVelocity(cm/s)	106±24	136±26	283±59	357±30	110±9.8	95±6.5	170±8.7	190±15.7	85±1.8	109±2.5	197±30	237±29
Pressure gradient	6.5±3.5	2.5±2.0	17.5±6.5	40.5±13.1	3.5±4.4	3.70±2.80	10±5.7	12±7.7	-2±3.04	1±4.49	8±0.87	15±2.05

Figure 5-1. Comparison of mean heart weight (HW,milligrams, mg) (A) mean body weight (BW,grams,g) (B) and normalized heart weight (H:BW, mg:g) (C) by genetic background in three month-old *Egfr* $^{wa2/wa2}$ mice, n=3 mice of each gender. Distribution of heart weight by age (in months) in B6-*Egfr* $^{wa2/wa2}$ male (solid circle) and female (open circle) mice (D). **p<0.05,**p<0.01, ****p<0.0001*

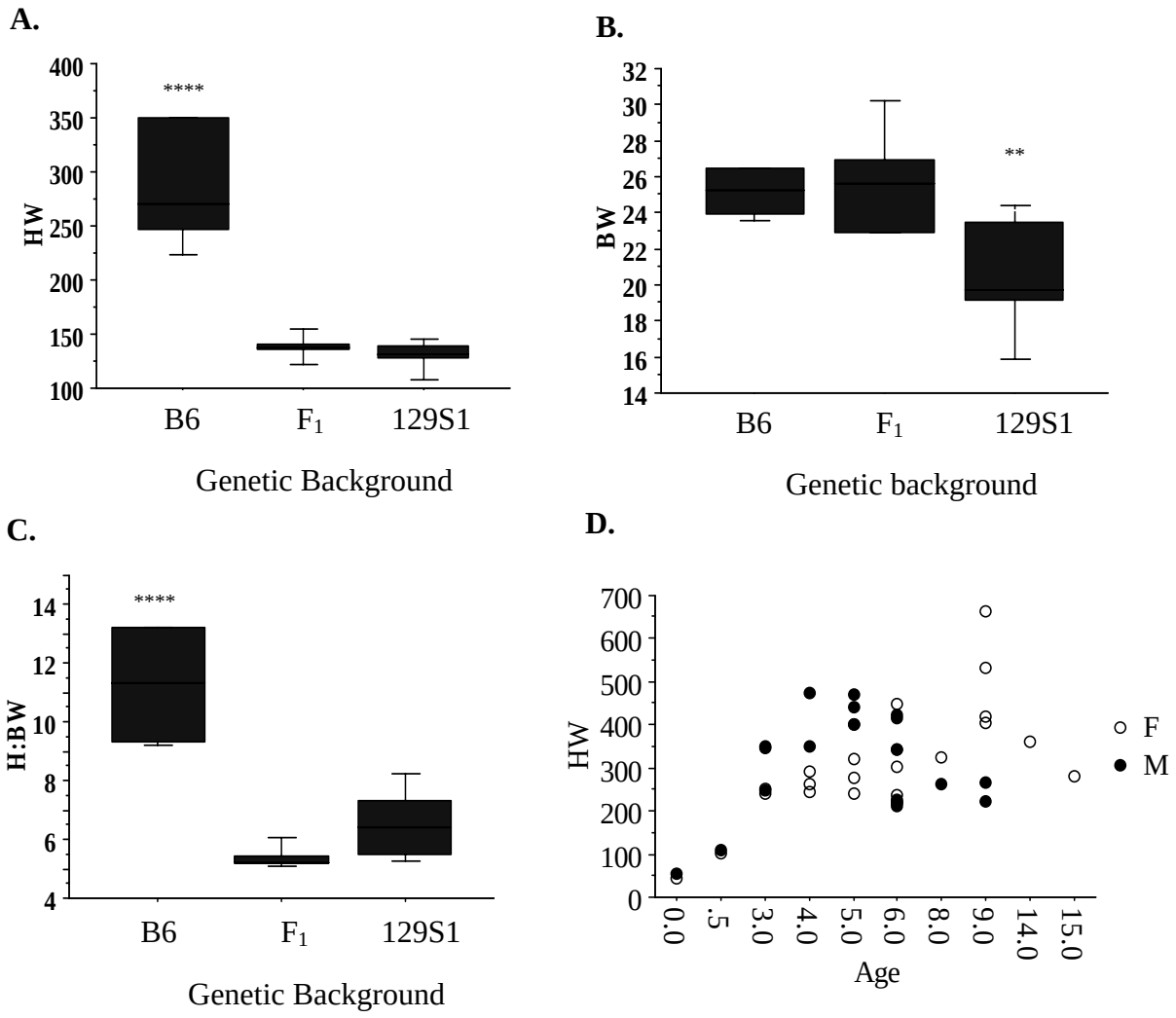

Figure 5-2 A. Distribution of heart weight in F_2 progeny. B. Scatter plot of HW in B6, F_1 (B6x129S1), 129S1 and F_2 *Egfr* $^{wa2/wa2}$ mice. C) Distribution of body weight (BW) in F_2 progeny. D. Scatter plot of BW in B6, F_1 (B6x129S1), 129S1, and F_2 *Egfr* $^{wa2/wa2}$ mice. E. Correlation between HW and BW in F_2 *Egfr* $^{wa2/wa2}$ mice. Blue arrow point to highest values from 129S1 *Egfr* $^{wa2/wa2}$ parentals and red arrow to lowest value from B6-*Egfr* $^{wa2/wa2}$ parentals.

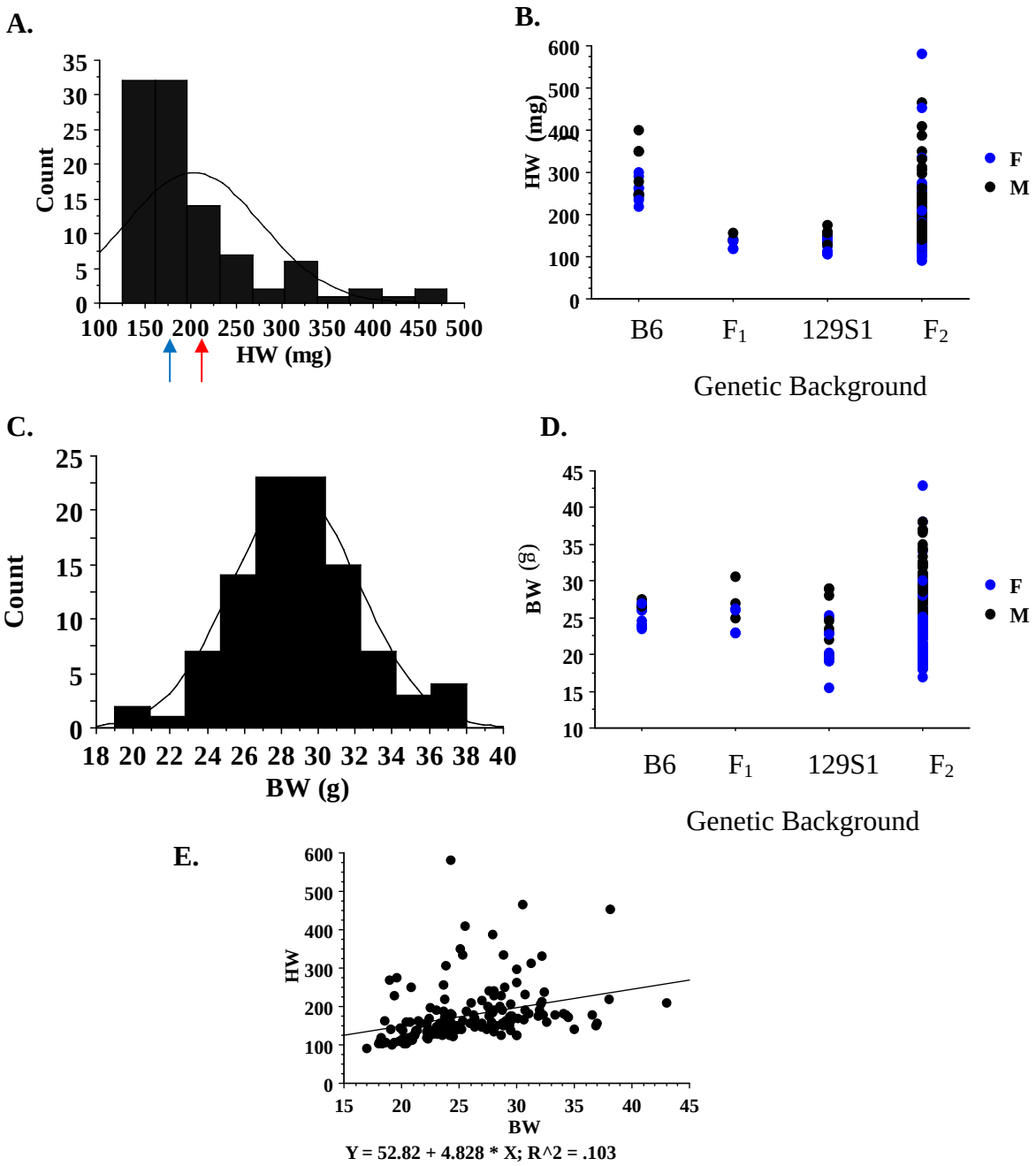

Table 5-4. Representative echocardiographic parameters and organ weights from F_2 *Egfr* $^{wa2/wa2}$ mice.

F_2 *Egfr* $^{wa2/wa2}$			
Mouse #	60	62	61
HW (mg)	176.9	190.1	332
H:BW (mg:g)	5.31	6.62	10.31
BW (g)	33.3	28.7	32.2
LVED, d (mm)	3.65±0.08	3.92±0.13	5.05±0.05
LVED, s (mm)	2.32±0.02	2.37±0.07	3.26±0.30
LVPW, d (mm)	0.75±0.08	1.09±0.06	0.79±0.16
LVPW, s (mm)	0.90±0.02	1.48±0.11	1.24±0.02
% FS	36.80±1.70	39.6±0.27	27.04±3.84
HR (BPM)	447±5	452±2	475±10

Figure 5-3. Representative histological sections from F_2 *Egfr* $^{wa2/wa2}$ three-month old littermates. Arrows point to aortic (AV) and pulmonary (PV) valves. A fibrotic region (FIB) near the apex of the most severely affected heart is also indicated. Magnification=1.6x.

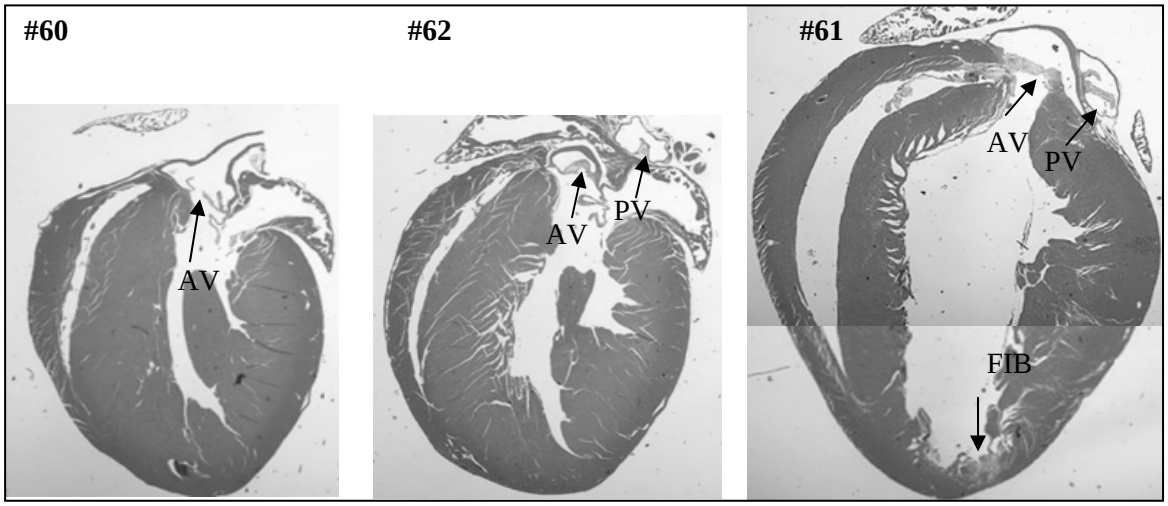

Figure 5-4. Single marker association tests for a whole genome scan performed on F_2 progeny, using sex as a covariate. Two suggestive QTLs were identified.

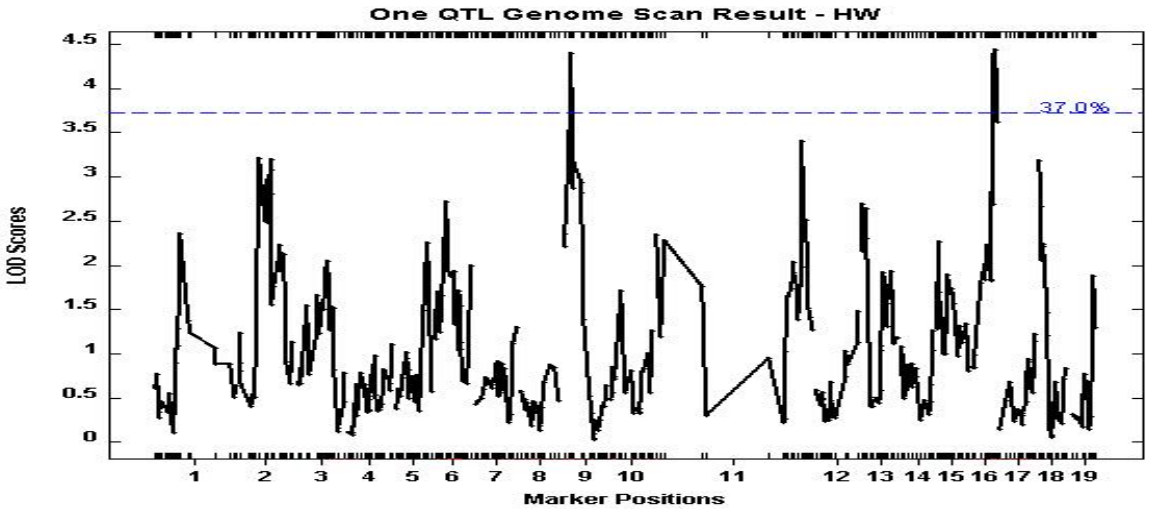

Figure 5-5. Single marker association tests for a whole genome scan performed on F_2 male progeny (A). Interval mapping of the Chromosome 9 locus in F_2 male mice and plot showing the relationship between cardiac weight and genotype at the 9.033.451 marker in F_2 progeny (B). Interval mapping of the Chromosome 12 locus in F_2 male mice and plot showing the relationship between cardiac weight and genotype at the rs3686531 marker in F_2 (F_1XF_1) progeny (C).

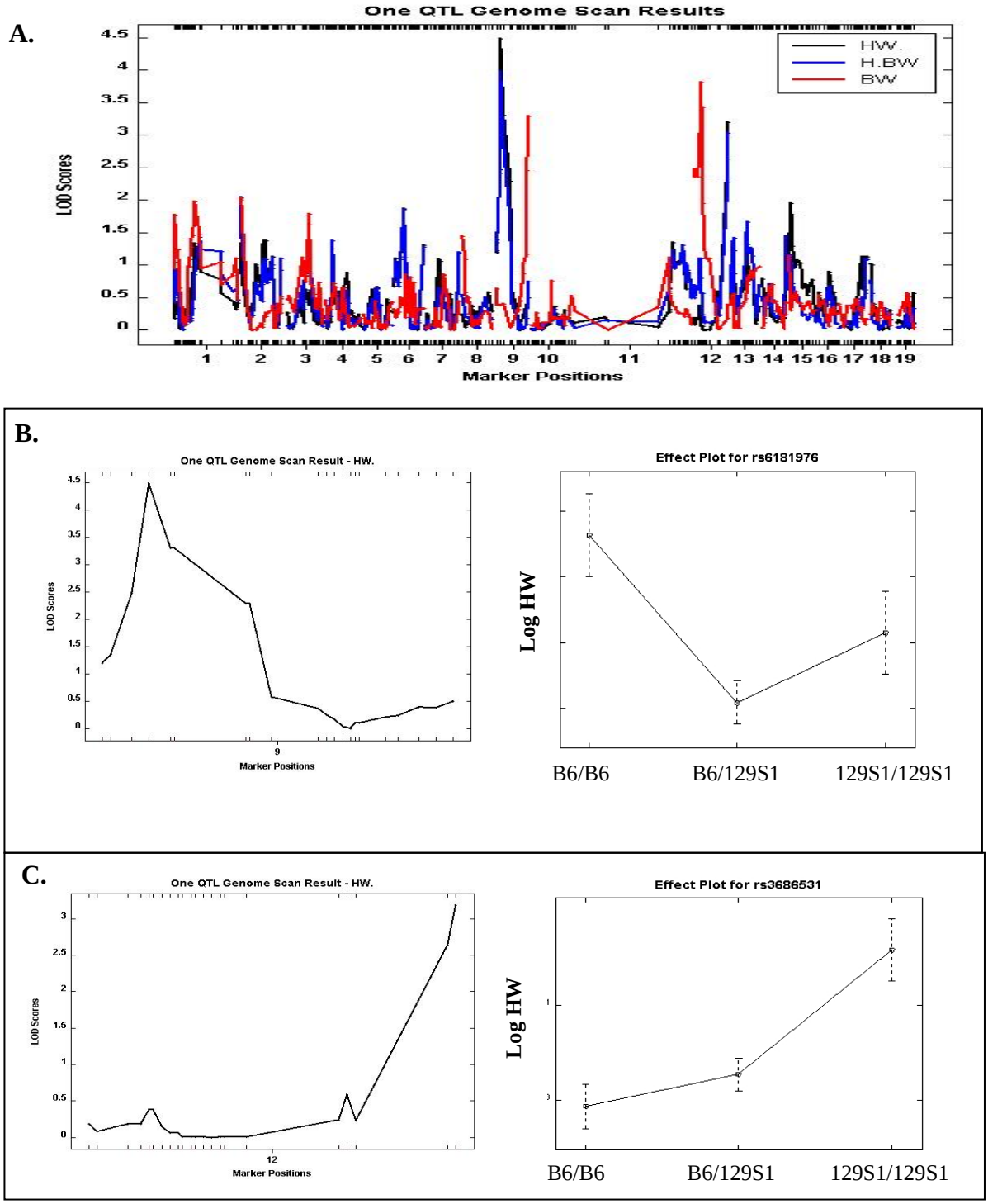

Figure 5-6. Single marker association test for heart weight (HW) in F_2 male mice using body weight (BW) as a covariate identified an additional QTL located on Chromosome 1 (near marker Gnf01.132) Suggestive (37.0%) significant (95.0%) and highly significant (99.0%) thresholds are indicated (A). Interval mapping and plot showing the relationship between HW and genotype at the Gnf01.132.831 marker in F_2 male progeny (B). Suggestive threshold is shown as a dotted line.

A.

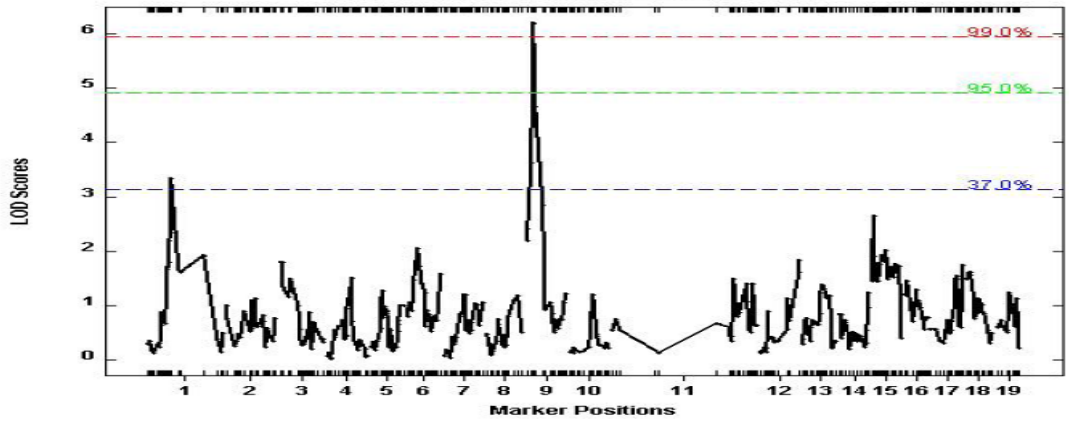

B. Chromosome 1

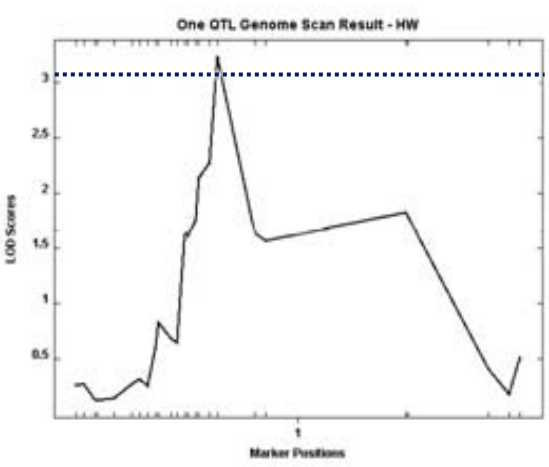

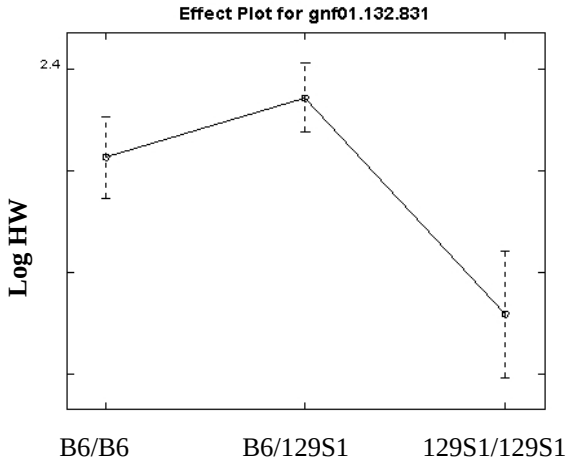

Figure 5-7. Interval mapping and plot showing the relationship between body weight (BW) and genotype at the rs8254399 marker on chromosome 9 (A) and rs13481367 markers on 12 (B) in F_2 male progeny.

A. Chromosome 9

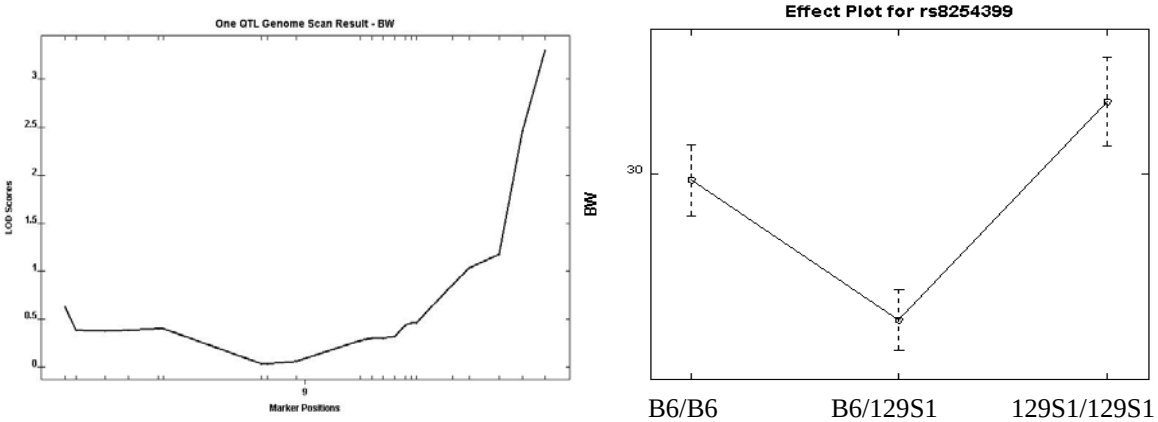

B. Chromosome 12

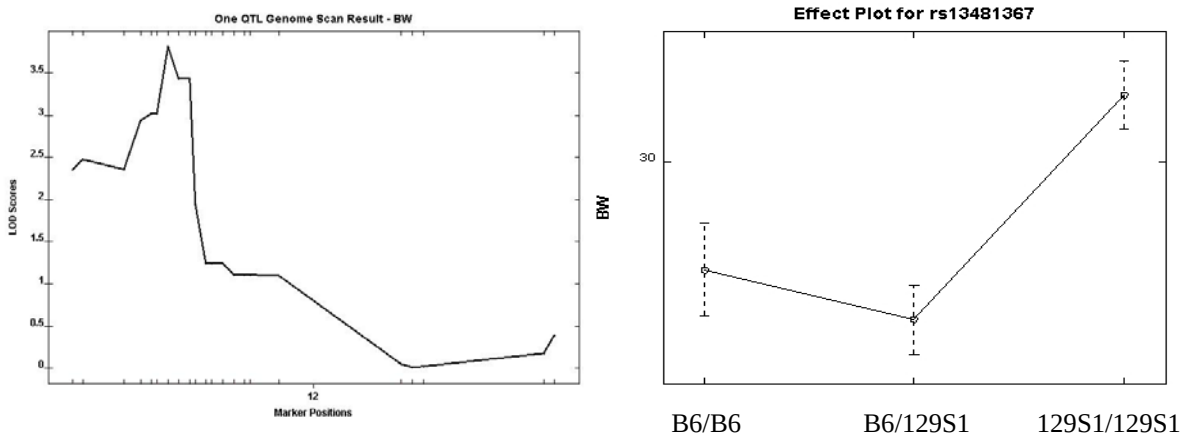

Figure 5-8. Single marker association test results for a whole genome scan performed on F_2 female mice. Each bar represents a single SNP marker (A). Interval mapping of chromosome 16 and plot showing the relationship between normalized cardiac weight and genotype at the chromosome 16 rs4220927 marker in F_2 female progeny (B). Suggestive threshold is represented as a dotted line.

A.

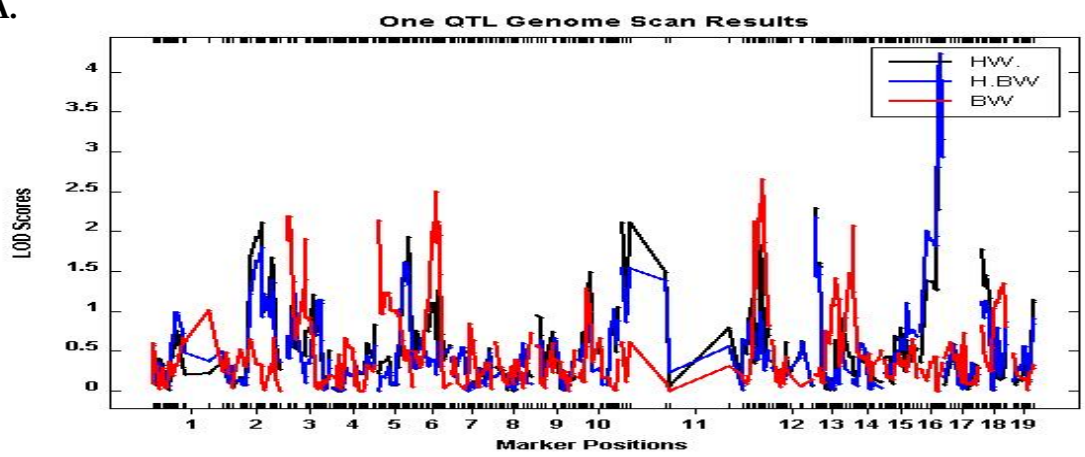

B. Chromosome 16

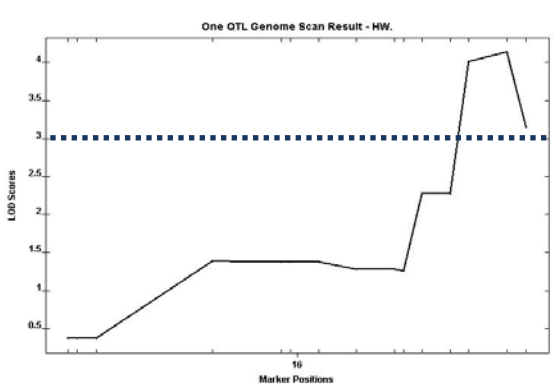

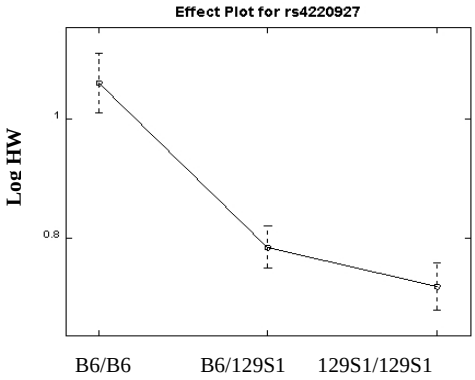

Figure 5-9. 1.5 LOD CI for QTLs on chromosome 9 (A) and 16 (B) linked to cardiac hypertrophy in male and female mice, respectively. Parenthesis denotes regions of high SNP variability between B6 and 129S1 strains. Grey bars represent the total number of SNPS genotyped per bin, while the red bars represent the number of SNPs per bin that differ between the specified strains.

A. Chromosome 9

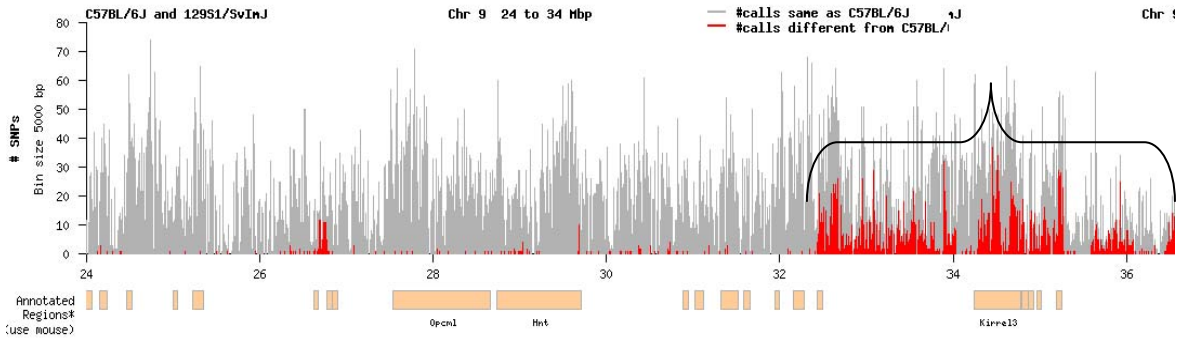

B. Chromosome 16

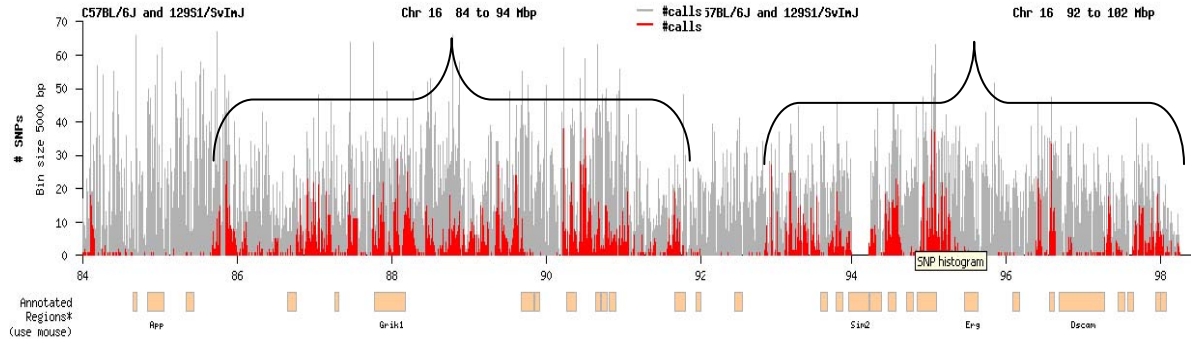

Table 5-5. Summary of modifier locus identified using the F_2-*Egfr* $^{wa2/wa2}$ panel.

Panel	**Phenotype**	**Chr**	**Marker**	**Peak position (cM)**	**Peak position (Mgb)**	***COVARIATE ANALYSIS***							
						None		*Sex*		*BW*		*Chr 9 and 16 QTLS*	
						LOD	***p*<**	**LOD**	***p*<**	**LOD**	***p*<**	**LOD**	***p*<**
Total	**HW**	1	rs3711079	6.12	22.14	_	_	–	–	–	–	7.32	*0.05*
		9	9.033.451	18.49	32.67	_	_	4.40	*0.63*	–	–	–	–
		15	rs13482485	9.05	25.55	–	–	–	–	–	–	4.72	*0.63*
		16	rs4220927	46.45	95.31	–	–	4.43	*0.63*	–	–	–	–
		19	rs1348389	48.97	57.36	–	–	–	–	–	–	5.37	*0.63*
Male	**HW**	1	Gnf01.132.831	52.04	113.12	–	–	–	–	3.23	*0.63*	–	–
		9	9.033.451	18.49	32.67	4.82	*0.05*	–	–	6.31	*0.01*	–	–
		12	rs3686531	82.40	117.52	3.03	*0.63*	–	–	–	–	–	–
	BW	9	rs8254399	86.37	123.75	3.29	*0.63*	–	–	–	–	–	–
		12	rs13481367	17.73	26.83	3.81	*0.63*	–	–	–	–	–	–
Female	**HW**	16	rs4220927	46.45	95.31	4.14	*0.63*	–	–	4.31	*ns*	–	–

References

1. Hammond, I.W., et al., *The prevalence and correlates of echocardiographic left ventricular hypertrophy among employed patients with uncomplicated hypertension.* J Am Coll Cardiol, 1986. **7**(3): p. 639-50.

2. Koren, M.J., et al., *Relation of left ventricular mass and geometry to morbidity and mortality in uncomplicated essential hypertension.* Ann Intern Med, 1991. **114**(5): p. 345-52.

3. Weber, K.T. and C.G. Brilla, *Pathological hypertrophy and cardiac interstitium. Fibrosis and renin-angiotensin-aldosterone system.* Circulation, 1991. **83**(6): p. 1849-65.

4. Muiesan, M.L., et al., *Association of change in left ventricular mass with prognosis during long-term antihypertensive treatment.* J Hypertens, 1995. **13**(10): p. 1091-5.

5. Brown, D.W., W.H. Giles, and J.B. Croft, *Left ventricular hypertrophy as a predictor of coronary heart disease mortality and the effect of hypertension.* Am Heart J, 2000. **140**(6): p. 848-56.

6. Devereux, R.B., et al., *Left ventricular hypertrophy and geometric remodeling in hypertension: stimuli, functional consequences and prognostic implications.* J Hypertens Suppl, 1994. **12**(10): p. S117-27.

7. Ganau, A., et al., *Patterns of left ventricular hypertrophy and geometric remodeling in essential hypertension.* J Am Coll Cardiol, 1992. **19**(7): p. 1550-8.

8. Levy, D., et al., *Prognostic implications of baseline electrocardiographic features and their serial changes in subjects with left ventricular hypertrophy.* Circulation, 1994. **90**(4): p. 1786-93.

9. Conrady, A.O., et al., *Prospective study of the changes in left ventricular mass and geometry patterns in hypertensive patients During 5 years of follow-up.* Circ J, 2005. **69**(11): p. 1374-9.

10. Wong, K.K., et al., *Genetic variants of proteins from the renin angiotensin system are associated with pressure load cardiac hypertrophy.* Clin Exp Pharmacol Physiol, 1996. **23**(6-7): p. 587-90.

11. Dellgren, G., et al., *Angiotensin-converting enzyme gene polymorphism influences degree of left ventricular hypertrophy and its regression in patients undergoing operation for aortic stenosis.* Am J Cardiol, 1999. **84**(8): p. 909-13.

12. Knez, I., et al., *Angiotensin-converting enzyme polymorphisms and their potential impact on left ventricular myocardial geometry after aortic valve surgery.* J Heart Valve Dis, 2003. **12**(6): p. 687-95.

13. Novaro, G.M., et al., *Association between apolipoprotein E alleles and calcific valvular heart disease.* Circulation, 2003. **108**(15): p. 1804-8.

14. Orlowska-Baranowska, E., et al., *Influence of ACE I/D genotypes on left ventricular hypertrophy in aortic stenosis: gender-related differences.* J Heart Valve Dis, 2004. **13**(4): p. 574-81.

15. Favero, L., et al., *Gender differences in left ventricular function in patients with isolated aortic stenosis.* J Heart Valve Dis, 2003. **12**(3): p. 313-8.

16. Rohde, L.E., et al., *Gender-associated differences in left ventricular geometry in patients with aortic valve disease and effect of distinct overload subsets.* Am J Cardiol, 1997. **80**(4): p. 475-80.

17. Roger, V.L., et al., *Progression of aortic stenosis in adults: new appraisal using Doppler echocardiography.* Am Heart J, 1990. **119**(2 Pt 1): p. 331-8.

18. Faggiano, P., et al., *Rate of progression of valvular aortic stenosis in adults.* Am J Cardiol, 1992. **70**(2): p. 229-33.

19. Peter, M., et al., *Progression of aortic stenosis. Role of age and concomitant coronary artery disease.* Chest, 1993. **103**(6): p. 1715-9.

20. Lester, S.J., et al., *The natural history and rate of progression of aortic stenosis.* Chest, 1998. **113**(4): p. 1109-14.

21. O'Brien, K.E., C.L. O'Bryan, and R. Saad, *Predictors of outcome in asymptomatic aortic stenosis.* N Engl J Med, 2001. **344**(3): p. 227-8; author reply 228-9.

22. Chambers, J., et al., *Determinants of left ventricular mass in aortic stenosis.* J Heart Valve Dis, 2004. **13**(6): p. 873-80.

23. Gharavi, A.G., et al., *Deletion polymorphism of the angiotensin-converting enzyme gene is independently associated with left ventricular mass and geometric remodeling in systemic hypertension.* Am J Cardiol, 1996. **77**(15): p. 1315-9.

24. Tripodi, G., et al., *Haplotype analysis of carnitine transporters and left ventricular mass in human essential hypertension.* J Ren Nutr, 2005. **15**(1): p. 2-7.

25. Deschepper, C.F., et al., *Functional alterations of the Nppa promoter are linked to cardiac ventricular hypertrophy in WKY/WKHA rat crosses.* Circ Res, 2001. **88**(2): p. 223-8.

26. Hamon, M., et al., *Association of angiotensin converting enzyme and angiotensin II type 1 receptor genotypes with left ventricular function and mass in patients with angiographically normal coronary arteries.* Heart, 1997. **77**(6): p. 502-5.

27. Liljedahl, U., et al., *Single nucleotide polymorphisms predict the change in left ventricular mass in response to antihypertensive treatment.* J Hypertens, 2004. **22**(12): p. 2321-8.

28. Osterop, A.P., et al., *AT1 receptor A/C1166 polymorphism contributes to cardiac hypertrophy in subjects with hypertrophic cardiomyopathy.* Hypertension, 1998. **32**(5): p. 825-30.

29. Rockman, H.A., et al., *Segregation of atrial-specific and inducible expression of an atrial natriuretic factor transgene in an in vivo murine model of cardiac hypertrophy.* Proc Natl Acad Sci U S A, 1991. **88**(18): p. 8277-81.

30. Liao, Y., et al., *Echocardiographic assessment of LV hypertrophy and function in aortic-banded mice: necropsy validation.* Am J Physiol Heart Circ Physiol, 2002. **282**(5): p. H1703-8.

31. Hu, P., et al., *Minimally invasive aortic banding in mice: effects of altered cardiomyocyte insulin signaling during pressure overload.* Am J Physiol Heart Circ Physiol, 2003. **285**(3): p. H1261-9.

32. Gao, X.M., et al., *Regression of pressure overload-induced left ventricular hypertrophy in mice.* Am J Physiol Heart Circ Physiol, 2005. **288**(6): p. H2702-7.

33. Perrino, C., et al., *Intermittent pressure overload triggers hypertrophy-independent cardiac dysfunction and vascular rarefaction.* J Clin Invest, 2006. **116**(6): p. 1547-60.

34. Barger, P.M. and D.P. Kelly, *Fatty acid utilization in the hypertrophied and failing heart: molecular regulatory mechanisms.* Am J Med Sci, 1999. **318**(1): p. 36-42.

35. Lygate, C.A., et al., *Serial high resolution 3D-MRI after aortic banding in mice: band internalization is a source of variability in the hypertrophic response.* Basic Res Cardiol, 2006. **101**(1): p. 8-16.

36. Li, Y.H., et al., *Doppler evaluation of peripheral vascular adaptations to transverse aortic banding in mice.* Ultrasound Med Biol, 2003. **29**(9): p. 1281-9.

37. Luetteke, N.C., et al., *The mouse waved-2 phenotype results from a point mutation in the EGF receptor tyrosine kinase.* Genes Dev, 1994. **8**(4): p. 399-413.

38. Chen, B., et al., *Mice mutant for Egfr and Shp2 have defective cardiac semilunar valvulogenesis.* Nat Genet, 2000. **24**(3): p. 296-9.

39. Mrosovsky, N., et al., *Masking in waved-2 mice: EGF receptor control of locomotion questioned.* Chronobiol Int, 2005. **22**(6): p. 963-74.

40. Moran, J.L., et al., *Utilization of a whole genome SNP panel for efficient genetic mapping in the mouse.* Genome Res, 2006. **16**(3): p. 436-40.

41. Ideraabdullah, F.Y., et al., *Rescue of the Mouse DDK Syndrome by Parent-of-Origin-Dependent Modifiers.* Biol Reprod, 2007. **76**(2): p. 286-293.

42. Broman, K.W., et al., *R/qtl: QTL mapping in experimental crosses.* Bioinformatics, 2003. **19**(7): p. 889-90.

43. Skavdahl, M., et al., *Estrogen receptor-beta mediates male-female differences in the development of pressure overload hypertrophy.* Am J Physiol Heart Circ Physiol, 2005. **288**(2): p. H469-76.

44. Wiltshire, T., et al., *Genome-wide single-nucleotide polymorphism analysis defines haplotype patterns in mouse.* Proc Natl Acad Sci U S A, 2003. **100**(6): p. 3380-5.

45. Yalcin, B., et al., *Unexpected complexity in the haplotypes of commonly used inbred strains of laboratory mice.* Proc Natl Acad Sci U S A, 2004. **101**(26): p. 9734-9.

46. Bonow, R.O., et al., *ACC/AHA 2006 guidelines for the management of patients with valvular heart disease: a report of the American College of Cardiology/American Heart Association Task Force on Practice Guidelines (writing committee to revise the 1998 Guidelines for the Management of Patients With Valvular Heart Disease): developed in collaboration with the Society of Cardiovascular Anesthesiologists: endorsed by the Society for Cardiovascular Angiography and Interventions and the Society of Thoracic Surgeons.* Circulation, 2006. **114**(5): p. e84-231.

47. Bonow, R.O., et al., *ACC/AHA Guidelines for the Management of Patients With Valvular Heart Disease. Executive Summary. A report of the American College of Cardiology/American Heart Association Task Force on Practice Guidelines (Committee on Management of Patients With Valvular Heart Disease).* J Heart Valve Dis, 1998. **7**(6): p. 672-707.

48. Zhai, P., et al., *An angiotensin II type 1 receptor mutant lacking epidermal growth factor receptor transactivation does not induce angiotensin II-mediated cardiac hypertrophy.* Circ Res, 2006. **99**(5): p. 528-36.

49. Iwamoto, R. and E. Mekada, *ErbB and HB-EGF signaling in heart development and function.* Cell Struct Funct, 2006. **31**(1): p. 1-14.

50. Chan, H.W., et al., *Tackling the EGFR in pathological tissue remodelling.* Pulm Pharmacol Ther, 2006. **19**(1): p. 74-8.

51. Ushikoshi, H., et al., *Local overexpression of HB-EGF exacerbates remodeling following myocardial infarction by activating noncardiomyocytes.* Lab Invest, 2005. **85**(7): p. 862-73.
52. Ohtsu, H., et al., *ADAM17 mediates epidermal growth factor receptor transactivation and vascular smooth muscle cell hypertrophy induced by angiotensin II.* Arterioscler Thromb Vasc Biol, 2006. **26**(9): p. e133-7.
53. Shah, B.H. and K.J. Catt, *Matrix metalloproteinase-dependent EGF receptor activation in hypertension and left ventricular hypertrophy.* Trends Endocrinol Metab, 2004. **15**(6): p. 241-3.
54. Shah, B.H. and K.J. Catt, *A central role of EGF receptor transactivation in angiotensin II -induced cardiac hypertrophy.* Trends Pharmacol Sci, 2003. **24**(5): p. 239-44.
55. Smith, N.J., et al., *Hijacking epidermal growth factor receptors by angiotensin II: new possibilities for understanding and treating cardiac hypertrophy.* Cell Mol Life Sci, 2004. **61**(21): p. 2695-703.
56. Asakura, M., et al., *Cardiac hypertrophy is inhibited by antagonism of ADAM12 processing of HB-EGF: metalloproteinase inhibitors as a new therapy.* Nat Med, 2002. **8**(1): p. 35-40.
57. Pareja, M., et al., *Activated epidermal growth factor receptor (ErbB1) protects the heart against stress-induced injury in mice.* Am J Physiol Regul Integr Comp Physiol, 2003. **285**(2): p. R455-62.
58. Lorita, J., et al., *Effects of epidermal growth factor on epinephrine-stimulated heart function in rodents.* Am J Physiol Heart Circ Physiol, 2002. **283**(5): p. H1887-95.
59. Tarnavski, O., et al., *Mouse cardiac surgery: comprehensive techniques for the generation of mouse models of human diseases and their application for genomic studies.* Physiol Genomics, 2004. **16**(3): p. 349-60.

CHAPTER 6

CONCLUSIONS AND FUTURE DIRECTIONS

EGFR activity is essential for proper tissue development, maintenance and repair in most organ systems. Conversely, EGFR overexpression or overactivation, particularly in epithelial tissues, promotes disease processes such as carcinogenesis. Thus, a continuous balance of EGFR signaling is required for overall fitness and health. A role for EGFR activity in adult tissue homeostasis is typically associated with organ systems that have high EGFR expression and retain proliferative or regenerative capacity, such as the skin, gut and liver. Since the ERBBs are expressed at relatively low levels in adult heart, and cardiomyocytes are terminally differentiated, the significant and lethal cardiomyopathy resulting from targeted inhibition of ERBB2/HER2 activity in cancer clinical trials was unexpected [1]. Assisted by genetically engineered mouse models, research has since advanced understanding about ERBB2 receptor signaling in cardiac homeostasis and disease, leading to the recent proposal to enhance ERBB2 activity via NRG1 stimulation as a strategy for treatment of heart failure and cardiotoxicity [2, 3]. Similarly, by using genetic and pharmaceutical models, the work presented herein explored the consequences of chronically suppressed EGFR/ERBB1 signaling on cardiac development and homeostasis. This effort is particularly timely for several reasons. First, due to innovations in cancer therapy and detection, cancer is frequently perceived and treated as a chronic disease [4]. As more patients are exposed to EGFR targeted therapies for longer duration, toxicities may

pose a greater health risk than predicted in short-term clinical trials, and adverse reactions associated with uncommon genetic polymorphisms may be uncovered. Secondly, inhibition of EGFR signaling has been proposed as a novel treatment for hypertension and LVH, meaning that patients with compromised cardiovascular function may also be chronically exposed to these drugs [5-7].

Since other EGFR-related phenotypes showed strain-dependent penetrance and severity [8, 9], we first asked if EGFR-related cardiovascular phenotypes are modulated by genetic background. Using congenic B6 and 129S11 *Egfr* ^{wa2} lines and their F_1 *Egfr* ^{wa2} offspring, we found significant genetic-background dependent variation in cardiac phenotypes, including congenital cardiomyocyte defects, LVH, and development of degenerative calcific AS, confirming our hypothesis. Since physiological studies suggested that B6 and 129S1 *Egfr* ^{wa2} mice had variable pressure differentials across the aortic valve, indicating differences in AS severity and load, we next asked if genetic background modified the cardiac response to afterload. By constricting the ascending aorta (TAC), we applied a similar afterload on the LV of adult wild type B6, 129S1 and F_1 male mice. We found significant genetic-background dependent variation in cardiac response to TAC, with B6 genetic modifiers promoting more rapid progression to heart failure accompanied by severe pathological responses. Although the duration of the pressure overload was shorter in the surgical model, and the cardiomyocytes of 129S1 mice did manifest a hypertrophic response, results of this study suggested that resistant 129S1 modifiers sustaining cardiomyocyte survival and function contributed to the variable cardiac phenotype. In order to partition EGFR congenital defects from effects on adult cardiac function, we conducted studies where adult B6 wild-type mice were chronically exposed to EGFR small molecule inhibitors. Left

ventricular wall thinning, depressed cardiac contractility and increased cardiac cell apoptosis, parameters which profoundly impact cardiac function, were observed with pharmaceutical inhibition of EGFR activity. Finally, we employed a genetic mapping study using an F_2 intercross strategy to broadly localize QTLs which modulated EGFR-related cardiac phenotypes. Consistent with observed sexual dimorphism in genetic and pharmaceutical studies, two QTLs were identified which were independently associated with cardiac hypertrophy in male and female F_2-*Egfr* $^{wa2/wa2}$ mice, respectively.

Ultimately, we hope that our studies will contribute to understanding EGFR function in cardiac biology, as well as provide improved mouse models of common cardiac diseases. Growing evidence implies that mitogenic signals activated by EGFR which induce proliferation in other cell types trigger a hypertrophic response in terminally differentiated cardiomyocytes. Consistent with other organ systems whose development is dependent upon EGFR, our observations suggest a balance of EGFR signaling is also important in cardiomyocyte homeostasis, where too much activity instigates a hypertrophic response, while too little activity compromises cardiomyocyte survival. During developmental timepoints prior to valve formation, we observed defective trabeculation and thinned chamber walls in B6 *Egfr* $^{wa2/wa2}$ embryos and increased cardiomyocyte apoptosis in B6 *Egfr* $^{wa2/wa2}$ neonatal pups, comparable to the congenital cardiomyocyte defects in *Erbb2* $^{-/-}$ embryos [10]. The cardiac phenotype observed with chronic dietary exposure to EGFR inhibitors (which probably also target ERBB2) had similarities to the dilated cardiomyopathy observed in mice with ventricular-specific ablation of *Erbb2* [11, 12]. Taken together, these observations suggest that signaling through EGFR/ERBB2 heterodimers or EGFR homodimers may also contribute to cardiomyocyte development and survival. In cancer

cells, EGFR/ERBB2 heterodimers generate potent mitogenic and cell survival signals and have prolonged signaling compared to EGFR homodimers because of differences in rate of receptor endocytosis [13, 14]. If signaling through EGFR/ERBB2 heterodimers is similarly prolonged in cardiomyocytes, the relative contribution from ERGFR/ERBB2 heterodimers could alter cardiomyocyte apoptosis or hypertrophy. One way to address this question might be through primary *Egfr* ^{wa2}cardiomyocyte cultures. A specific *Erbb2* inhibitor, such as Herceptin/trastuzumab, could be applied to cultures of *Egfr* $^{wa2/wa2}$ and *Egfr* $^{wa2/+}$ cardiomyocytes and effects on apoptosis, AKT activity and levels of phosphorylated pro and anti-apoptotic proteins assessed. Alternatively, *Egfr* $^{wa2/wa2}$ mice could be crossed to *Erbb2* cardiac restricted knock-out mice to test the consequences *in vivo* of reduced EGFR activity on the *Erbb2* cardiac phenotype. Given the development of dual inhibitors targeting both EGFR and ERBB2 signaling [15, 16], and the recent proposal to target ERBB signaling for the treatment of cardiovascular diseases where cardiomyocyte function may be impaired, it follows that the relative contributions of ERBB members to cardiac survival should be investigated.

A requirement for EGFR signaling in cardiac valve development has consistently been reported [17, 18]. Our studies extend these observations, suggesting that EGFR signaling may prevent degenerative pathological processes associated with valvular disease. Since we found evidence of significant valvular interstitial cell proliferation and altered extracellular matrix (ECM) composition in adult B6 *Egfr* $^{wa2/wa2}$ mice, we hypothesize that EGFR signaling normally checks valve cellular proliferation and may also play a role in ECM stratification or organization during valve remodeling stages. Decreased EGFR signaling delays wound healing and exacerbates inflammation in several injury models [19-

22] and misregulation of these processes may worsen or accelerate valvular disease on the sensitive B6 genetic background. Initial results from pharmaceutical studies appeared to reinforce our hypothesis, as 100% of the EKB-569 inhibitor treated mice had evidence of calcification, compared to 38% of the controls; in addition mean thickness of aortic valve leaflets was associated with diet. However, valve thickening was seen in mice fed both treated and control diets compared to mice receiving normal chow, while calcification was present in valves from all mice fed the control diet in later experiments. Repeating these experiments with a different base diet or inbred strain, and performing histological analysis of calcification, ECM composition and cellular proliferation would be important in light of the *Egfr* ^{wa2} developmental and post-natal cardiac valve phenotypes. Additionally, the chick embryo cardiac cushion explant system might be useful to determine if EGFR inhibitors enhance calcification, VIC proliferation or ECM composition in a more controlled environment. In addition, by using lower drug concentrations, these *in vitro* studies would reduce off-target effects.

A conditional *Egfr* allele (*Egfr* ^{flox}) using a LoxP strategy has been developed in the lab, making inactivation of *Egfr* in specific cell types possible. By crossing the *Egfr* ^{flox} line to lines with cardiomyocyte-restricted Cre recombinase expression, we can obtain mice with cardiomyocyte-specific deletion of *Egfr*. This strategy should allow us to discriminate *Egfr*-related effects on cardiac muscle from secondary effects due to congenital valve enlargement. Preliminary characterization of *Egfr* $^{flox/flox}$ mice that express Cre recombinase under the control of the *myosin light chain 2v* locus *(MLC2v* $^{Cre/+}$*)* has revealed no significant differences in survival, baseline cardiac function or cardiac or other organ weights compared to *Egfr* $^{flox/flox}$ or *Egfr* $^{flox/+}$ *MLC2v* $^{Cre/+}$ controls. However, these mice are on mixed B6/129S1

genetic background and recombination efficiency has not been assessed. Additionally, it is possible that cardiac phenotypes arising from cardiomyocyte specific EGFR inactivity may be subtle without challenge. Currently, we have B6 *Egfr* ^{flox} congenic lines (N10) and have ongoing crosses to both MLC2v and α-cardiac myosin heavy chain (αMHC) Cre mice. Characterization of cardiac phenotypes of these mice at baseline, and in response to stimuli such as pressure overload induced by aortic banding or β-adrenergic stimulation via isoprotenol exposure, would further define the role of EGFR signaling in cardiomyocyte function and survival.

A significant portion of interindividual variability in both tumor response to EGFR targeted therapies and toxicities appears to be the result of genetic variations both in the individual and in the neoplasia [23-25]. Positive response and skin toxicity have been connected to germline EGFR polymorphisms within intron 1 that alter its expression (Veronese, 2005[26, 27]. Polymorphisms correlating to low EGFR expression and tumor resistance to EGFR targeted therapy are found more frequently in persons of Asian ethnicity [28, 29]. A rare, but potentially fatal complication of EGFR inhibitor therapy is interstitial lung disease, and Japanese patients appear to be at a higher risk for this rare toxicity than patients from other nationalities [30]. Sexual dimorphism in EGFR somatic mutations, clinical outcome and toxicities with EGFR targeted therapies has also been reported [31]. Females more often experience tumor response and positive outcome in cancer clinical trials using the EGFR TKI Iressa/Gefinitib for the treatment of non-small lung cell cancer [32-34]. Since phenotypes of mice with reduced or absent EGFR are highly dependent upon genetic background and mimic patient toxicities observed with EGFR targeted therapies, these mouse models may prove useful in identifying genetic modifiers of EGFR activity [35].

Preliminary studies are underway profiling expression of genes residing within the identical by descent (IBD) region of the Chromosome 9 QTL in *Egfr* $^{wa2/wa2}$ LV and aortic outflow tracts. Our laboratory has also backcrossed the *Egfr* ^{wa2} mutation onto the A/J and BTBR T^{+} tf/J genetic backgrounds. Comparison of cardiac phenotypes of these mice coupled with haplotype analysis may narrow the candidate region even further. Transgenic bacterial artificial chromosomes (BAC) mice harboring overlapping candidate regions of 129S1 chromosome 9 QTL on the B6 genetic background could be created and crossed to B6 *Egfr* $^{wa2/wa2}$ mice. Amelioration of cardiac hypertrophy in *Egfr* $^{wa2/wa2}$ mice would provide strong evidence of protective 129S1 modifiers. Successful identification of genes modulating the *Egfr* ^{wa2} cardiac phenotypes would advance understanding about the role of EGFR in cardiac development and homeostasis, may uncover novel targets for the treatment of common cardiac diseases, and assist prediction of cardiotoxicity in sensitive populations.

References

1. Ewer, M.S., et al., *Cardiotoxicity in patients receiving transtuzumab (Herceptin): primary toxicity, synergistic or sequential stress, or surveillance artifact?* Semin Oncol, 1999. **26**(4 Suppl 12): p. 96-101.

2. Liu, X., et al., *Neuregulin-1/erbB-activation improves cardiac function and survival in models of ischemic, dilated, and viral cardiomyopathy.* J Am Coll Cardiol, 2006. **48**(7): p. 1438-47.

3. Freedman, N.J. and G.S. Ginsburg, *Novel--and "neu"--therapeutic possibilities for heart failure.* J Am Coll Cardiol, 2006. **48**(7): p. 1448-50.

4. Force, T., D.S. Krause, and R.A. Van Etten, *Molecular mechanisms of cardiotoxicity of tyrosine kinase inhibition.* Nat Rev Cancer, 2007. **7**(5): p. 332-44.

5. Asakura, M., et al., *Cardiac hypertrophy is inhibited by antagonism of ADAM12 processing of HB-EGF: metalloproteinase inhibitors as a new therapy.* Nat Med, 2002. **8**(1): p. 35-40.

6. Shah, B.H. and K.J. Catt, *Matrix metalloproteinase-dependent EGF receptor activation in hypertension and left ventricular hypertrophy.* Trends Endocrinol Metab, 2004. **15**(6): p. 241-3.

7. Smith, N.J., et al., *Hijacking epidermal growth factor receptors by angiotensin II: new possibilities for understanding and treating cardiac hypertrophy.* Cell Mol Life Sci, 2004. **61**(21): p. 2695-703.

8. Threadgill, D.W., et al., *Targeted disruption of mouse EGF receptor: effect of genetic background on mutant phenotype.* Science, 1995. **269**(5221): p. 230-4.

9. Strunk, K.E., V. Amann, and D.W. Threadgill, *Phenotypic variation resulting from a deficiency of epidermal growth factor receptor in mice is caused by extensive genetic heterogeneity that can be genetically and molecularly partitioned.* Genetics, 2004. **167**(4): p. 1821-32.

10. Lee, K.F., et al., *Requirement for neuregulin receptor erbB2 in neural and cardiac development.* Nature, 1995. **378**(6555): p. 394-8.

11. Crone, S.A., et al., *ErbB2 is essential in the prevention of dilated cardiomyopathy.* Nat Med, 2002. **8**(5): p. 459-65.

12. Ozcelik, C., et al., *Conditional mutation of the ErbB2 (HER2) receptor in cardiomyocytes leads to dilated cardiomyopathy.* Proc Natl Acad Sci U S A, 2002. **99**(13): p. 8880-5.

13. Muthuswamy, S.K., M. Gilman, and J.S. Brugge, *Controlled dimerization of ErbB receptors provides evidence for differential signaling by homo- and heterodimers.* Mol Cell Biol, 1999. **19**(10): p. 6845-57.

14. Pinkas-Kramarski, R., et al., *Diversification of Neu differentiation factor and epidermal growth factor signaling by combinatorial receptor interactions.* Embo J, 1996. **15**(10): p. 2452-67.

15. Burris, H.A., 3rd, et al., *Phase I safety, pharmacokinetics, and clinical activity study of lapatinib (GW572016), a reversible dual inhibitor of epidermal growth factor receptor tyrosine kinases, in heavily pretreated patients with metastatic carcinomas.* J Clin Oncol, 2005. **23**(23): p. 5305-13.

16. Wong, T.W., et al., *Preclinical antitumor activity of BMS-599626, a pan-HER kinase inhibitor that inhibits HER1/HER2 homodimer and heterodimer signaling.* Clin Cancer Res, 2006. **12**(20 Pt 1): p. 6186-93.

17. Jackson, L.F., et al., *Defective valvulogenesis in HB-EGF and TACE-null mice is associated with aberrant BMP signaling.* Embo J, 2003. **22**(11): p. 2704-16.

18. Chen, B., et al., *Mice mutant for Egfr and Shp2 have defective cardiac semilunar valvulogenesis.* Nat Genet, 2000. **24**(3): p. 296-9.

19. Yin, J., et al., *Wound-induced ATP release and EGF receptor activation in epithelial cells.* J Cell Sci, 2007. **120**(Pt 5): p. 815-25.

20. Repertinger, S.K., et al., *EGFR enhances early healing after cutaneous incisional wounding.* J Invest Dermatol, 2004. **123**(5): p. 982-9.

21. O'Brien, D.P., et al., *Selective inhibition of the epidermal growth factor receptor impairs intestinal adaptation after small bowel resection.* J Surg Res, 2002. **105**(1): p. 25-30.

22. Beuerman, R.W. and H.W. Thompson, *Molecular and cellular responses of the corneal epithelium to wound healing.* Acta Ophthalmol Suppl, 1992(202): p. 7-12.

23. Li, J., et al., *CYP3A phenotyping approach to predict systemic exposure to EGFR tyrosine kinase inhibitors.* J Natl Cancer Inst, 2006. **98**(23): p. 1714-23.

24. Li, J., et al., *Association of Variant ABCG2 and the Pharmacokinetics of Epidermal Growth factor Receptor Tyrosine Kinase Inhibitors in Cancer Patients.* Cancer Biol Ther, 2007. **6**(3): p. 432-8.

25. Jimeno, A. and M. Hidalgo, *Pharmacogenomics of epidermal growth factor receptor (EGFR) tyrosine kinase inhibitors.* Biochim Biophys Acta, 2006. **1766**(2): p. 217-29.

26. Amador, M.L., et al., *An epidermal growth factor receptor intron 1 polymorphism mediates response to epidermal growth factor receptor inhibitors.* Cancer Res, 2004. **64**(24): p. 9139-43.

27. Liu, G., et al., *Epidermal growth factor receptor polymorphisms and clinical outcomes in non-small-cell lung cancer patients treated with gefitinib.* Pharmacogenomics J, 2007.

28. Zhou, Q., et al., *EGFR Intron 1 polymorphism in Asian Populations and its correlation with EGFR gene expression and amplification in breast tumor tissues.* Cancer Biol Ther, 2006. **5**(11): p. 1445-9.

29. Buerger, H., et al., *Allelic length of a CA dinucleotide repeat in the egfr gene correlates with the frequency of amplifications of this sequence--first results of an inter-ethnic breast cancer study.* J Pathol, 2004. **203**(1): p. 545-50.

30. Cersosimo, R.J., *Gefitinib: an adverse effects profile.* Expert Opin Drug Saf, 2006. **5**(3): p. 469-79.

31. Sasaki, H., et al., *EGFR Mutation status in Japanese lung cancer patients: genotyping analysis using LightCycler.* Clin Cancer Res, 2005. **11**(8): p. 2924-9.

32. Janne, P.A., et al., *Outcomes of patients with advanced non-small cell lung cancer treated with gefitinib (ZD1839, "Iressa") on an expanded access study.* Lung Cancer, 2004. **44**(2): p. 221-30.

33. Zhang, X.T., et al., *[Treatment of non-small cell lung cancer with gefitinib.].* Zhonghua Jie He He Hu Xi Za Zhi, 2005. **28**(3): p. 180-3.

34. Konishi, J., et al., *Analysis of the response and toxicity to gefitinib of non-small cell lung cancer.* Anticancer Res, 2005. **25**(1B): p. 435-41.

35. Roberts, R.B., C.L. Arteaga, and D.W. Threadgill, *Modeling the cancer patient with genetically engineered mice: prediction of toxicity from molecule-targeted therapies.* Cancer Cell, 2004. **5**(2): p. 115-20.